CRYSTAL CORED OPTICAL WAVEGUIDES

A thesis submitted for the degree
of Doctor of Philosphy in the
University of London

by

BIMAL KUMAR NAYAR B.Sc.(Eng.)

Department of Electrical Engineering,
Imperial College,
London, SW7 2BT.

November, 1983.

ABSTRACT

Optical fibres normally have isotropic non-crystalline core and cladding materials. The thesis describes a study of the theory, practicability, and possible applications of fibres with crystalline, non-centrosymmetric core and glass cladding. The wave propagation in such a dielectric waveguide has been studied and dispersion characteristics determined for a uniaxial crystal cored fibre with its crystal c-axis along the fibre axis. In addition the possibility of second harmonic generation (SHG) in these fibres is considered. It is shown, using coupled mode analysis that these guides can be designed such that a wave at the fundamental frequency in the HE_{11} mode can be phase matched with a SH guided mode. Alternatively, lower efficiencies of generation are shown to be easy to implement when the fundamental wave is the guided HE_{11} mode and the SH wave is in the radiation field.

The fabrication of these crystal cored fibres is described in some detail. The basic technique used is to draw down capillaries of an appropriate glass having bore diameters <10μm, followed by growth of an orientated organic single crystal in the hollow region. The growth mechanism was crystallization from the melt by a modified vertical Bridgeman technique. The criteria used to select suitable organic crystal materials for SHG are discussed. It was found that acetamide and benzil were potentially suitable materials. Benzil was finally preferred and studied in more depth, largely because of the hygroscopic nature of acetamide. The above method of crystal growth was successfully used to fabricate single mode, void free benzil crystal cored fibres of lengths upto 50mm.

The experimental SHG has been demonstrated with a 1.06μm. fundamental wavelength in benzil cored fibres where the SH wave is in the radiation field. Possible implications of this work for guided wave non-linear interactions are considered.

ACKNOWLEDGEMENTS

It is a pleasure to be able to record formally my thanks to Dr. J.R. Cozens for his advice and guidance throughout the course of my studies at Imperial College. Thanks are also due to Mr. R.B. Dyott for guidance, useful discussions and encouragement during the course of this work. The genial company of research students in the electromagnetic wave group was always a fortunate asset. In particular I would like to thank V.Henderek for allowing the use of his furnace for drawing capillaries and N.Nourshargh and S. Al-Shukari for stimulating discussions.

I would also like to thank R.Kashyap and D.R.Smith of British Telecom Research Labs. for arranging the use of Nd:YAG laser for optical SHG demonstration.

Personal thanks are due to my wife and family for constant support.

CONTENTS

		Page
Introduction		7
Chapter 1	Second Harmonic Generation	8
1.0.	Introduction	8
1.1.	Non-linear phenomena	8
1.2.	Optical SHG in the bulk media	15
1.3.	Phase-matching techniques	18
	1.Birefringent phase matching	19
	2.Quasi-phase matching methods	22
	3.Phase matching using guidance properties of optical waveguides	24
Chapter 2	Wave propagation in isotropic and anisotropic cored fibres	29
2.0.	Introduction	29
2.1.	Wave propagation in isotropic cored fibres	29
2.2.	Weakly guiding approximations	36
2.3.	Wave propagation in uniaxial crystal cored fibre	40
2.4.	Wave propagation in biaxial crystal cored fibres	44
2.5.	Wave propagation in uniaxial cored fibres with crystal axis not along the fibre axis	46
2.6.	Wave propagation in fibres with dispersive core	48
Chapter 3	Theoretical analysis of optical SHG in crystal cored fibres	49
3.0.	Introduction	49
3.1.	Qualitative description of SHG in crystal cored fibres	49
	1.Coupling the fundamental into a SH guided mode	50

		Page
	2.Coupling the fundamental guided mode into the SH radiation field	52
3.2.	Analysis of SHG in crystal cored fibres	52
3.3.	Discussion	62
Chapter 4	Materials for growth in glass capillaries	66
4.0.	Introduction	66
4.1.	Selection criteria used for growth of crystals in glass capillaries	66
4.2.	Crystal materials used for growth in glass capillaries	69
4.3.	Purification of commercially avialable materials	71
	1.Purification of benzil	71
4.4.	Growth of bulk benzil single crystals	73
4.5.	Assessment and discussion of properties of benzil	75
	1.Benzil's dispersion	75
	2.Benzil's non-linear tensor coefficients	77
	3.Transmission spectrum of benzil	77
Chapter 5	Growth of crystal cored optical fibres	80
5.0.	Introduction	80
5.1.	Growth of acetamide single crystals in glass capillaries	80
5.2.	Selection of capillary glass for the fabrication of benzil crystal cored fibres	94
5.3.	Prepration of glass capillaries	95
5.4.	Change in glass refractive on capillary drawing	96
5.5.	Growth of benzil in small bore capillaries	99
Chapter 6	Optical SHG experiments using benzil crystal cored fibres	102
6.0.	Introduction	102
6.1.	SHG experiments using GaAs laser	102

Page

6.2. SHG experiments using Nd:YAG laser 106

Conclusion 109

Appendix 1: Description and listing of the computer program used to determine propagation constants of modes in fibres 113

Appendix 2: Evaluation of the field overlap integral for SHG in crystal cored fibres 119

References 121

Publications 124

INTRODUCTION

The enormous bandwidth potential in the use of optical fibres, as the transmission media, for communication systems was recoganised soon after Kao and Hockam(1966) demonstrated transmission of optical signals in glass fibres. The research effort over the last fifteen years has cumilated in the installation of fully engineered graded index fibre systems in several European countries, Japan and USA. At the present time single mode fibre systems, which offer even greater bandwidths, are being installed. These systems are however not fully 'optic' as the information processing and amplification at the repeater stage is carried out electronically. The endevour to make active optical devices has resulted in the development of integrated optic devices for modulation, switching and other information processing functions. These devices are of planar geometry and in general make use of the electro-optic and acusto-optic effects. For parametric amplification it is necessary to use the material's second order susceptiblity. A number of researchers have been investigating three wave mixing in planar waveguides but the efficiency of these interactions has been low due to difficulties in phase matching and low value of the material's second order susceptibilty. In recent years a number of organic materials with very large second order susceptibilty have been realised by molecular engineering. These materials also tend to exhibit resistance to damage at high optical intensities. The prospect of realisation of efficient non-linear optical devices using these materials seems to be very promising. In this work a study of fabrication of crystal cored fibres using organic materials was carried out with the intention of making waveguiding structures for non-linear optical interactions. The waveguide fabrication method used is particularly useful as some of these materials lack mechanical strength and are susceptiable to chemical attack because the molecular sites are bound only by relatively weak Van der Waals forces. Also, the cylinderical geometry of these fibres will make their coupling to the silica fibres, used for communication, relatively easy.

CHAPTER 1

SECOND HARMONIC GENERATION

1.0 Introduction:

The first non-linear optics experiment was carried out by Franken et al(1961) using the then newly invented Ruby laser to demonstrate optical second harmonic generation. In the last two decades the subject has developed extensively, both theoretically and experimentally, and it is now possible to generate second and third harmonic frequencies of intense laser beams with efficiencies approaching 50%. Non-linear optical techniques are now widely used to produce coherent light over a wide range of frequencies from the ultra-violet to far infra-red. Non-linear optics is a generic term for a number of diverse optical phenomena which arise with high optical intensities. In this chapter a review of second harmonic generation and methods of phase matching the interacting waves is presented.

1.1 Non-linear Phenomena:

When a dielectric medium is subjected to electromagnetic radiation it tends to become polarized due to distortion of its internal charge distribution under the influence of electric field, $\underline{E}$, associated with the radiation. The resultant electric dipole moment per unit volume is defined as electric polarization, $\underline{P}$. For weak fields the induced polarization is linear and proportional to the applied field and is given by

$$\underline{P} = \underline{P_L} = \epsilon_o \hat{\chi}_L^{(1)} . \underline{E} \qquad (1.1.1)$$

where

ϵ_0 is the permittivity of the free space.

$\hat{\chi}_L^{(1)}$ is the linear susceptibility tensor of second rank.

Dielectric constant of the medium is defined in terms of linear

susceptibility tensor as

$$\hat{\varepsilon} = \varepsilon_o(\hat{1} + \hat{\chi}_L^{(1)}) \qquad (1.1.2)$$

and, hence

$$\underline{D} = \hat{\varepsilon}\underline{E} \qquad (1.1.3)$$

However, with intense fields the polarization is no longer linear and can be represented as a power series of the inducing field

$$\underline{P} = \underline{P_L} + \underline{P_{NL}} = \varepsilon_o(\hat{\chi}_L^{(1)} \cdot \underline{E} + \hat{\chi}_{NL}^{(2)} : \underline{E}\ \underline{E} + \hat{\chi}_{NL}^{(3)} \vdots \underline{E}\ \underline{E}\ \underline{E} + \ldots.) \qquad (1.1.4)$$

where, the first term on R.H.S. is the previously defined linear polarization while the subsequent terms are due to the non-linear polarization. Non-linear susceptibilities $\hat{\chi}_{NL}^{(2)}$, $\hat{\chi}_{NL}^{(3)}$, ... are tensors of the second, third and higher ranks. A number of diverse optical phenomena are due to the first three terms in the above expansion, i.e.

$\hat{\chi}_L^{(1)}$ is responsible for the linear optical properties, such as reflection and refraction.

$\hat{\chi}_{NL}^{(2)}$ gives rise to second harmonic generation(SHG), parametric amplification, sum and difference frequency generation, d.c. rectification and linear electro-optic effect.

$\hat{\chi}_{NL}^{(3)}$ gives rise to third harmonic generation, four wave mixing processes, quadratic electro-optic effect, two photon absorption, and stimulated Raman, Brillouin and Rayleigh scattering.

The second order non-linear polarization is of particular interest as it affords the possibility of second harmonic generation and parametric amplification with modest powers in optical waveguides. The second order non-linear susceptibility tensor is non-zero in only non-centrosymmteric materials. In centrosymmetric materials polarization reverses the sign for reversal of the electric field and as a consequence the terms containing even powers of the field in the polarization expansion become zero. The polarization in both centrosymmetric and non-centrosymmetric materials as a function of applied field is shown in figure 1.1. The non-linearities in both the

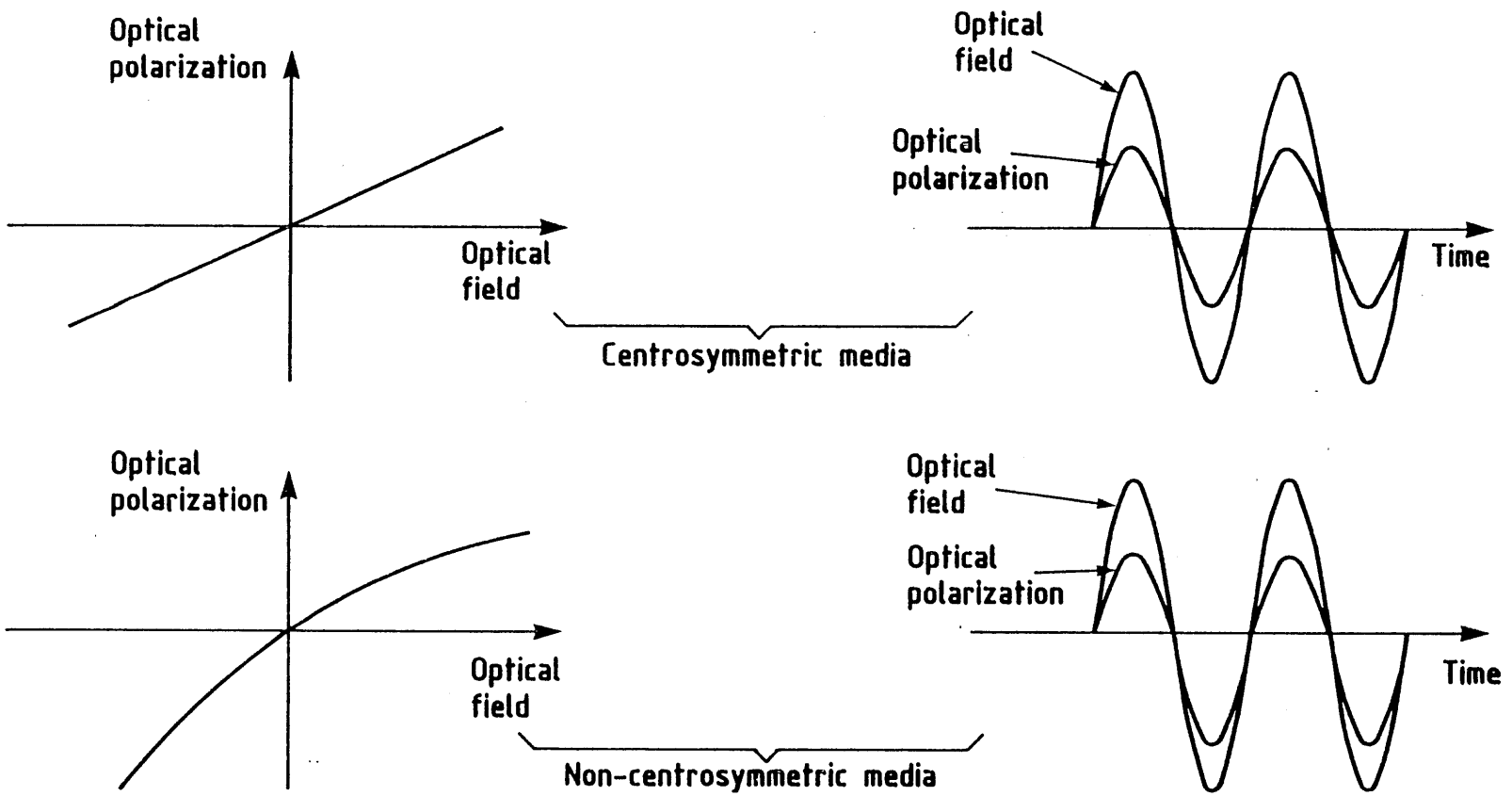

Figure 1.1: Response of crystalline material to incident optical field.

cases have been exaggerated.

In the subsequent analysis the third and higher order terms in the polarization expansion have been neglected and the non-linear polarization will be considered as

$$\underline{P}_{NL} = \varepsilon_o \hat{\chi}^{(2)}_{NL} : \underline{E}\,\underline{E} \qquad (1.1.5)$$

The tensor properties of $\hat{\chi}^{(2)}_{NL}$ are better appericiated by writing its full form rather than the condensed notation used above

$$\underline{P}_{NL} = \underline{P}_i(t) = \varepsilon_o \sum_{ijk} \hat{\chi}^{(2)}_{ijk} : \underline{E}_j(t)\underline{E}_k(t) \qquad (1.1.6)$$

Where, instantaneous electric field and polarization can be written in terms of their Fourier components as

$$\underline{E}(\underline{r},t) = 1/2[\underline{E}(\underline{r},\omega)e^{j(\underline{k}.\underline{r}-\omega t)} + c.c.] \qquad (1.1.7)$$

$$\underline{P}(\underline{r},t) = 1/2[\underline{P}(\underline{r},\omega)e^{j(\underline{k}.\underline{r}-\omega t)} + c.c.] \qquad (1.1.8)$$

Susceptibility tensor $\hat{\chi}^{(2)}_{ijk}(-\omega_3, \omega_2, \omega_1)$ is then defined in terms of Fourier amplitude relation as

$$\underline{P}_i(r,\omega_3) = \frac{1}{2}\varepsilon_o \sum_{ijk} \hat{\chi}^{(2)}_{ijk}(-\omega_3,\omega_2,\omega_1) : \underline{E}_j(r,\omega_2)\underline{E}_k(r,\omega_1)\, e^{j(\underline{k}_1 + \underline{k}_2 - \underline{k}_3).\underline{r}} \qquad (1.1.9)$$

where, $\omega_3 = \omega_1 + \omega_2$

For SHG, $\omega_1 = \omega_2$, and the susceptibility tensor becomes $\hat{\chi}^{(2)}_{ijk}(-2\omega,\omega,\omega)$

In literature experimentalists adopt a different notation for SHG tensor, namely $d_{ijk}(-2\omega,\omega,\omega)$. The two are same expect for a factor of '2' and their relationship is (Kaminow 1974)

$$\hat{\chi}^{(2)}_{ijk}(-2\omega,\omega,\omega) = 2d_{ijk}(-2\omega,\omega,\omega) \qquad (1.1.10)$$

Non-linear polarization for SHG can then be expressed using SH tensor, d, as

$$\underline{P}_i(\omega_3) = \epsilon_o \sum_{ijk} d_{ijk}(-\omega_3, \omega, \omega) : \underline{E}_j(\omega) . \underline{E}_k(\omega) e^{j(2\underline{k}-\underline{k}_3)\cdot \underline{r}} \qquad (1.1.11)$$

where, $\omega_3 = 2\omega$

Or, in condensed notation as

$$\underline{P}_i(2\omega) = \epsilon_0 d_{ijk} : \underline{E}_j(\omega) . \underline{E}_k(\omega) \qquad (1.1.12)$$

SH tensor d_{ijk} has in general twenty-seven independent elements. However, as no physical significance can be attached in interchanging $\underline{E}_j$ and $\underline{E}_k$, it follows that $d_{ijk} = d_{ikj}$ and the number of independent tensor elements reduce to eighteen. A contracted notation d_{im} is used for d_{ijk} ie

(jk)	=	(11)	(22)	(33)	(23)	(13)	(12)
m	=	1	2	3	4	5	6

Using this contracted notation for the indices, equation (1.1.12) becomes

$$\begin{vmatrix} \underline{P}_x \\ \underline{P}_y \\ \underline{P}_z \end{vmatrix} = \epsilon_o \begin{vmatrix} d_{11} & d_{12} & d_{13} & d_{14} & d_{15} & d_{16} \\ d_{21} & d_{22} & d_{23} & d_{24} & d_{25} & d_{26} \\ d_{31} & d_{32} & d_{33} & d_{34} & d_{35} & d_{36} \end{vmatrix} \begin{vmatrix} \underline{E}_x^2 \\ \underline{E}_y^2 \\ \underline{E}_z^2 \\ 2\underline{E}_y\underline{E}_z \\ 2\underline{E}_z\underline{E}_x \\ 2\underline{E}_x\underline{E}_y \end{vmatrix} \qquad (1.1.13)$$

A further reduction in the number of independent elements is possible due to Klienman's conjecture (Klienman 1962). That is in a lossless medium the permutation of frequencies is irrelevant and d_{ijk} is symmetric under any permutation of its indices. As a result the number of independent tensor elements reduce from eighteen to ten. The equation (1.1.13) therefore can be rewritten as

$$\begin{vmatrix} \underline{P}_x \\ \underline{P}_y \\ \underline{P}_z \end{vmatrix} = \varepsilon_o \begin{vmatrix} d_{11} & d_{12} & d_{13} & d_{14} & d_{15} & d_{16} \\ d_{16} & d_{22} & d_{23} & d_{24} & d_{14} & d_{12} \\ d_{15} & d_{24} & d_{33} & d_{23} & d_{13} & d_{14} \end{vmatrix} \begin{vmatrix} \underline{E}_x^2 \\ \underline{E}_y^2 \\ \underline{E}_z^2 \\ 2\underline{E}_y \underline{E}_z \\ 2\underline{E}_z \underline{E}_x \\ 2\underline{E}_x \underline{E}_y \end{vmatrix} \quad (1.1.14)$$

In practice most of the materials possess only a few non-zero tensor elements and the optical SH tensor forms for all the crystal classes are listed in standard texts on non-linear optics (Singh 1971, Yariv 1975).

An estimate of magnitude of one dimensional non-linear SH coefficient is possible from the analysis of an anharmonic oscillator. This model representation of a crystal is similar to the Drude-Lorentz model for the valence electrons. It was first used by Bloembergen (1965) and has since also been used other researchers (Lax 1962, Garrett et al 1966, Kurtz et al 1967, Robinson 1967, Garrett 1968) to obtain an order of magnitude of the effect in various crystals. The equation of motion for an anharmonic oscillator is given by

$$\ddot{x} + \gamma\dot{x} + \omega_o^2 x + \nu x^2 = \left(\frac{e}{m}\right) E(\omega,t) \quad (1.1.15)$$

where

$x(t)$ is the deviation of the electron from its equilbrium position.

γ is the damping constant.

ω_o is the linear resonance frequency.

ν is the anharmonic force constant.

e and m are the electronic charge and the mass respectively.

$E(\omega,t)$ is the electric field of the light wave varying with the frequency, ω.

The induced polarization due to this field is given by

$$P = Nex(t) = \varepsilon_o \chi_L E(\omega,t) \qquad (1.1.16)$$

where

N, is the number of electrons per unit volume.

Solving equation (1.1.15) and using (1.1.16) it can be shown that linear susceptibilities, $\chi_L^{(\omega)}$ and $\chi_L^{(2\omega)}$, at ω and 2ω respectively are given by

$$\chi_L^{(\omega)} = \frac{Ne^2}{m\varepsilon_o} \frac{1}{D(\omega)}$$

$$\chi_L^{(2\omega)} = \frac{Ne^2}{m\varepsilon_o} \frac{1}{D(2\omega)} \qquad (1.1.17)$$

where

$$D(\omega) = \omega_o^2 - \omega^2 + i\gamma\omega$$

$$D(2\omega) = \omega_o^2 - 4\omega^2 + 2i\gamma\omega$$

It can be further shown that the SH non-linear coefficient is given by

$$d = -\frac{Ne^3\nu}{m^2\varepsilon_o} \frac{1}{D(2\omega)\, D^2(\omega)} \qquad (1.1.18)$$

This can be expressed in terms of linear susceptibilities $\chi_L^{(\omega)}$ and $\chi_L^{(2\omega)}$ as

$$d = \frac{m\nu\varepsilon_o^2}{N^2|e|^3} \chi_L^{(\omega)^2} \chi_L^{(2\omega)} \qquad (1.1.19)$$

Garrett and Robinson (1966) have defined a coefficient 'δ', such that

$$|\delta| = \frac{d}{\varepsilon_o \chi_L^{(\omega)^2} \chi_L^{(2\omega)}} = \frac{m\nu\varepsilon_o}{N^2 e^3} \qquad (1.1.20)$$

Its three dimensional analog is known as 'Millers-Delta' and is defined as

$$\delta_{ijk} = \frac{d_{ijk}}{\varepsilon_o \chi_{ii}^{(2\omega)} \chi_{jj}^{(\omega)} \chi_{kk}^{(\omega)}} \qquad (1.1.21)$$

Miller (1964a) found that the above quantity was nearly constant for a

large number of materials. It is approximately equal to 3×10^{-6} esu (7×10^{-2} m^2/C). There are no known materials having δ above 20×10^{6} esu and a very few have a value below 0.2×10^{6} esu. However, d can vary over four orders of magnitude. Hence an order of magnitude estimate for d of various materials can be made from their refractive index data ie

$$d = \varepsilon_o \chi_L^{(\omega)^2} \chi_L^{(2\omega)} \delta \approx \varepsilon_o (n^2 - 1)^3 \delta \approx \varepsilon_o n^6 \delta \qquad (1.1.22)$$

where, it has been assumed that $n^{\omega} = n^{2\omega}$, and δ can be assumed to have an approximate constant value of 0.07 m^2/C.

1.2 Optical SHG In The Bulk Media :

In the previous section it was stated that for large optical fields in non-centrosymmetric crystals, a non-linear polarization wave is induced whose SH component gives rise to a SH light wave. The SH power generated in the bulk crystal in this manner can be derived using the coupled wave formalism and is given in various texts on the subject (Yariv (1975), Zernike and Midwinter (1973)). The expression for SH power, $P^{2\omega}$, generated by a single mode gaussian beam of power, P^{ω}, incident along a principal plane of a parallel slab of thickness, L, of a lossless crystal is given by (Singh (1971)),

$$P^{2\omega} = \frac{2(\mu_o)^{3/2}(\varepsilon_o)^{1/2}\omega^2 d_{im}^2 (P^{\omega})^2 L^2}{\pi W_o^2 n^{2\omega} (n^{\omega})^2} \left[\frac{\mathrm{Sin}(\Delta k \frac{L}{2})}{\Delta k \frac{L}{2}}\right]^2 \qquad (1.2.1)$$

where

ε_o and μ_o are the free space permittivity and permeability respectively.

ω is the fundamental frequency.

W_o is the spot radius of the fundamental beam.

d_{im} is the pertinent SH tensor coefficient.

$\Delta k = k^{2\omega} - 2k^{\omega}$, is the phase mismatch in the propagation constants of the fundamental and SH waves.

n^{ω} and $n^{2\omega}$ are the bulk refractive indices at the fundamental and SH frequencies respectively.

The maximum SH power is obtained for $\Delta k=0$. This requirement corresponds to the phase matching of fundamental and SH light wave velocities. It can be seen from the above equation that the SH power goes through a series of maxima and minima for $\Delta k \neq 0$ and is maximum when

$$\frac{1}{2}\Delta kL = (2n+1)\frac{\pi}{2} \qquad \text{for, } n = 0,1,2,3,\ldots$$

or, when the crystal length is given by

$$L = \frac{\pi}{\Delta k}, \frac{3\pi}{\Delta k}, \quad \ldots$$

Maker et al (1962) were first to observe this periodic variation of the SH intensity by tilting a thin quartz crystal plate in the path of a Ruby laser beam. Also, when $\Delta k \neq 0$ and $\Delta kL = (2n+1)\pi$, the effective SH tensor coefficient is reduced by a factor of $2/(2n+1)\pi$. A plot of SH amplitude normalized to initial amplitude of the fundamental wave as a function of distance inside the crystal for various degrees of phase mismatch is given in figure 1.2. The crystal length which gives the first maxima is defined as the 'Coherence Length', L_c and is given in terms of crystal indices as

$$L_C = \frac{\pi}{\Delta k} = \frac{\pi}{k^{2\omega} - 2k^{\omega}} = \frac{\lambda}{4[n^{2\omega} - n^{\omega}]} \qquad (1.2.2)$$

The variation of SH power as a function of crystal length can be described in terms of a simple physical effect. The SH polarization wave travels in the bulk material with a phase velocity which is same as that of the inducing fundamental light wave ie $v^{\omega} = c/n^{\omega}$. However, as the most materials are positively dispersive the SH light wave travels with a velocity, $v^{2\omega} = c/n^{2\omega}$, which is different from that of the fundamental wave. Consequently the SH light wave generated at any instant will be slightly out of phase with the SH light wave generated an instant earlier. The two waves have a phase difference of π after a distance equal to the coherence length. In order to eliminate this phase mismatch various methods have been devised to phase match the fundamental and SH light waves and are described below.

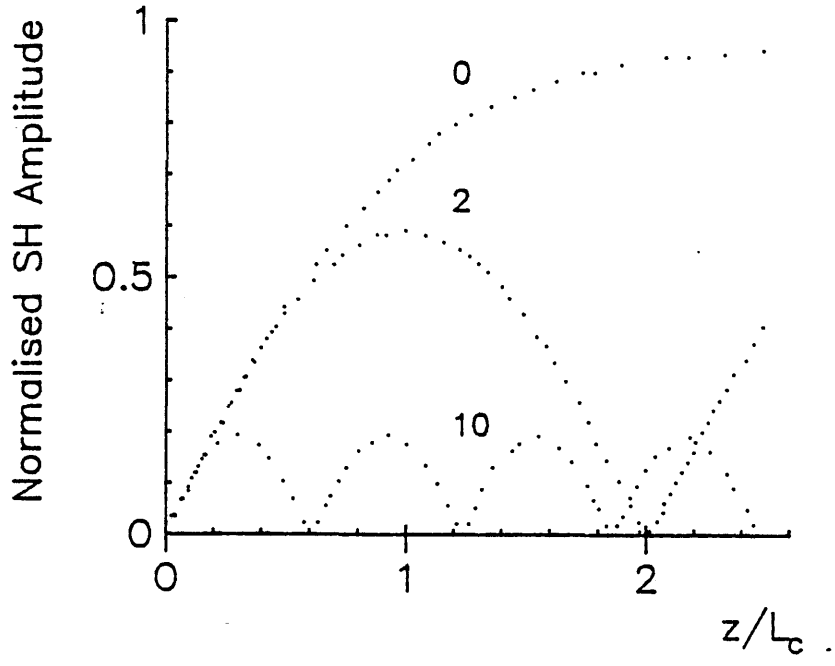

Figure 1.2: Normalized SH amplitude as a function of the distance inside the crystal for various degrees of phase mismatch.

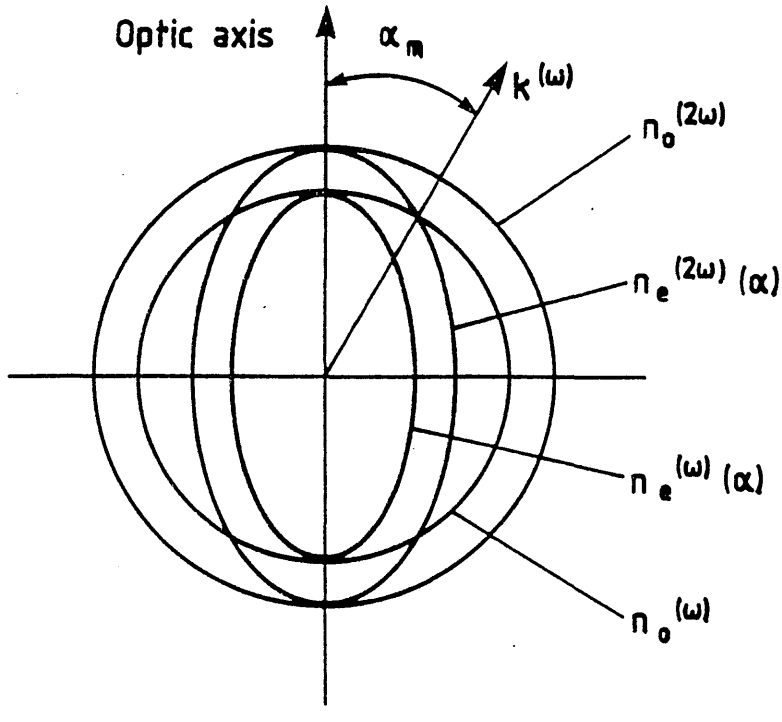

Figure 1.3: Angle phase matching in a negative uniaxial crystal.

1.3 Phase-Matching Techniques:

There are seven crystal classes of which those belonging to one ie Cubic, are isotropic while the rest are anisotropic. The refractive index of anisotropic crystals is not only frequency dependent but is also dependent upon the state of polarisation of the light wave and its direction of propagation relative to the crystal c-axis. Anisotropic crystals can be either uniaxial or biaxial depending upon whether they possess two or three independent refractive indices. This crystal property is referred to as birefringence and is responsible for the double refraction phenomenon. Unpolarised light on entering a birefringent media is resolved into two orthogonal components. In an uniaxial crystal the refractive index of the component of light rays polarised normal to the c-axis is independent of the direction of propagation and they are referred to as ordinary rays. However, the refractive index of the component of light rays polarised parallel to c-axis varies with the direction of propagation relative to the c-axis. These rays because of their unusual behaviour are referred to as extraordinary rays. In general if 'α' is the angle between the direction of propagation and the optic or c-axis, the refractive index for the e-rays is given by

$$n_e(\alpha) = [(\mathrm{Cos}\alpha/n_o)^2 + (\mathrm{Sin}\alpha/n_e)^2]^{-1/2} \qquad (1.3.1)$$

where

n_o and n_e are the refractive indicies along the two principal crystal axes.

The difference in refractive indices along the two principal directions of an uniaxial crystal gives its birefringence. Uniaxial crystal can be positive or negative depending on whether n_e is greater or less than n_o. In some crystals it is possible to exploit their natural birefringence to phase match the fundamental and SH waves. The other methods which can also be used to obtain phase matched optical SHG are

1. Quasi-phase matching methods.
2. Phase matching using guidance properties of optical waveguides.

These methods are discussed below in greater detail.

1.3.1 Birefringent Phase Matching:

The use of natural crystal birefringence to overcome material dispersion for phase matched SHG was first realised independently by Maker et al (1962) and Giordmaine (1962). The principle of this method of phase matching can be illustrated by considering phase matching in the case of potassium-di-hydrogen phosphate (KDP) crystal. KDP is a negative uniaxial crystal belonging to $\bar{4}2m$ point group. In figure 1.3 index surfaces of KDP are shown for frequencies ω and 2ω. It can be seen from the figure that if the direction of propagation is at an angle 'α_m' to the crystal axis, $n_o^{\omega} = n_e^{2\omega}$. Hence, if the fundamental beam is launched at an angle 'α_m' to the crystal c-axis as an ordinary wave, the phase matched SH beam will exit as an extraordinary wave along the same direction. The phase matching angle in this case is given by

$$\mathrm{Sin}^2\alpha_m = \frac{[(n_o^{\omega})^{-2} - (n_o^{2\omega})^{-2}]}{[(n_e^{2\omega})^{-2} - (n_o^{2\omega})^{-2}]} \qquad (1.3.2)$$

The phase matching is only possible if the dispersion is less than the crystal birefringence ie $|n_o^{2\omega} - n_o^{\omega}| < |n_e^{2\omega} - n_o^{2\omega}|$. This type of phase matching is termed as 'collinear' as the fundamental and the SH propagate along the same direction. This can further be of type 1 or type 2 depending upon the state of polarization of the fundamental optical beam. In type 1 phase matching the fundamental waves have parallel polarization whereas in type 2 phase matching they have orthogonal polarizations. These two phase matching conditions for a negative uniaxial crystal can be written as

$$\text{type1:} \quad n_o^{\omega} = n_e^{2\omega}(\alpha_m) \quad ; \; o^{\omega}+o^{\omega} \rightarrow e^{2\omega}$$

$$\text{type2:} \quad 1/2[n_o^{\omega}+n_e^{\omega}(\alpha_m)] = n_e^{2\omega}(\alpha_m) \quad ; \; o^{\omega}+e^{\omega} \rightarrow e^{2\omega} \qquad (1.3.3)$$

and for a positive uniaxial crystal they are

$$\text{type1:} \quad n_e^{\omega}(\alpha_m) = n_o^{2\omega} \quad ; \; e^{\omega}+e^{\omega} \rightarrow o^{2\omega}$$

type2: $1/2[n_e^{\omega}(\alpha_m)+n_o^{\omega}] = n_o^{2\omega}$; $e^{\omega}+o^{\omega} \rightarrow o^{2\omega}$ (1.3.4)

The phase matching angles for a given crystal and phase matching type can be evaluated using the appropriate condition, from above, and equation (1.3.1).

The SHG efficiency with birefringent phase matching is usually small because of the double refraction effect. This effect results in the fundamental and the SH waves not overlapping over the entire crystal length and is referred to as 'Poynting Walk Off'. This is shown in figure 1.4 for type 1 phase matching in a negative uniaxial crystal. The angle, ρ, between the SH wavevector and the direction of power flow for type 1 phase matching in a negative uniaxial crystal is given by

$$\rho \approx \tan \rho = \frac{(n_o^{\omega})^2}{2}\left[\frac{1}{(n_e^{2\omega})^2} - \frac{1}{(n_o^{2\omega})^2}\right] \text{Sin } 2\alpha \qquad (1.3.5)$$

The ray and wave normal are parallel for $\alpha_m = 0°$ or $90°$ and in this case there is no walk off. The phase matching is then said to be non-critical and very efficient conversion can be obtained. The effect of 'Poynting Walk Off' is more serious for type 2 phase matching as in this case when the two fundamental waves do not overlap, non-linear polarization is not generated and hence no SH light wave.

For some crystal materials which have phase matching angle close to $90°$ it is possible to achieve non-critical phase matching by varying the crystal temperature to change its birefringence. A temperature dependent change in birefringence occurs as extraordinary index is in general much more temperature dependent than the ordinary index. The phase match temperature, T_m, at which $n^{2\omega} = n^{\omega}$ can be calculated using the following equation

$$T_m = T_o + \frac{n^{\omega} - n^{2\omega}}{\frac{dn^{2\omega}}{dT} - \frac{dn^{\omega}}{dT}} \qquad (1.3.6)$$

where

T_o, is the ambient temperature.

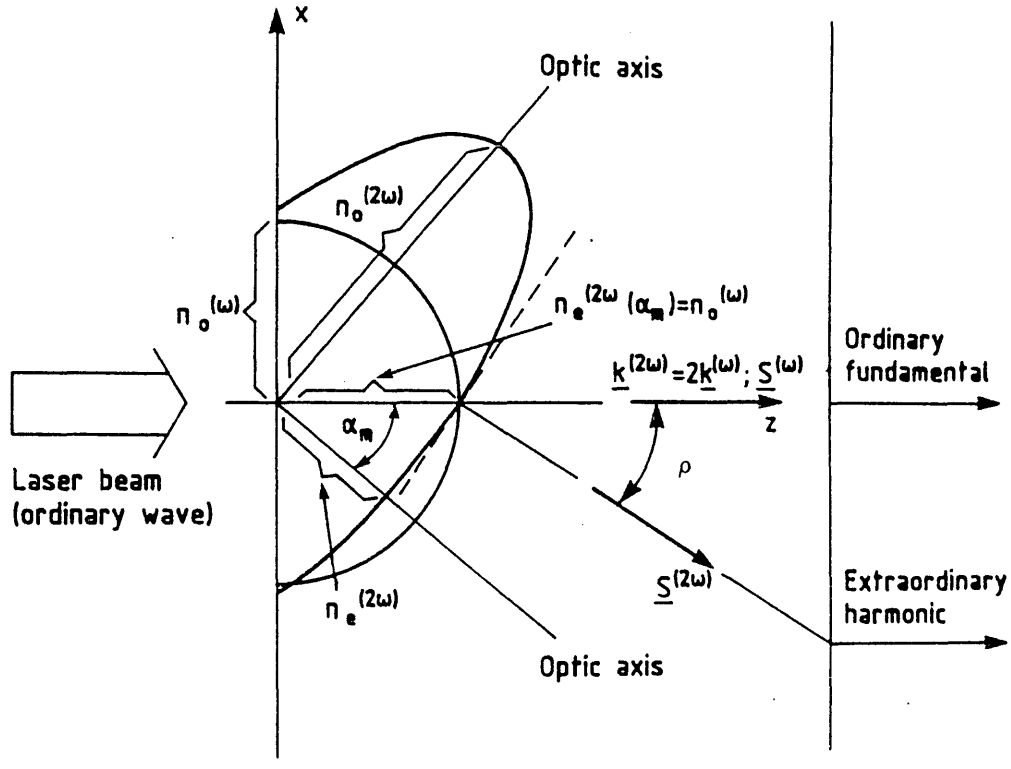

Figure 1.4: 'Walk-Off' effect for SHG with type 1 phase matching in a negative uniaxial crystal.

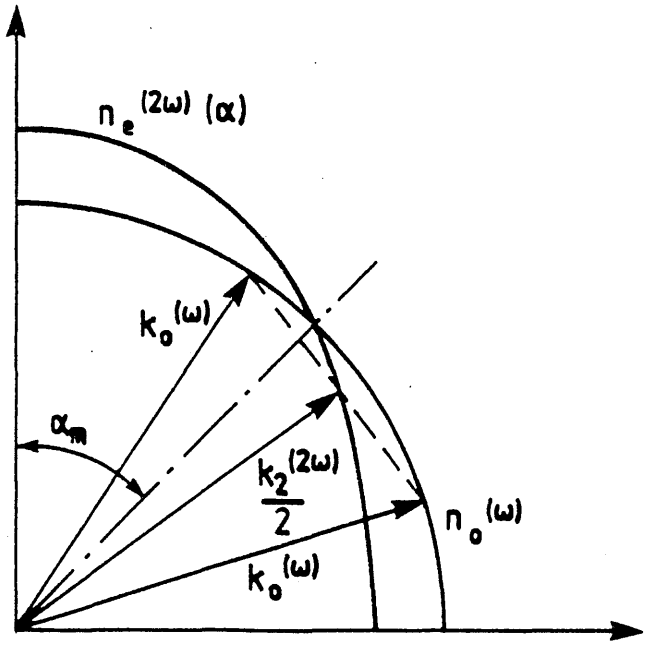

Figure 1.5: Non-collinear phase matching.

This method was first used by Miller et al (1965) to obtain non-critical phase matching in $LiNbO_3$ crystal at fundamental wavelengths of 1.058μm and 1.153μm. More recently this method was used by Useugi et al (1976) to compensate phase mismatch introduced during the fabrication of stripe guide in $LiNbO_3$ for SHG.

Also, for efficient SHG it is necessary to have an optimum degree of focussing of the fundamental beam in the crystal. If the beam's cross-sectional area is large, the intensity of the fundamental beam may not be large enough to generate SH, whereas if it is too small the interaction length will be limited due to excessive divergence and result in low SHG efficiency.

In contrast with the 'Collinear Phase Matching' described above it is also possible to obtain 'Non-collinear Phase Matching'. This technique has been demonstrated by Giordmaine (1962) and Maker et al (1962). In this method two fundamental non-collinear beams are used to produce phase matched SH beam. However either of the two beams on their own cannot generate SH beam. The principle of this method is illustrated in figure 1.5 for the case of KDP crystal.

The theory of birefringence phase matching is now well understood and all the commercially avialable SH generators exploit this form of phase matching.

1.3.2 Quasi-Phase Matching Methods:

The birefringence phase matching method disscussed in the previous section is not applicable to materials having inadequate birefringence e.g. quartz, or those which are isotropic e.g. GaAs. In these materials it is possible to correct the phase mismatch and for this reason phase matching in such materials is referred to as quasi-phase matching. Armstrong and co-workers (1962) were first to propose a number of methods to achieve quasi-phase matching.

One of the method's suggested was the use of periodic variation in the SH tensor co-efficient. This can be achieved by using a periodic structure of crystal plates having the same thickness but with the

crystal axis of the adjacent plates orientated in the opposite direction. The maximum SH intensity is obtained when the thickness of the crystal plates is equal to the 'Coherence Length'. In which case at the end of the first crystal plate there is maximum transfer of energy from the polarization wave into the SH light wave but the two lag in phase by 180°. By having the second plate orientated in the opposite direction, the sign of the SH tensor coefficient reverses for the electric field directed along the original direction. This shifts the phase of the polarization wave by 180° and as a result at the end of the second crystal plate also the SH power grows instead of diminishing as in the case of the bulk crystal. The SH power in this case is reduced by a factor of $(4/\pi^2)$ cf bulk phase matched case. This method of phase matching has been studied in detail by Yacoby et al (1973) and Szilagyi et al (1976). Franken et al (1963) demonstrated enhanced SHG by this method using quartz crystal plates. In their experiment the thickness of the crystal plates was not equal to an odd multiple of the coherence length and as a consequence they had to orientate the stack at 24° to the direction of the laser beam to observe the build up of the SH power. The SH wave in there case was greatly attenuated due to the Fresnel reflection losses at each interface between the plates. Recently, Szilagyi et al (1976) and Thompson et al (1976) eliminated Fresnel reflection losses by propagating the fundamental wave at Brewster's angle with respect to a stack of GaAs plates to generate SH of 10.6μm radiation. Miller (1964b) has shown that this type of structure can occur in polydomain crystals. In an another experiment Dewey(1975) obtained enhanced SHG in single rotationally twinned ZnSe crystal. The non-linear properties of a crystal containing rotational twins are equivalent to that of a stack of crystal plates having periodic variation of SH tensor coefficient and thickness equal to the twin plane spacing.

Another method to correct the phase mismatch uses phase change on total-internal reflection. In a slab of a crystal both the fundamental and the SH waves can be made to undergo multiple reflections at the crystal-air interface. The angle of reflection can be so chosen that the phase mismatch accumulated in every pass between the two reflecting sides is just cancelled by the differential phase change between the fundamental and the SH wave.

This technique has been implemented by Boyd et al (1966).

Bloembergen et al (1970) have suggested the use of periodic variation of the refractive index to achieve quasi-phase matching. In this technique alternate thin layers of different non-linear materials are epitaxially grown to form a periodic laminated structure. Such a periodic structure exhibits frequency stop band in its linear dispersion curve and the characteristic bending of the curve near the stop band is used to obtain phase matching. The detailed behaviour of this type of phase matching has been analysed by Tang and Bey (1973). Van der Ziel (1976a) has verified this form of phase matching by frequency doubling of 2μm radiation using 17 alternating pairs of GaAs and $Al_{0.3}Ga_{0.7}As$.

1.3.3 Phase Matching Using Guidance Properties Of Optical Waveguides:

The advent of integrated optics has highlighted advantages of using waveguiding structures for non-linear interactions and these have been exploited by a number of researchers for optical SHG and mixing. These advantages are:

1. Phase matching can be achieved using waveguide dispersion. Waveguide dispersion arises because the phase velocity of a light wave of a given wavelength in a waveguide is determined by the guiding region dimensions, refractive index difference between the guiding region and the substrate, and the mode of propagation. In practice this is achieved by suitably tailoring the guiding region dimensions and/or the refractive index difference. Thus it is possible to also use materials which are isotropic or have inadequate birefringence for angle phase matching.
2. The dimensions of the guiding region for optical wavelengths are of the order of micrometers and as a result it is possible to have large optical intensities, required for non-linear interactions, with modest optical powers. Also, as the optical energy is guided it is possible to have long interaction lengths. An approximate comparision of the efficiency of the SHG process in a bulk medium and that in a waveguiding structure can be made by considering the product of the intensity of the input beam at frequency, ω, and the interaction length.

For bulk material:

$$I_\omega L = (P/\pi w_o)(\pi w_o/\lambda) = P/\lambda \qquad (1.3.7)$$

where, gaussian beam diffraction has been assumed and w_o is the beam radius at the focus.

Whereas, for a three dimensional guide:

$$I_\omega L = (P/\lambda^2)L = (P/\lambda)(L/\lambda) \qquad (1.3.8)$$

where, it has been assumed that the guide dimensions are comparable to the wavelength of the fundamental wave.

The advantages described above of using waveguiding structures can cancel out if the field overlap integral of the interacting modes is small. This arises since the SHG efficiency is proportional to it ie

$$\eta_{SH} \propto \int \underline{E}_\omega \cdot \underline{E}_{2\omega} \, dA \qquad (1.3.9)$$

where,

$\underline{E}_\omega$ is the electric field distribution of the fundamental mode.

$\underline{E}_{2\omega}$ is the electric field distribution of the SH mode.

A is the waveguide cross-sectional area.

The overlap integral places constraints on mode types into which SH can be coupled and is maximum when both the fundamental and the SH propagate as the fundamental waveguide modes. In practice, phase matching is generally achieved for SH as a higher order mode due to waveguide dispersion characteristic and this leads to low conversion efficiencies.

Planar optical waveguides can be fabricated by a number of well established technologies eg sputtering, in- and out-diffusion, epitaxial growth, ion-exchange, etc. The phase matched SHG in planar optical waveguides has been demonstrated by a number of researchers using one of the following configuratios:

1. A non-linear guide on a linear substrate - (Anderson et al (1971), Zemon et al(1972), Ito et al (1974), Van der Ziel et al (1976b))

The phase matching between the fundamental and SH modes is achieved by the correct choice of the guide thickness. In all the above reports, with the exception of that by Van der Ziel, phase matching was achieved for SH wave propagating as a higher order mode than the fundamental. As a result SHG efficiencies obtained were low due to small value of the field overlap integral. Van der Ziel et al were able to demonstrate phase matching between the fundamental TE_0 and the SH TM_0 modes by etching a grating on one side of the guide to compensate for the phase mis-match. In practice there is some tapering in the guide thickness and this tends to give broadband SHG, but with lower efficiency due to reduced interaction length.

2. A non-linear guide on a non-linear substrate - (Hopkins et al (1974), Van der Ziel et al (1974), Uesugi et al (1976 and 1979).

In this method also phase matching between the fundamental and the harmonic modes is achieved by precise control of the guide thickness. Hopkins et al (1974) were first to report SHG using such a structure. They formed optical waveguides in barium sodium niobate by introducing hydrogen during poling and used these guides to generate phase matched SH by varying the crystal temperature (to tune the waveguide dispersion). The use of temperature dependence of the refractive index to vary the waveguide dispersion relaxes the stringent requirements on the guide dimensions. Uesugi et al (1976) also used temperature dependence of refractive index to achieve phase matching between the lowest order fundamental and SH modes in a Ti-indiffused $LiNbO_3$ waveguide. More recently Uesugi et al (1979) used a bias electric field to achieve the same effect.In this case the bias electric field changes the refractive index and hence the waveguide dispersion via the linear electro-optic effect.

3. A linear guide on a non-linear substrate - (Tien et al (1970), Chen et al (1974))

In this method evanescent field of the fundamental mode excites a

non-linear polarization wave in the substrate which gives rise to a SH light wave. By suitably selecting the guide thickness it is possible to arrange that the non-linear polarization wave travels at a velocity faster than that of the SH polarization wave in the substrate medium. Consequently the non-linear polarization wave radiates SH light wave as a Cerenkov radiation. The cosine of the Cerenkov angle at which the SH is emitted is given by the ratio of the phase velocities of the SH light wave to that of the non-linear polarization wave. In this method tolerances on the waveguide thickness are not severe and broadband SH can be generated. However, efficiency of this method is low as the overlap between the fundamental and the SH fields is small.

4. A linear guide on a non-linear substrate with harmonic as a guided mode - (Suematsu et al (1973), Burns et al (1974) and Chen et al (1974))

In this method non-linear polarization wave excited in the substrate generates a SH light wave which can be guided in the waveguide. The phase matching in this case also is critically dependent on the guide thickness. Burns et al (1974) achieved non-critical phase matching in liquid/TiO_2/quartz waveguide by varying the liquid refractive index by temperature tuning to give phase matching between the lowest order fundamental TE_0 and SH TM_0 modes.

It was stated above that the efficiency for SHG is low, in thin film and stripe waveguides, if the coupling does not take place between the lowest order modes. A possible way for compensating the phase mismatch between the modes is by introducing some form of perturbation equal to the phase mismatch in the waveguide structure. Somekh et al (1972a and 1972b) were first to propose the use of a periodic modulation of the waveguide thickness or the non-linear coefficient to couple the fundamental into the SH wave. Van der Ziel et al (1976b) were first to demonstrate coupling between the lowest order fundamental and the SH mode using a grating etched on the interface of GaAs waveguide. The periodic grating modulated both the linear and the non-linear susceptibilites at frequency $\rho=2\pi/\tau$, where τ is the grating period. The grating period is so chosen to allow

$\delta\beta=\rho$,where $\delta\beta=\beta^{2\omega} - 2\beta^{\omega}$. Levine et al (1975) have used the above concept to obtain phase matched SHG in a nitrobenzene waveguide. They used a periodic modulation of the sign of the non-linear susceptibility with a spatially periodic dc electric field to align the dipoles. Chen et al (1976) also used the above concept to couple the fundamental mode into the SH radiation field which then propagates in the substrate.

Ito et al (1978) have demonstrated phase matching between the low order fundamental and the SH mode using a four layered structure. This structure consists of both linear and non-linear materials such that guidance occurs in both the materials. The phase matching is obtained by the judious choice of layer thickness. However in this case tolerances reported are not as severe as in the other methods discussed above.

It has not been possible, up to now, to realise an efficient non-linear optical device using these structures due to a number of factors in addition to the constraints placed by the overlap integral. The most stringent requirement that has been difficult to achieve is the need to maintain the guide dimensions to within a few percent over the waveguide length to maintain phase matching. The best reports are of interaction lengths between 10 to 20mm. The other problems that have been serious are the scattering losses at the guide-substrate interface and the optical damage as a result of high optical intensities.

This problem of variation of thickness of the guiding region is anticipated to be less severe for crystals grown in glass capillaries as it is possible to draw capillaries with uniform dimensions. It is, therefore expected that the optical SHG in crystal cored optical fibres will be more efficient as compared to that in the planar waveguides. Also, it opens up the possibilities of performing optical parametric amplification for optical fibre communication systems.

CHAPTER2

Wave Propagation in Isotropic and Anisotropic Cored Fibres

2.0 Introduction:

An optical fibre is a cylinderical waveguiding structure and consists of a high refractive index core surrounded by a low refractive index cladding. Light can be guided in these fibres by total internal reflection at the core-cladding interface. The exact description of guiding properties of such a fibre is found from the solution of its wave equation. In this chapter mode theory of wave propagation in both isotropic and anisotropic fibres is presented and is used in the subsequent chapter for the theoretical analysis of SHG in the crystal cored fibres.

2.1 Wave Propagation In Isotropic Cored Fibres:

The optical fibres used in communication systems have an isotropic core and cladding ie glass or silica. The theory of wave propagation in these fibres is well established and documented in a number of texts on the subject (Kapany (1967), Kapany and Burke (1972), Marcuse (1972 and 1974), Midwinter (1979)). The cross-section of a typical step-index optical fibre is given in figure 2.1. Here the fibre core radius is 'a' and the core and cladding refractive indices are n_1 and n_2 respectively. An outline of the derivation of mode solution for such a fibre with the key results is presented below:

The wave equation can be derived using Maxwell's equations ie

$$\nabla \times \underline{E} = -\frac{\partial \underline{B}}{\partial t} \qquad (2.1.0)$$

$$\nabla \times \underline{H} = \underline{J} + \frac{\partial \underline{D}}{\partial t} \qquad (2.1.1)$$

$$\nabla . \underline{D} = \rho \qquad (2.1.2)$$

$$\nabla . \underline{B} = 0 \qquad (2.1.3)$$

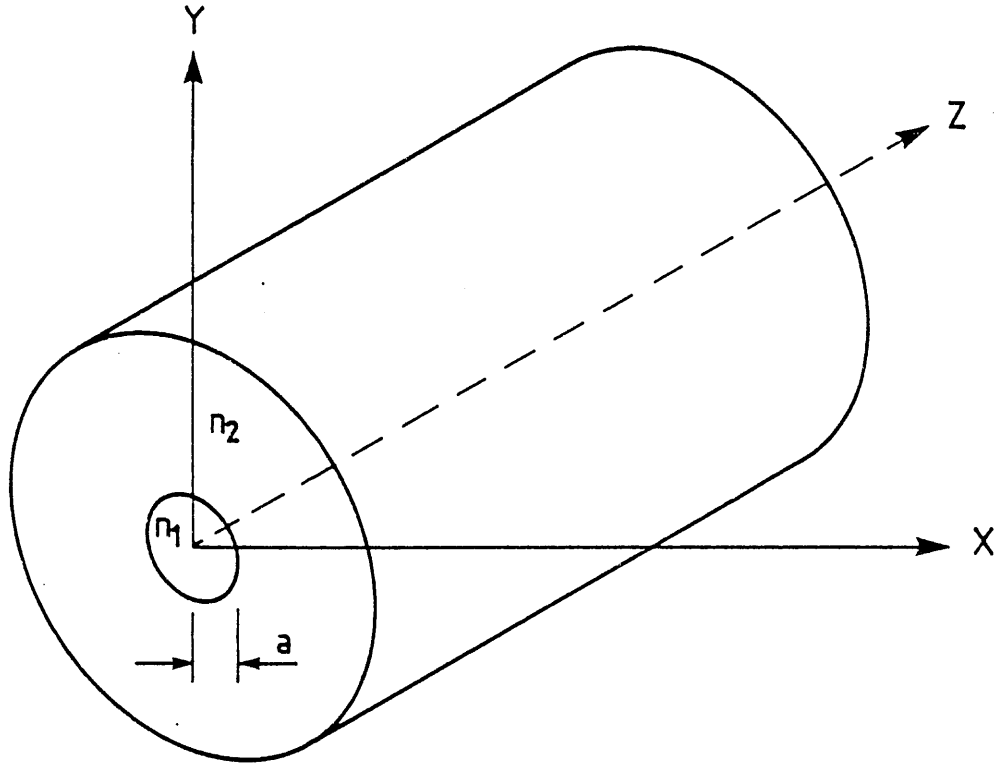

Figure 2.1: Cross-section of an optical fibre.

where

$\underline{E}$ is electric field strength.

$\underline{B}$ is the magnetic flux density.

$\underline{H}$ is the magnetic field strength.

$\underline{J}$ is the current density.

$\underline{D}$ is the electric displacement.

ρ is the charge density.

The electric displacement and magnetic flux density are related to electic field strength and magnetic field strength respectively by

$$\underline{D} = \epsilon_o \epsilon_r \underline{E} \qquad (2.1.4)$$

$$B = \mu_o \mu_r \underline{H} \qquad (2.1.5)$$

where,

ϵ_o and μ_o are the free space permittivity and permeability respectively.

ϵ_r and μ_r are the relative permittivity and permeability respectively.

For a charge free, non-magnetic and uniform isotropic media ie $\underline{J}= \rho =0$ and $\mu_r =1$, the Maxwell's equations become

$$\nabla \times \underline{E} = -\mu_o \frac{\partial \underline{H}}{\partial t} \qquad (2.1.6)$$

$$\nabla \times \underline{H} = \varepsilon_o \varepsilon_r \frac{\partial \underline{E}}{\partial t} \qquad (2.1.7)$$

$$\nabla . \underline{E} = 0 \qquad (2.1.8)$$

$$\nabla . \underline{H} = 0 \qquad (2.1.9)$$

Taking curl of equation(2.1.6) and, using (2.1.7) and (2.1.8) gives vector wave equation ie

$$\nabla^2 \underline{E} - \mu_o \varepsilon_r \varepsilon_o \frac{\partial^2 \underline{E}}{\partial t^2} = 0 \qquad (2.2.10)$$

Assuming the direction of propagation to be along the z-axis and the fields of the form

$$\begin{bmatrix} \underline{E} \\ \underline{H} \end{bmatrix} = \begin{bmatrix} \underline{\mathcal{E}} \\ \underline{\mathcal{H}} \end{bmatrix} e^{j(\omega t - \beta z)} \qquad (2.1.11)$$

where, β and ω are the propagation constant and the frequency of the wave respectively.

Transforming the wave equation (2.1.10) into cylinderical co-ordinate system, r, ϕ, and z, with z- along the waveguide, gives

$$\left[\frac{\partial^2}{\partial r^2} + \frac{1}{r}\frac{\partial}{\partial r} + \frac{1}{r^2}\frac{\partial^2}{\partial \phi^2}\right] \underline{\mathcal{E}} + \left[k^2 - \beta^2\right] \underline{\mathcal{E}} = 0 \qquad (2.1.12)$$

where

$$k^2 = \epsilon_r k_0^2 = \epsilon_r \epsilon_o \mu_o \omega^2 \qquad (2.1.13)$$

and k_0 is the free space propagation constant.

The solutions for the above wave equation can be obtained in terms of longitudnal field components. Trying a solution of the form

$$\begin{bmatrix} \mathcal{E}_z \\ \mathcal{H}_z \end{bmatrix} = \begin{bmatrix} A \\ B \end{bmatrix} F(r)\, e^{j\nu\phi} \qquad (2.1.14)$$

where, A and B are the amplitude coefficients.

Gives, scalar wave equation

$$\frac{\partial^2 F}{\partial r^2} + \frac{1}{r}\frac{\partial F}{\partial r} + (k^2 - \beta^2 - \frac{\nu^2}{r^2})F = 0 \qquad (2.1.15)$$

where

ν , can be positive or negative, however it must be an integer as otherwise fields will not be periodic in ϕ with period 2π.

The function F(r) has to be so chosen that it is finite at r=0 and tends to zero for $r \to \infty$. For r<a, the function can be taken to correspond to Bessel's function of the first kind, so that,

$$\begin{bmatrix} \mathcal{E}_z \\ \mathcal{H}_z \end{bmatrix} = \begin{bmatrix} A \\ B \end{bmatrix} J_\nu(U\frac{r}{a})\, e^{j\nu\phi} \qquad (2.1.16)$$

where

$$U = a(k_1^2 - \beta^2)^{\frac{1}{2}} \qquad (2.1.17)$$

$$k_1 = k_0 n_1$$

For r>a, the appropriate Bessel's function is the modified Hankel's function, hence

$$\begin{bmatrix} \mathcal{E}_z \\ \mathcal{H}_z \end{bmatrix} = \begin{bmatrix} C \\ D \end{bmatrix} K_\nu(W\frac{r}{a})\, e^{j\nu\phi} \qquad (2.1.18)$$

where
C and D are the amplitude coefficients.

$$W = a(\beta^2 - k_2^2)^{\frac{1}{2}} \qquad (2.1.19)$$

$$k_2 = k_0 n_2$$

The solution for propagation constant, β, can be obtained by ensuring continuity of the tangential field components at the core-cladding interface. This condition gives four homogenous equations with four unknown coefficients i.e. A, B, C, D. However if the determinant of the coefficients is equal to zero then a solution can be found for wave propagation in the waveguide. The determinant is the transcendental equation for the β ie

$$\left[\frac{J_\nu^1(U)}{UJ_\nu(U)} + \frac{K_\nu^1(W)}{WK_\nu(W)}\right]\left[\frac{k_1^2a^2}{U}\,\frac{J_\nu^1(U)}{J_\nu(U)} + \frac{k_2^2a^2}{W}\,\frac{K_\nu^1(W)}{K_\nu(W)}\right] = \nu^2\beta_\nu^2a^2\left[\frac{1}{U^2} + \frac{1}{W^2}\right] \qquad (2.1.20)$$

where, primed Bessel and Hankel functions are equal to their derivatives with respect to their argument.

The solution to the above equation exists for discerte values of β's corresponding to various modes that can propagate in the fibre. For $\nu = 0$, the modes that can propagate are Transverse Magnetic (TM), and Transverse Electric (TE). These modes are radially symmetric and for a given ν there exist μ roots such that $\beta_{\nu\mu} \geq k_2$, as the J-Bessel functions are oscillatory. For $\nu \geq 1$, the modes cannot be desiganated as pure TE or TM modes as they both have non-zero longitudnal field components. These modes are designated as $HE_{\nu\mu}$ or $EH_{\nu\mu}$ depending

upon whether they are more charcteristically like TM or TE modes.

The mode cut-off's can be obtained using equation (2.1.20) and the condition $W \longrightarrow 0$. It can be shown that

$$J_\nu(U_c) = 0 \begin{cases} HE_{1\mu} \\ EH_{\nu\mu} \end{cases} \qquad (2.1.21)$$

$$\left[\left(\frac{n_1}{n_2}\right)^2 + 1\right] J_{\nu-1}(U_c) = \frac{U_c}{\nu - 1} J_\nu(U_c) \quad \begin{cases} HE_{\nu\mu} \\ \nu = 2,3,4 \end{cases} \qquad (2.1.22)$$

$$J_o(U_c) = 0 \begin{cases} TE_{o\mu} \\ TM_{o\mu} \end{cases} \qquad (2.1.23)$$

For HE_{11} mode there does not exist a cut-off frequency. Hence, single mode fibres can be fabricated if all the modes other than the HE_{11} have their propagation constants beyond cut-off. In literature, V-value is used to give an estimate of the number of modes a guide can support. This is referred to as 'Normalised Frequency' and is given by

$$V^2 = k_o^2 a^2 (n_1^2 - n_2^2) = U^2 + W^2 \qquad (2.1.24)$$

Mode cut-off is defined by the condition, W=0. Hence, single mode operation is possible for

$$V \leq 2.405 \qquad (2.1.25)$$

where, 2.405 is the first root of $J_0(U_c) = 0$

The propragation characteristics of an optical fibre can be shown on a ω-β diagram. In figure 2.2, ω-β diagram for a low moded fibre is given. Here the core-cladding refractive index difference has been greatly exaggerated for clarity. The values of propagation constant for the various modes can be computed from the solution of the transcendental equation (2.1.20). A computer program was written to compute the propagation constants for the modes in an uniaxial

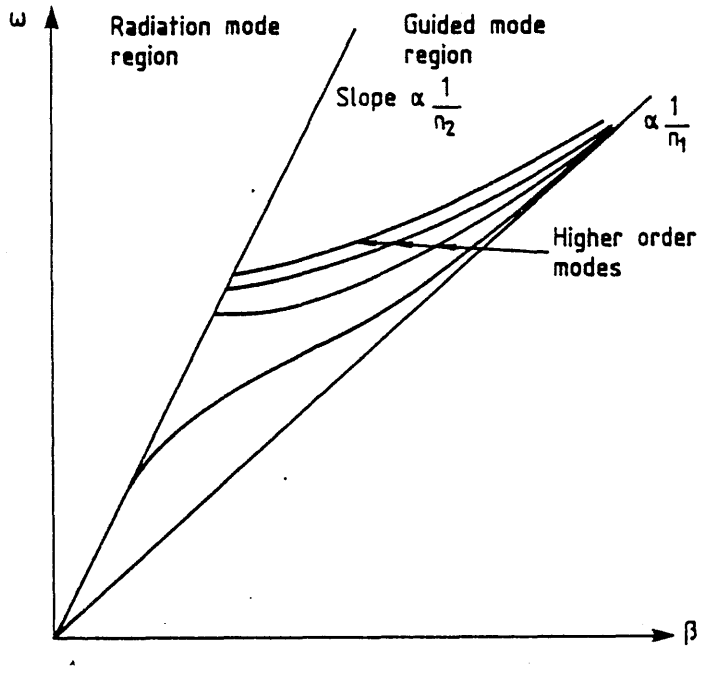

Figure 2.2: ω-β diagram for a low moded optical fibre.

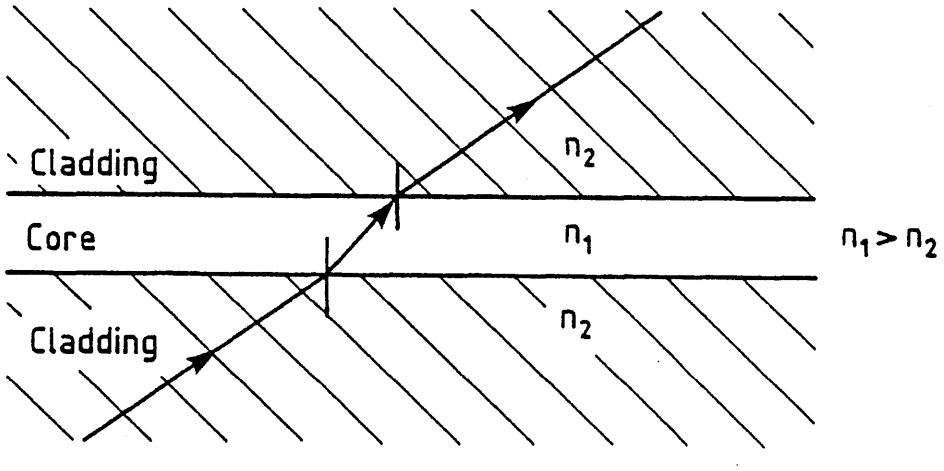

Figure 2.3: Radiation mode representation.

crystal cored fibre and this program can also be used, as described in Appendix 1, to determine propagation constants of modes of isotropic cored fibres.

The region given by $0 \leq \beta \leq k_2$ has been indicated in figure 2.2 as the radiation mode region. The radiation modes are also solutions of the wave equation for an optical fibre as they too satisfy the boundry conditions at the core-cladding interface. These modes are neither bound to the core and nor do they decay outside the core. They are equivalent to a ray incident at the core-cladding interface such that it exits into the cladding after refracting through the core, see figure 2.3. As there can be continuum of angles at which these rays can be incident at the core-cladding interface, β's of the radition field form a continuum. The field expressions for radiation modes have been derived by Marcuse (1974). The expressions for radiation modes in a weakly guiding are given in section 2.2. In addition to the propagating radiation modes described above there exist a continuum of evanescent modes having imaginary β's in the range $0 \leq \beta \leq j\infty$.

2.2 Weakly Guiding Fibre Approximations:

The optical fibres used for communications are weakly guiding structures as the refractive index difference between their core and cladding is very small. Typically 'Δ' is in the range 0.001 to 0.02, and is defined as

$$\Delta = 1 - \left(\frac{n_2}{n_1}\right)^2 \qquad (2.2.1)$$

Snyder (1969) and Gloge(1971) used this approximation to obtain linearly polarized transverse field components as solution of the wave equation. A consequence of this approximation is that it can be shown that the ratio of the magnitude of the longitudnal and transverse field components is of the order of $\Delta^{1/2}$. The transverse field components have been obtained in the above papers for a weakly guiding fibre and are discussed in a greater detail by Marcuse (1974). The transverse field components for one polarization are (Marcuse (1974))

For r<a

$$\mathcal{E}_y = A J_\nu(U \frac{r}{a}) \begin{Bmatrix}\cos \nu\phi \\ \sin \nu\phi\end{Bmatrix} \tag{2.2.2}$$

$$\mathcal{H}_x = - nA\left(\frac{\varepsilon_o}{\mu_o}\right)^{\frac{1}{2}} J_\nu(U\frac{r}{a}) \begin{Bmatrix}\cos \nu\phi \\ \sin \nu\phi\end{Bmatrix} \tag{2.2.3}$$

$$\mathcal{E}_x = 0 \tag{2.2.4}$$

$$\mathcal{H}_y = 0 \tag{2.2.5}$$

For r>a

$$\mathcal{E}_y = A \frac{J_\nu(U)}{K_\nu(W)} K_\nu(W\frac{r}{a}) \begin{Bmatrix}\cos \nu\phi \\ \sin \nu\phi\end{Bmatrix} \tag{2.2.6}$$

$$\mathcal{H}_x = -nA\left(\frac{\varepsilon_o}{\mu_o}\right)^{\frac{1}{2}} \frac{J_\nu(U)}{K_\nu(W)} K_\nu(W\frac{r}{a}) \begin{Bmatrix}\cos \nu\phi \\ \sin \nu\phi\end{Bmatrix}$$

$$\mathcal{E}_x = \mathcal{H}_y = 0 \tag{2.2.7}$$

where

The choice of Cos $\nu\phi$ and Sin $\nu\phi$ in the above expressions is arbitary as two degenerate sets of modes rotated at $\pi/2$ from each other can exist.

$\underline{\mathcal{H}}_t = \frac{1}{Z} \hat{e}_Z \times \underline{\mathcal{E}}_t$ has been assumed as $|\underline{\mathcal{E}}_z| < < |\underline{\mathcal{E}}_t|$ and Z is the wave impedence.

$n = (n_1 + n_2)/2.$

The amplitude coefficient 'A' can be evaluated in terms of the power carried by the modes using the following orthogonality relation

$$P = \frac{1}{2} \int_{-\infty}^{\infty} \int_{-\infty}^{\infty} \hat{e}_z.(\underline{\mathcal{E}}_t \times \underline{\mathcal{H}}_t^*)dxdy \tag{2.2.8}$$

Marcuse (1974) has shown that using the above orthogonality relation 'A' is given by

$$A = \left[\frac{4(\mu_o/\varepsilon_o)^{\frac{1}{2}} W^2 P}{e_\nu \pi a^2 V^2 |J_{\nu-1}(U) J_{\nu+1}(U)|}\right]^{\frac{1}{2}} \tag{2.2.9}$$

where,

$$e_\nu = \begin{cases} 2 \text{ for } \nu = 0 \\ 1 \text{ for } \nu \neq 0 \end{cases}$$

Note: P is the power normalization coefficient and is same for all the modes. The power carried by individual modes is found from their mode amplitudes ie power carried by ν^{th} mode is $P|A_\nu|^2$.

The transcendental equation for a weakly guiding fibre simplifies to

$$\frac{UJ_\nu(U)}{J_{\nu\pm1}(U)} = \pm \frac{WK_\nu(W)}{K_{\nu\pm1}(W)} \qquad (2.2.10)$$

Snyder (1971) has shown that the values of U_c evaluated using the above equation are accurate to within 1% for $\Delta \leq 0.2$ and less than 10% when $\Delta = 0.5$. Hence the above description of linearly polarized waves can be used with confidence for $\Delta < 0.5$. The mode solutions obtained from the above equation are characterized in the literature as $LP_{\nu\mu}$ modes. For $\nu > 0$, each $LP_{\nu\mu}$ mode consists of two $HE_{\nu+1,\mu}$ modes and two $EH_{\nu-1,\mu}$ modes which are doubly degenerate. The $\nu = 0$, modes corresponds to $HE_{1\mu}$ modes.

The description of radiation modes can also be simplified using the weakly guiding approximations. The radiation modes have fields which are transverse to their direction of propagation and as such they can have substaintial field component along the fibre axis. However, radiation modes having β slightly less than k_2 are very nearly transverse. The transverse field components for one polarization are (Marcuse (1974))

For $r < a$

$$\mathcal{E}_y = A' J_\nu(\sigma r) \begin{Bmatrix} \text{Cos } \nu\phi \\ \text{Sin } \nu\phi \end{Bmatrix} \qquad (2.2.11)$$

$$\mathcal{H}_x = -nA' \left(\frac{\varepsilon_o}{\mu_o}\right)^{\frac{1}{2}} J_\nu(\sigma r) \begin{Bmatrix} \text{Cos } \nu\phi \\ \text{Sin } \nu\phi \end{Bmatrix} \qquad (2.2.12)$$

$$\mathcal{E}_x = \mathcal{H}_y = 0 \qquad (2.2.13)$$

where

$$\sigma = (n_1^2 k_0^2 - \beta^2)^{\frac{1}{2}} \tag{2.2.14}$$

and A' is the amplitude coefficient.

For $r > a$

$$\mathcal{E}_y = B' \left[H_\nu^{(1)}(\rho r) + C' H_\nu^{(2)}(\rho r) \right] \begin{Bmatrix} \cos \nu\phi \\ \sin \nu\phi \end{Bmatrix} \tag{2.2.15}$$

$$\mathcal{H}_x = - nB' \left(\frac{\varepsilon_o}{\mu_o} \right)^{\frac{1}{2}} \left[H_\nu^{(1)}(\rho r) + C' H_\nu^{(2)}(\rho r) \right] \begin{Bmatrix} \cos \nu\phi \\ \sin \nu\phi \end{Bmatrix} \tag{2.2.16}$$

$$\mathcal{E}_x = \mathcal{H}_y = 0 \tag{2.2.17}$$

where

$$\rho = (n_2^2 k_o^2 - \beta^2)^{\frac{1}{2}} \tag{2.2.18}$$

B' and C' are the amplitude coefficients.
$H_\nu^{(1)}$ and $H_\nu^{(2)}$ are the Hankel functions of the first and second kind respectively and are related to the modified K-Bessel functions by

$$K_n(x) = \frac{\pi}{2} j^{(n+1)} H_n^{(1)}(jx) \tag{2.2.19}$$

$$K_n(x) = \frac{\pi}{2} (-j)^{(n+1)} H_n^{(2)}(-jx) \tag{2.2.20}$$

Marcuse (1974) has derived expressions for amplitude coefficients using the following orthogonality relation

$$\frac{1}{2} \int_{-\infty}^{\infty} \int_{-\infty}^{\infty} \hat{e}_z \cdot (\underline{\mathcal{E}}_t \times \underline{\mathcal{H}}_t^*) dxdy = P\delta(\rho - \rho') \tag{2.2.21}$$

where, $\delta(\rho-\rho')$ is the Dirac-Delta function and is infinite for $\rho=\rho'$.

The amplitude coefficient A' is given by(Marcuse(1974))

$$A' = \frac{(\mu_o/\varepsilon_o)^{\frac{1}{4}} \{8\rho P\}^{\frac{1}{2}}}{(e_\nu n)^{\frac{1}{2}} a\pi^{3/2} |\sigma J_{\nu-1}(\sigma a)H_\nu^{(1)}(\rho a) - \rho J_\nu(\sigma a)H_{\nu-1}^{(1)}(\rho a)|} \qquad (2.2.22)$$

where

$$e_\nu = \begin{cases} 2 \text{ for } \nu = 0 \\ 1 \text{ for } \nu \neq 0 \end{cases}$$

The amplitude coefficients B' and C' can be found in terms of A', Marcuse(1974).

2.3 Wave Propagation In Uniaxial Crystal Cored Fibres:

The propagation of modes in a uniaxial dielectric rod was first studied by Longaker and Roberts (1963), and Rosenbaum (1965). They considered propagation of only the low order modes as their study was dircted towards laser cavity design. Cozens (1976) has recently discussed wave propagation in anisotropic crystal cored fibres. Also, Rosenbaum and Kraus (1977) have considered wave propagation in weakly guiding uniaxially cored fibres. However their study was restricted to guides having small anisotropy ie $\frac{|n_e - n_o|}{n_o} \ll 1$.

The wave equation for uniaxial crystal cored fibre is given by

$$\nabla(\nabla.\underline{E}) - \nabla^2\underline{E} = -\mu_o\hat{\varepsilon}\frac{\partial^2\underline{E}}{\partial t^2} \qquad (2.3.1)$$

where

$\hat{\varepsilon}$ is the permittivity tensor and for the case of principal crystal direction parallel to the guide co-ordinate system is given by

$$\hat{\varepsilon} = \begin{vmatrix} \varepsilon_{xx} & 0 & 0 \\ 0 & \varepsilon_{yy} & 0 \\ 0 & 0 & \varepsilon_{zz} \end{vmatrix} \qquad (2.3.2)$$

An exact solution exists only when the extraordinary permittivity of the crystal is along the fibre axis ie $\epsilon_{xx}=\epsilon_{yy}=\epsilon_1\neq\epsilon_{zz}=\epsilon_z$.

Therefore in this case the extraordinary crystal index, n_z, is along the fibre axis while the ordinary index, n_1, is along the axes transverse to the direction of propagation. The solution of the wave equation can then be obtained in similar manner as in the case of isotropic cored fibre. The longitudnal field components can be taken as

For $r < a$

$$\mathcal{E}_z = AJ_\nu\left(U\left(\frac{n_z}{n_1}\right)\frac{r}{a}\right) e^{j\nu\phi} \tag{2.3.3}$$

$$\mathcal{H}_z = BJ_\nu\left(U\frac{r}{a}\right) e^{j\nu\phi} \tag{2.3.4}$$

For $r > a$

$$\mathcal{E}_z = CK_\nu\left(W\frac{r}{a}\right) e^{j\nu\phi} \tag{2.3.5}$$

$$\mathcal{H}_z = DK_\nu\left(W\frac{r}{a}\right) e^{j\nu\phi} \tag{2.3.6}$$

where

All the terms have same meaning as in the isotropic cored case.

Cozens(1976) has shown that the transcendental equation for this case is given by

$$\left[\frac{1}{U}\frac{J'_\nu(U)}{J_\nu(U)} + \frac{1}{W}\frac{K'_\nu(W)}{K_\nu(W)}\right]\left[\frac{k_1 k_z a^2}{U}\frac{J'_\nu\left(\frac{n_z}{n_1}U\right)}{J_\nu\left(\frac{n_z}{n_1}U\right)} + \frac{k_2^2 a^2}{W}\frac{K'_\nu(W)}{K_\nu(W)}\right] = \nu^2\beta_\nu^2 a^2\left[\frac{1}{U^2} + \frac{1}{W^2}\right] \tag{2.3.7}$$

The mode cut-off frequencies are obtained from the above transcendental equation with the condition $W \to 0$ and can be shown to be given by

For TE modes

$$f_{c,E} = \frac{2.405}{2\pi a\left[\mu_o\varepsilon_o(n_1^2 - n_2^2)\right]^{\frac{1}{2}}} \tag{2.3.8}$$

This is same as for isotropic cored fibre.

For TM modes

$$f_{c,m} = \frac{n_1}{n_z} f_{c,E} \qquad (2.3.9)$$

Hence, for $n_z > n_1$, single mode operation occurs at a frequency lower than that for the isotropic case.

For $\upsilon = 1$, the cut-off frequencies are given by

$$U_c = 0 \qquad (2.3.10)$$

$$J_1(U_c) = 0 \qquad (2.3.11)$$

$$J_1\left(\frac{n_z}{n_1} U_c\right) = 0 \qquad (2.3.12)$$

$U_c = 0$, implies zero cut-off frequency and this occurs for the HE_{11} mode. The cut-off frequencies of $EH_{\upsilon\mu}$ modes are given by the equation (2.3.11) and those for $HE_{1,\mu+1}$ modes where, $\mu=1,2,3,..,$ are given by the equation (2.3.12).

For $HE_{\upsilon\mu}$ modes with $\upsilon \geq 2$, cut-off frequencies can be obtained from the solution of the following equation.

$$\left\{\frac{n_1 n_z}{n_2^2} J_{\nu-1}\left(\frac{n_z}{n_1} U\right) J_\nu(U) + J_{\nu-1}(U)\, J_\nu\left(\frac{n_z}{n_1} U\right) - \frac{U}{(\nu - 1)} J_\nu(U) J_\nu\left(\frac{n_z}{n_1} U\right)\right\} = 0 \qquad (2.3.13)$$

The change in the cut-off values for the TM and HE modes of isotropic cored case, is to be expected as their longitudnal electric field component is greater than that of the TE and EH modes. A computer program was written to obtain the values of propagation constants of various modes. The computer listing along with the description of the computational method used is given in Appendix 1. A plot of normalised propagation constant, $\beta_n = \beta/k_o$, as a function of the product of free space propagation constant and the core radius, $k_o a$, was computed for HE_{11}, HE_{12} and HE_{21} modes of a negative uniaxial crystal cored fibre and is given in figure 2.4. These mode dispersion characteristics are very similar to those of isotropic cored fibres. In order to compare the difference in the normalised propagation constants of an uniaxial crystal cored fibre with that of

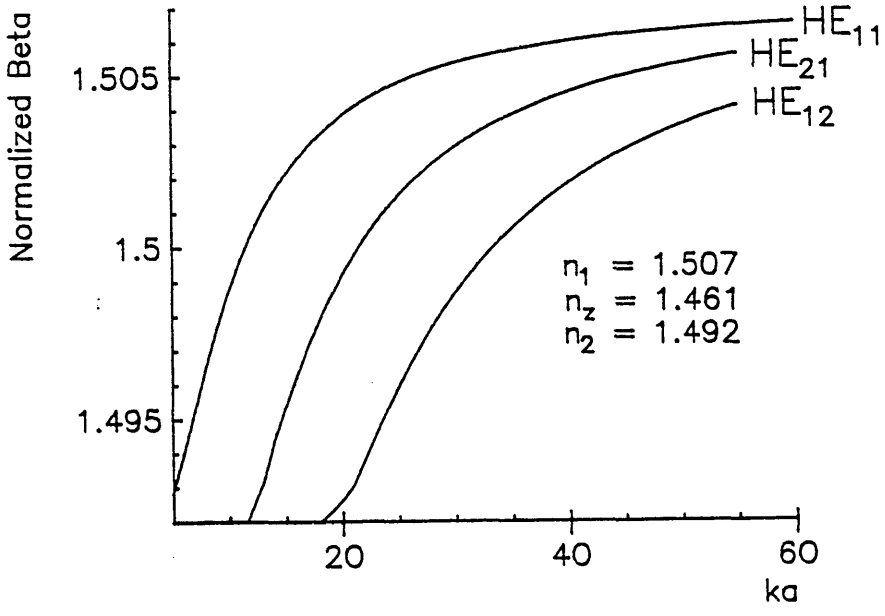

Figure 2.4: Plot of β_n as a function of $k_0 a$ for various modes of a negative uniaxial crystal cored fibre.

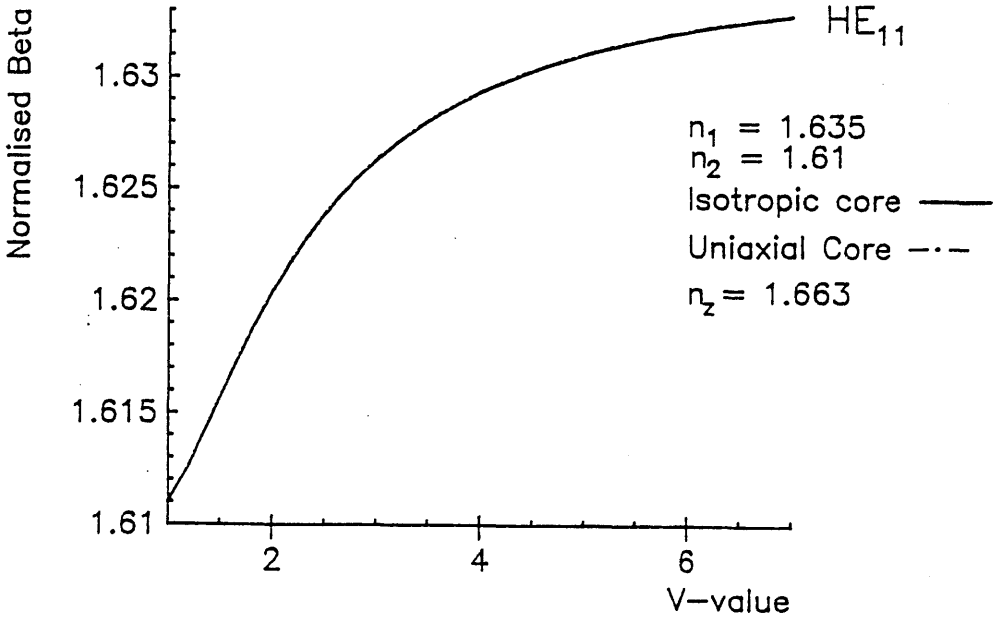

Figure 2.5: Plot of β_n of the HE_{11} mode as a function of the fibre V-value for 1. a benzil crystal cored fibre (—·—) and 2. an isotropic cored fibre, $n_z = n_1$, (———).

an isotropic cored fibre, values of β_n of the HE_{11} mode were computed as a function of fibre V-value for a benzil crystal cored fibre and an isotropic cored fibre having the same core refractive index as the ordinary refractive index of benzil. These have been plotted in figure 2.5. It can be seen that the values of β_n are virtually similar for both the fibres. The maximum percentage variation in β_n is 0.0047 at V = 2.1. However, it is more meaningful to evaluate the maximum percentage difference in β_n as a function of the core-cladding refractive index difference, δn, and this has a value of 0.3. This is also small as the extraordinary refractive index of benzil is greater than the ordinary refractive index by only about 1.7%. In order to consider larger differences in the transverse and longitudnal indices of the fibre, the propagation constants were computed for HE_{11} mode in fibres with longitudnal index greater and less than the transverse index by 10% and these have been plotted in figure 2.6. It can be seen that the normalised propagation constant has a value greater or less than that in an isotropic cored fibre depending upon whether the crystal core is a positive or a negative uniaxial material. The maximum percentage difference in β_n as a function of δn is 1.72. These results show, as expected, that small crystal birefringence is unlikely to significantly effect the propagation constants in a weakly guiding uniaxial crystal cored fibres as the fields are very nearly transverse. This also implies that for small crystal birefringence the transverse fields in a weakly guiding uniaxial crystal cored fibre will be very similar to those in an isotropic cored fibre.

2.4 Wave Propagation In Biaxial Crystal Cored Fibres:

In the case of biaxial cored fibres it is not possible to obtain an analytical solution of the wave equation. However, it is possible to obtain numerically the fields and propagation constants of various modes. Cozens (1976) has proposed a simple computational method for evaluation of the propagation constants. The biaxial guide is considered as a perturbed ideal guide (perturbation of dielectric constant) and hence the change in the propagation constant due to the perturbation can be evaluated using the coupled mode theory. Hence, the propagation constant of a mode of a biaxial cored fibre can be

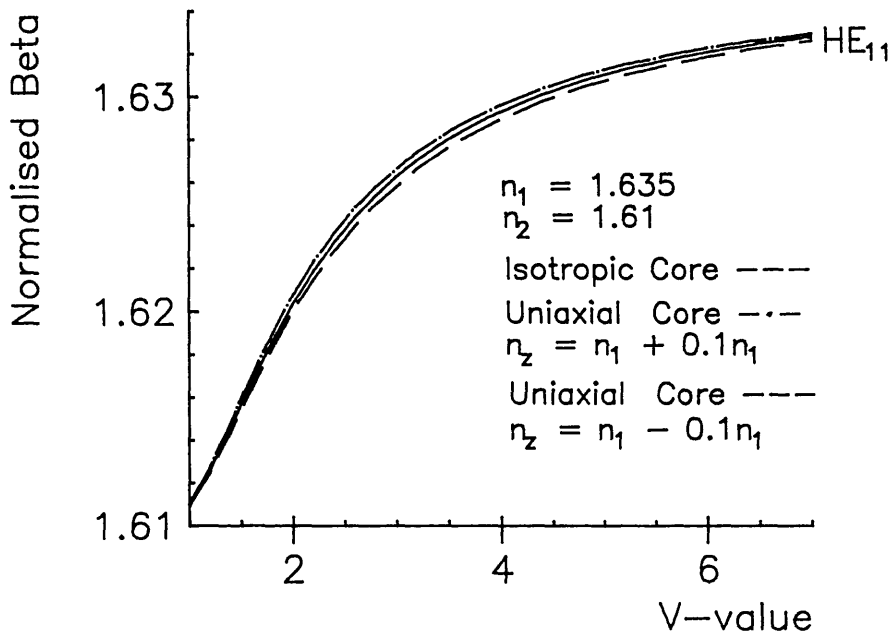

Figure 2.6: Plot of β_n of the HE_{11} mode as a function of the fibre V-value for 1. Isotropic core 2. positive uniaxial crystal core and 3. negative uniaxial crystal core.

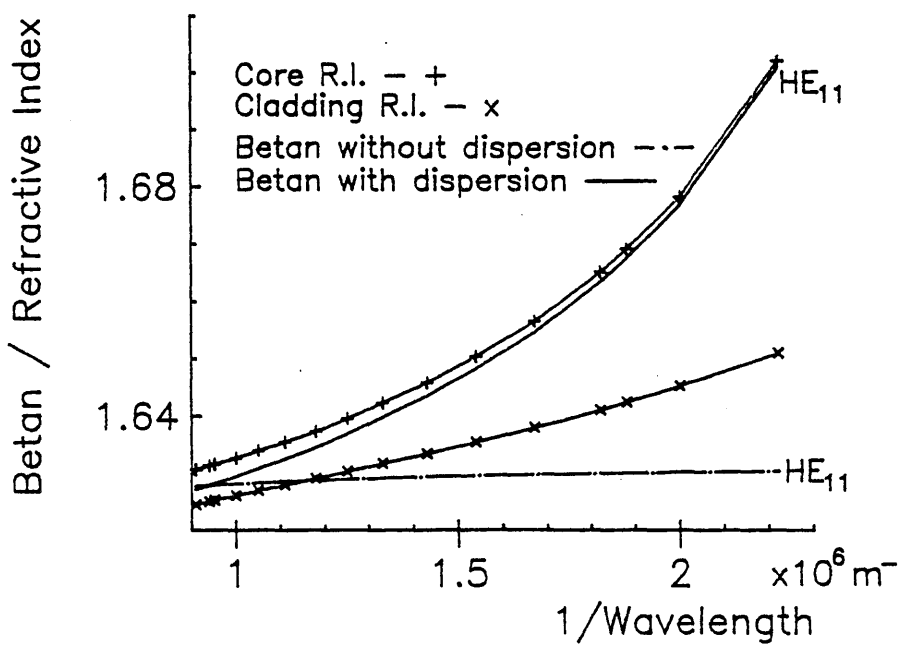

Figure 2.7: Plot of β_n of the HE_{11} mode in a benzil crystal cored fibre as a function of λ^{-1}; 1. computed using refractive index values of the core and cladding at each wavelength and 2. using the refractive index data at λ=1.064μm. Also plotted are the ordinary refractive index of benzil and the cladding refractive index.

given by

$$\beta_\nu' = \beta_\nu + \Delta\beta \qquad (2.4.1)$$

where

β_ν is the propagation constant of the ν^{th} mode of the ideal guide.

$$\Delta\beta = \frac{\omega}{P}\int_0^{2\pi}\int_0^{a}\Big[(\varepsilon_x-\varepsilon_1)\,\underline{\mathcal{E}}_{x\nu}\cdot\underline{\mathcal{E}}^*_{x\nu} + (\varepsilon_y-\varepsilon_1)\,\underline{\mathcal{E}}_{y\nu}\cdot\underline{\mathcal{E}}^*_{y\nu} + (\varepsilon_z-\varepsilon_1)\left(\frac{\varepsilon_1}{\varepsilon_z}\right)\underline{\mathcal{E}}_{z\nu}\cdot\underline{\mathcal{E}}^*_{z\nu}\Big]\,r\,dr\,d\phi \qquad (2.4.2)$$

here P is the power normalization factor and $\underline{\mathcal{E}}_{x\nu}$ etc. are the known fields of the ideal mode.

The above expression is valid provided $\Delta\beta << \beta_\nu$. A consequence of this requirement is that the above method is only applicable to biaxial crystal cored fibres with small crystal anisotropy. The accuracy of the above method can be improved by using the modes of a uniaxial cored fibre as the ideal modes of the perturbed guide.

2.5 Wave Propagation In Uniaxial Cored Fibres With Crystal Axis Not Along The Direction Of Propagation:

It was observed in some of the benzil crystal cored fibres that the crystal c-axis was not along the fibre axis. The deviations were generally small i.e. < 5°, however in some extreme cases deviations as large as 10° were also observed (Chapter 5). If the crystal c-axis makes an angle 'α' to the direction of propagation i.e. z-axis, the permittivity tensor in the wave equation is then given by

$$\hat{\varepsilon} = \tilde{T}\,\hat{\varepsilon}'\,T \qquad (2.5.1)$$

where

T is the transformation matrix and for this case becomes

$$T = \begin{pmatrix} 1 & 0 & 0 \\ 0 & \cos\alpha & \sin\alpha \\ 0 & -\sin\alpha & \cos\alpha \end{pmatrix} \qquad (2.5.2)$$

$\tilde{T}$ is the transpose of T.

$\hat{\epsilon}'$ is the permittivity tensor of uniaxial crystal in its principal co-ordinate system.

$$\therefore \hat{\epsilon} = \begin{pmatrix} \epsilon_{xx} & 0 & 0 \\ 0 & \epsilon_{yy} & \epsilon_{yz} \\ 0 & \epsilon_{zy} & \epsilon_{zz} \end{pmatrix} \qquad (2.5.3)$$

and the matrix elements are

$$\epsilon_{xx} = \epsilon_1 = \epsilon_0 n_o^2$$

$$\epsilon_{yy} = \epsilon_1 \text{Cos}^2\alpha + \epsilon_z \text{Sin}^2\alpha = \epsilon_0(n_o^2\text{Cos}^2\alpha + n_e^2\text{Sin}^2\alpha)$$

$$\epsilon_{zy} = \epsilon_{yz} = \frac{1}{2}(\epsilon_1 - \epsilon_z)\text{Sin}2\alpha = \frac{1}{2}\epsilon_0(n_o^2 - n_e^2)\text{Sin}2\alpha$$

$$\epsilon_{zz} = \epsilon_z \text{Cos}^2\alpha + \epsilon_1 \text{Sin}^2\alpha = \epsilon_0(n_e^2\text{Cos}^2\alpha + n_o^2\text{Sin}^2\alpha)$$

The wave equation in this case also has to be numerically solved as no analytical solution exists. For crystal cored fibres where the deviation of the crystal axis from the fibre axis is not large , the propagation constant can be calculated using the perturbation method discussed in the previous section. In this case ideal modes of the perturbed guide will be those of an uniaxial guide with its crystal axis along the fibre axis. Hence, the change in the propagation constant, $\Delta\beta$, from that of the ideal modes is given by

$$\Delta\beta = \frac{\omega}{P}\int_0^{2\pi}\int_0^{a}\left[(\epsilon_{y'} - \epsilon_1)\ \underline{\mathcal{E}}_{y\nu} \cdot \underline{\mathcal{E}}^*_{y\nu} + (\epsilon_{z'} - \epsilon_z)\left(\frac{\epsilon_z}{\epsilon_{z'}}\right)\right.$$

$$\left.\underline{\mathcal{E}}_{z\nu} \cdot \underline{\mathcal{E}}^*_{z\nu}\right] r\,dr\,d\phi \qquad (2.5.4)$$

where

$\epsilon_{y'}$ and $\epsilon_{z'}$ are components of permittivity of the crystal along the fibre y- and z-axis.

2.6 Wave Propagation In Fibres With Dispersive Core:

The majority of organic crystals with large second order susceptibilities also have strong absorption in the near UV region of the spectrum and as a result the dispersion between the fundamental and SH wavelengths is generally large. Therefore it is necessary to also take dispersion into account when determining the phase matching requirements for non-linear interactions in crystal cored fibres. The effect of dispersion can be incorporated in the computer program, used to evaluate fibre propagation constants, by using Sellimer's formulae to compute the core and cladding refractive indices at the appropriate wavelengths. In figure 2.7, normalised propagation constant of the HE_{11} mode in a benzil crystal cored fibre has been plotted along with variation of core and cladding refractive indices with the wavelength. Also included is a plot of normalised propagation constant of the HE_{11} mode computed in absence of dispersion and with core and cladding refractive index values at 1.064μm wavelength. It can be seen from the above plots that in crystal cored fibres it is necessary to take into account core and cladding dispersion as otherwise errors in evaluation of propagation constants of the modes can be very large. This curve also shows that for fundamental wavelength of 1.064μm the SH will be in the radiation field.

CHAPTER 3

Theoretical Analysis Of Optical Second Harmonic Generation In Crystal Cored Fibres

3.0 Introduction:

Optical fibres are attractive for non-linear interactions as it is possible to draw long lengths of fibre having constant normalised frequency. Stolen et al(1974) were first to demonstrate phase matched four wave mixing in optical fibres. These days fibres are used to realise fibre Raman laser in the 1.06μm to 1.7μm wavelength range, generation of short pulses using pulse compression in fibres and in the study of soliton propagation for communication applications. These effects occur due to the third order non-linear susceptibilty of fused silica and self-focussing effect. Optical fibres cannot however be used for optical SHG or parametric amplification as the second order non-linear susceptibility in silica and glass is zero. The crystal cored fibres unlike optical fibres have a non-centrosymmetric core material and can be used for three wave mixing processes.

In this chapter principles of phase matched SHG in crystal cored fibres are presented and expressions for SH power generated are derived using coupled mode analysis. The analysis presented in this chapter could also be used for the study of other three wave interactions.

3.1 Qualitative Description Of SHG In Crystal Cored Fibres:

A high intensity field in the core of a crystal cored fibre generates a non-linear polarization wave which then gives rise to a SH light wave in a same way as in a bulk crystal. There is however no appericiable build up of the SH power if the fundamental and SH modes are not phase matched. The phase matching between these two modes can be achieved using waveguide dispersion as discussed in chapter 1. In crystal cored fibres it is possible to implement phase matching, as

in planar and stripe waveguiding structures, by either of the following two methods:

1. Coupling the fundamental mode into a SH guided mode.
2. Coupling the fundamental mode into the SH radiation field.

In both the above methods for SHG it is desirable to have monomode operation at the fundamental frequency so that all the launched power is avialable for SHG. This is because the launched power in a multimode fibre is distributed among all the modes which are supported by the fibre and consequently power in any one mode is small. Also, in multimode fibres, the power in the modes varies continously as even small perturbations can cause mode coupling. These two methods are discussed below in a greater detail.

3.1.1 Coupling the fundamental mode into a SH guided mode:

This method of phase matching is preferable as it is more efficient of the above two methods(see section 3.2). The phase matching condition for optical SHG is $\beta^{2\omega} = 2\beta^{\omega}$, where β^{ω} and $\beta^{2\omega}$ are the propagation constants of the fundamental and the SH modes respectively. The SH guided mode into which the coupling can take place is determined by the solution of the fibre's eigenvalue equation ie equation (2.3.7). The waveguide dispersion characteristic for the HE_{11} mode does not allow phase matching between the fundamental and the SH HE_{11} modes and as a result the fundamental mode has to be phase matched to a higher order SH mode. This form of phase-matching is shown on a ω-β diagram in figure 3.1. Here the core-cladding refractive index difference has been exaggerated to show the principle of phase matching. It is also necessary, as discussed in chapter 1, to ensure that the field overlap integral is non-zero for coupling to take place. The field overlap integral for SHG in crystal cored fibres is given in Appendix 2. It is non-zero for coupling the fundamental HE_{11} mode into SH $HE_{1\mu}$ modes and has a maximum value for coupling into the SH HE_{11} mode. In practice, as the phase matching requirement is not necessarily satisfied for a given waveguide dispersion it is difficult to implement this form of phase matching. In some cases it should be possible to use temperature dependent change in refractive index to optimise the

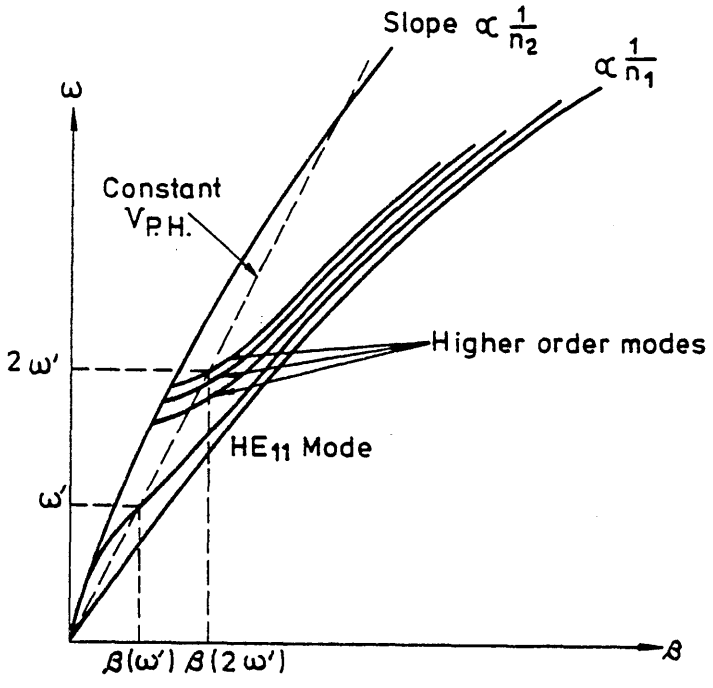

Figure 3.1: ω-β diagram showing phase-matching scheme for guided wave optical SHG.

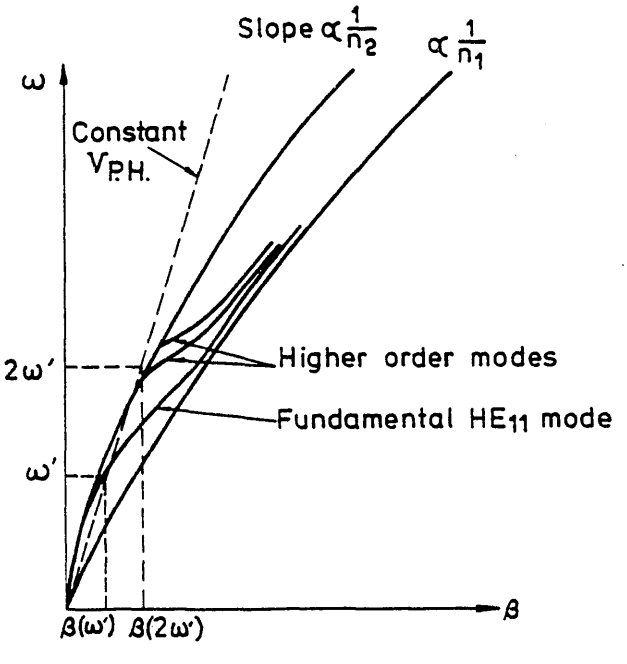

Figure 3.2: ω-β diagram showing phase-matching scheme for optical SHG in the radiation field.

waveguide dispersion to achieve phase matching.

3.1.2 Coupling the fundamental guided mode into the SH radiation field:

This form of phase matching is possible only if the fibre core and cladding materials are dispersive. As this is generally the case it is relatively easy to implement. In this case it is only necessary to arrange that the propagation constant of the SH light wave, $\beta^{2\omega}$, lies in the continuum of radiation field ie $\beta^{2\omega} < n_2^{2\omega} k_0^{2\omega}$. This form of phase matching has been shown on a ω-β diagram in figure 3.2. As for phase matching $\beta^{2\omega} = 2\beta^{\omega}$, where β^{ω} is the propagation constant of the fundamental HE_{11} mode, the condition necessary to couple the SH into the radiation field becomes

$$\beta^{\omega}/k_0^{\omega} < n_2^{2\omega} \qquad (3.1.1)$$

Therfore the chromatic dispersion δn, where $\delta n = n_2^{2\omega} - n_2^{\omega}$, required in the cladding glass is given by

$$\delta n > [\beta^{\omega}/k_0^{\omega} - n_2^{\omega}] \qquad (3.1.2)$$

It is also necessary to ensure that $n_1^{2\omega} > n_2^{2\omega}$. The precise value of chromatic dispersion required is dependent on the fibre V-value, at the fundamental frequency, but it will always be less than the core cladding refractive index, Δn, at the fundamental frequency. As in weakly guiding fibres $\Delta n << 0.2$, the chromatic dispersion required can be obtained by using commercially avialable glasses. The SH radiation in this case will exit from the fibre core at an angle, α, given by

$$\text{Cos}\alpha = \beta^{2\omega}/(k_0^{2\omega} n_2^{2\omega}) \qquad (3.1.3)$$

For values of $\beta^{2\omega}$ slightly less than $k_0^{2\omega} n_2^{2\omega}$, the angle α is of the order of few degrees and therefore the SH will be guided in the cladding.

3.2 Analysis Of SHG In Crystal Cored Fibres:

The process of optical SHG in crystal cored fibres can be treated as a coupled mode interaction in which the second order susceptibility of the fibre core acts as the perturbation resulting in the fundamental power to couple into the SH wave. Here it is assumed that the fibre core is uniaxial with its crystal axis along the fibre axis and the SH is generated from a input fibre mode at the fundamental frequency $\omega/2$ by coupling to a guided mode or radiation field at frequency ω. The coupled wave equations in this case can be derived using Maxwell's equations. For a charge free and non-magnetic region these are

$$\nabla \times \underline{E} = -\frac{\partial \underline{B}}{\partial t} \qquad (3.2.1)$$

$$\nabla \times \underline{H} = \frac{\partial \underline{D}}{\partial t} \qquad (3.2.2)$$

where

$$\underline{B} = \mu_0 \underline{H} \qquad (3.2.3)$$

$$\underline{D} = \epsilon_0 \underline{E} + \underline{P} \qquad (3.2.4)$$

For optical SHG, the polarization term, $\underline{P}$, consists of both the linear and non-linear components ie

$$\underline{P} = \underline{P}_L + \underline{P}_{NL} = \epsilon_o \chi_L^{(1)} \underline{E} + \underline{P}_{NL} \qquad (3.2.5)$$

However as the permittivity, ϵ, of the medium is related to its linear susceptibility by

$$\hat{\epsilon} = \epsilon_o(\hat{1} + \hat{\chi}_L^{(1)}) \qquad (3.2.6)$$

The electric displacement vector becomes

$$\underline{D} = \hat{\epsilon}\underline{E} + \underline{P}_{NL} \qquad (3.2.7)$$

The equations (3.2.1) and (3.2.2) can then be written as

$$\nabla \times \underline{E} = -\mu_o \frac{\partial \underline{H}}{\partial t} \qquad (3.2.8)$$

$$\nabla \times \underline{H} = \hat{\epsilon} \frac{\partial \underline{E}}{\partial t} + \frac{\partial \underline{P}_{NL}}{\partial t} \qquad (3.2.9)$$

where, permittivity tensor is given by

$$\hat{\varepsilon} = \begin{vmatrix} \varepsilon_1 & o & o \\ o & \varepsilon_1 & o \\ o & o & \varepsilon_z \end{vmatrix} \qquad (3.2.10)$$

Taking curl of equation (3.2.8) gives the vector wave equation

$$\nabla(\nabla.\underline{E}) - \nabla^2\underline{E} = -\mu_o \frac{\partial}{\partial t}(\nabla X\underline{H}) \qquad (3.2.11)$$

In the subsequent analysis it is assumed that the crystal cored fibre is weakly guiding ie $\Delta << 1$. In practice this can easily be arranged by selecting a suitable cladding glass for a given core material. For a weakly guiding fibre, as was discussed in chapter 2, field components of the guided modes can be taken to be very nearly transverse. The same also holds for the radiation modes having β values slightly less than $n_2 k_0$, the region of interest for SHG. This assumption is not however valid for $|\beta|$ values much less than $n_2 k_0$. Also, in the subsequent analysis longitudnal component of the non-linear polarization wave has been neglected and in general this may not be justifiable.

The transverse wave equation for the fibre can then be shown using equation (3.2.11) to be given by

$$\nabla_t \left(\nabla_t.\underline{E}_t + \frac{\partial E_z}{\partial z}\right) - \left(\nabla_t^2 + \frac{\partial^2}{\partial z^2}\right) \underline{E}_t = -\mu_o \frac{\partial}{\partial t} (\nabla x\underline{H})_t \qquad (3.2.12)$$

For a charge free region

$$\nabla.\underline{D} = \nabla.(\hat{\varepsilon}\underline{E}) = 0 \qquad (3.2.13)$$

ie

$$\frac{\partial \underline{E}_z}{\partial z} = -\frac{\varepsilon_1}{\varepsilon_z}(\nabla_t.\underline{E}_t) \qquad (3.2.14)$$

and as

$$(\nabla X\underline{H})_t = \varepsilon_1 \frac{\partial}{\partial t} \underline{E}_t + \frac{\partial}{\partial t} \underline{P}_{NLt} \qquad (3.2.15)$$

The transverse wave equation can be re-written as

$$\left(\nabla_t^2 + \frac{\partial^2}{\partial z^2} - \mu_o \varepsilon_1 \frac{\partial^2}{\partial t^2}\right) \underline{E}_t - \nabla_t (\nabla_t . \underline{E}_t) \left(1 - \frac{\varepsilon_1}{\varepsilon_z}\right) = \mu_o \frac{\partial^2}{\partial t^2} \underline{P}_{NLt} \quad (3.2.16)$$

The non-linear polarization can be regarded as a form of perturbation i.e. non-linear guide can be considered as a perturbation of an ideal guide. The wave equation for an unperturbed guide ie $\underline{P}_{NL} = 0$, is

$$\left(\nabla_t^2 + \frac{\partial^2}{\partial z^2} - \mu_o \varepsilon_1 \frac{\partial^2}{\partial t^2}\right) \underline{E}_t - \nabla_t (\nabla_t . \underline{E}_t) \left(1 - \frac{\varepsilon_1}{\varepsilon_z}\right) = 0 \quad (3.2.17)$$

An unpertubed uniaxial cored fibre will support a discrete number of guided modes and a continuum of radiation modes. The radiation modes have propagation constant, β, which lies in the range $-k_2 \leq \beta \leq k_2$, where, $k_2 = n_2 k_0$. Also there are evanescent modes with a continous spectrum of imaginary values in the range $-j\infty < \beta < j\infty$ and the complete set of radiation modes are described by parameter, ρ, where

$$\rho = (k_2^2 - \beta^2)^{1/2} \quad (3.2.18)$$

and it lies in the range $0 \leq \rho < \infty$.

The transverse field distribution of the perturbed guide supporting N guided modes and a continuum of radiation modes can be expressed by the expansion

$$\underline{E}_t = \sum_{\mu=1}^{N} a_\mu (z) \underline{\mathcal{E}}_{\mu t} e^{j(\omega t - \beta_\mu z)} + \sum \int_0^\infty a_\rho (z,\rho) \underline{\mathcal{E}}_{\rho\tau} e^{j(\omega t - \beta z)} d\rho \quad (3.2.19)$$

The summation in front of the integral indicates summation over all types of radiation modes. However, for SHG the radiation modes of interest are only those with $\beta \approx n_2 k_0$. The expansion coefficients are taken to be only z-dependent while the fields have been assumed to be of the form $e^{j(\omega t - \beta z)}$. The field distribution terms in the expansion are same as those given in chapter 2 for the fibre modes. Substituting (3.2.19) into (3.2.16) gives

$$\sum_{\mu}\left\{ a_\mu\left[(\nabla_t^2+(k_1^2-\beta_\mu^2))\underline{\mathcal{E}}_{\mu t}\, e^{j(\omega t-\beta_\mu z)} - \nabla_t\left(\nabla_t.\underline{\mathcal{E}}_{\mu t}\, e^{j(\omega t-\beta_\mu z)}\right)\left(1-\frac{\varepsilon_1}{\varepsilon_z}\right)\right]\right.$$
$$\left. +\left[\frac{d^2a_\mu}{dz^2}-2j\beta_\mu\frac{da_\mu}{dz}\right]\underline{\mathcal{E}}_{\mu t}\, e^{j(\omega t-\beta_\mu z)}\right\}$$
$$+\sum\left\{\int_0^\infty a_\rho\, d\rho\left[(\nabla_t^2+(k_1^2-\beta^2))\,\underline{\mathcal{E}}_{\rho t}\, e^{j(\omega t-\beta z)} - \nabla_t\left(\nabla_t.\underline{\mathcal{E}}_{\rho t}\, e^{j(\omega t-\beta z)}\right)\left(1-\frac{\varepsilon_1}{\varepsilon_z}\right)\right]\right.$$
$$\left. +\int_0^\infty\left[\frac{d^2a_\rho}{dz^2}-2j\beta\frac{da_\rho}{dz}\right]\underline{\mathcal{E}}_{\rho t}\, e^{j(\omega t-\beta z)}\, d\rho\right\} = \mu_o\frac{\partial^2\underline{P}_{NLt}}{\partial t^2} \qquad (3.2.20)$$

where, $k_1 = \omega\sqrt{\mu_o\epsilon_1} = n_1 k_0$ (3.2.21)

In an unperturbed guide, each discrete guided mode satisfies

$$[\nabla_t^2+(k_1^2-\beta_\mu^2)]\;\underline{\mathcal{E}}_{\mu t}\, e^{j(\omega t-\beta_\mu z)} - \nabla_t(\nabla_t.\underline{\mathcal{E}}_{\mu t}\, e^{j(\omega t-\beta_\mu z)})\;(1-\frac{\varepsilon_1}{\varepsilon_z})=0 \qquad (3.2.22)$$

and the radiation modes satisfy

$$[\nabla_t^2+(k_1^2-\beta^2)]\;\underline{\mathcal{E}}_{\rho t}\, e^{j(\omega t-\beta z)} - \nabla_t\,(\nabla_t.\underline{\mathcal{E}}_{\rho t}\, e^{j(\omega t-\beta z)})\;(1-\frac{\varepsilon_1}{\varepsilon_z})=0 \qquad (3.2.23)$$

Using (3.2.22) and (3.2.23), equation (3.2.20) becomes

$$\sum_{\mu}\left[\frac{d^2a_\mu}{dz^2}-2j\beta_\mu\frac{da_\mu}{dz}\right]\underline{\mathcal{E}}_{\mu t}\, e^{j(\omega t-\beta_\mu z)}$$
$$+\sum\int_0^\infty\left[\frac{d^2a_\rho}{dz}-2j\beta\frac{da_\rho}{dz}\right]\underline{\mathcal{E}}_{\rho t}\, e^{j(\omega t-\beta z)}d\rho = \mu_o\frac{\partial^2\underline{P}_{NLt}}{\partial t^2} \qquad (3.2.24)$$

The discrete guided modes satisfy the following orthogonality relationship

$$\tfrac{1}{2}\int_{-\infty}^{\infty}\int_{-\infty}^{\infty}\underline{e}_z.\;(\underline{\mathcal{E}}_{nt}\times\underline{\mathcal{H}}^*_{mt})\,dxdy = P \text{ for } m=n$$
$$= 0 \text{ otherwise} \qquad (3.2.25)$$

This is the fimilar Poynting vector used for the calculation of power in an e-m wave and was also used to calculate fibre mode amplitudes in chapter 2.

The radiation modes satisfy the following orthogonality relationship,

$$\tfrac{1}{2}\int_{-\infty}^{\infty}\int_{-\infty}^{\infty} \underline{e}_z \cdot \left(\underline{\mathcal{E}}_{\rho t} \times \underline{\mathcal{H}}^*_{\rho t}\right) dxdy = P\delta(\rho-\rho^1) \qquad (3.2.26)$$

Where, $\delta(\rho-\rho')$ is the Dirac-Delta function. According to this relation the integral becomes infinitly large if the modes are identical and zero if they are different. This was also used to calculate the mode amplitudes of the radiation modes.

Taking the cross product of both sides of the equation (3.2.24) with $\underline{\mathcal{H}}^*_{\mu t}$ and then taking scalar product with a unit vector in z-direction, gives after integration over guide cross-section and using the orthogonality relation in equation (3.2.25)

$$\left[\frac{d^2a_\mu}{dz^2} - 2j\beta_\mu \frac{da_\mu}{dz}\right] e^{j(\omega t-\beta_\mu z)} = \frac{\mu_o}{2P} \frac{\partial^2}{\partial t^2}\int_{-\infty}^{\infty}\int_{-\infty}^{\infty} \underline{e}_z \cdot (\underline{P}_{NLt} \times \underline{\mathcal{H}}^*_{\mu t})dxdy \qquad (3.2.27)$$

If the mode amplitude a_μ changes only slowly in a distance of a wavelength, then its second derivative can be neglected ie for slow variations, $|d^2a_\mu/dz^2| << \beta_\mu |da_\mu/dz|$. The equation (3.2.27) then becomes

$$\frac{da_\mu}{dz} e^{j(\omega t-\beta_\mu z)} = \frac{-\mu_o}{4j\beta_\mu P} \frac{\partial^2}{\partial t^2}\int_{-\infty}^{\infty}\int_{-\infty}^{\infty} e_z \cdot (\underline{P}_{NLt} \times \underline{\mathcal{H}}^*_{\mu t})\, dxdy \qquad (3.2.28)$$

Integrand on the R.H.S. after simplification is given by

$$\frac{\beta}{\omega\mu_o} \underline{P}_{NLt} \cdot \left[\underline{\mathcal{E}}^*_{\mu t} - \frac{j}{\beta_\mu} \nabla_t \underline{\mathcal{E}}^*_{\mu z}\right]$$

Now $\frac{1}{\beta_\mu}\frac{\partial \underline{\mathcal{E}}^*_{\mu z}}{\partial x}$ and $\frac{1}{\beta_\mu}\frac{\partial \underline{\mathcal{E}}^*_{\mu z}}{\partial y}$ are of the order of $\frac{\underline{\mathcal{E}}^*_{\mu z}}{\beta_\mu a}$ and as β_μ a is of the order of unity for optical fibres $\frac{\underline{\mathcal{E}}^*_{\mu z}}{\beta_\mu a}$ will be approximately equal to $\underline{\mathcal{E}}^*_{\mu z}$. Also, as in weakly guiding fibres $|\underline{\mathcal{E}}_z| << |\underline{\mathcal{E}}_t|$, it is reasonable to assume that $\frac{1}{\beta_\mu} \nabla_t \underline{\mathcal{E}}^*_{\mu z} << \underline{\mathcal{E}}^*_{\mu t}$. Hence equation (3.2.28) can be written as

$$\frac{da_\mu}{dz} e^{j(\omega t-\beta_\mu z)} = \frac{-1}{4j\omega P} \frac{\partial^2}{\partial t^2} \int_{-\infty}^{\infty}\int_{-\infty}^{\infty} \underline{P}_{NLt} \cdot \underline{\mathcal{E}}^*_{\mu t}\, dxdy \qquad (3.2.29)$$

The orthogonality relation (3.2.26) can be used in the case of radiation modes to similarly give

$$\frac{da_\rho}{dz} e^{j(\omega t-\beta z)} = \frac{-1}{4j\omega P} \frac{\partial^2}{\partial t^2} \int_{-\infty}^{\infty}\int_{-\infty}^{\infty} \underline{P}_{NLt} \cdot \underline{\mathcal{E}}^*_{\rho t}\, dxdy \qquad (3.2.30)$$

For SHG non-linear polarization is given by (chapter 1)

$$\underline{P}_{NL} = \underline{P}^{(\omega)} = \varepsilon_o d_{ijk} : E_j^{(\omega/2)} E_k^{(\omega/2)} e^{j\omega t} \qquad (3.2.31)$$

In the above expression for non-linear polarization, the fields are transverse. For single mode propagation at the fundamental frequency we have $E_j = E_k = E_t$. Here for the sake of generality we assume that all the power at the fundamental frequency is in the ν^{th} guided mode and having transverse field distribution given by

$$\underline{E}_{\nu t} = a_\nu^{(\omega/2)}(z)\, \underline{\mathcal{E}}_{\nu t}^{(\omega/2)} e^{j((\omega/2)t-\beta_\nu z)} \qquad (3.2.32)$$

Using (3.2.31) and (3.2.32), equations (3.2.29) and (3.2.30) can be written as

For guided mode SHG

$$\frac{da_\mu^{(\omega)}}{dz} = \frac{\omega\varepsilon_o d_{im}}{4jP} \left[a_\nu^{(\omega/2)}(z)\right]^2 e^{j\Delta\beta z} \int_{-\infty}^{\infty}\int_{-\infty}^{\infty} \underline{\mathcal{E}}_{\nu t}^{(\omega/2)^2} \cdot \underline{\mathcal{E}}_{\mu t}^{(\omega)*} dxdy \qquad (3.2.33)$$

For SHG in radiation field

$$\frac{da_\rho^{(\omega)}}{dz} = \frac{\omega\varepsilon_o d_{im}}{4jP} \left[a_\nu^{(\omega/2)}(z)\right]^2 e^{j\Delta\beta z} \int_{-\infty}^{\infty}\int_{-\infty}^{\infty} \underline{\mathcal{E}}_{\nu t}^{(\omega/2)^2} \cdot \underline{\mathcal{E}}_{\rho t}^{(\omega)*} dxdy \qquad (3.2.34)$$

where

$$\Delta\beta = \beta_\mu^{(\omega)} - 2\beta_{\nu,\rho}^{(\omega/2)} \qquad (3.2.35)$$

and d_{im} is the pertinent SH tensor element.

In equations (3.2.33) and (3.2.34) the integral on the R.H.S. represents transverse overlap integral. It specifies the modes among which the coupling can take place and also determines the strength of coupling. It can be evaluated by substitution of field expressions, given in chapter 2, for guided modes and radiation field followed by integration over the core crossection. In appendix 2 its evaluation and significance is discussed in greater detail. In the subsequent analysis this integral will be designated as I_g and I_r corresponding to equations (3.2.33) and (3.2.34) respectively. Assuming weak coupling ie $a^{\omega/2}$ remains constant over the interaction length, L, the SH guided mode amplitude after distance, L, can be found by integrating equation (3.2.33). The square of the amplitude of the SH guided mode is then

$$|a_\mu^{(\omega)}(L)|^2 = \frac{\omega^2 \varepsilon_o^2 d_{im}^2}{16P^2} [a_\nu^{(\omega/2)}]^4 I_g^2 L^2 \left[\frac{\mathrm{Sin}(\Delta\beta L/2)}{\Delta\beta L/2}\right]^2 \qquad (3.2.36)$$

Total power flow through a plane perpendicular to the fibre is equal to the sum of guided and radiation field power and is given by

$$P_T = P\left\{\sum_\nu |a_\nu|^2 + \sum \int_0^{n_2 k_o} |a_\rho|^2 d\rho\right\} \qquad (3.2.37)$$

In the above expression power flow in the -ve z-direction has been neglected. P is a normalization factor and is same for all the modes. This was also used in chapter 2 for calculation of mode amplitudes.

Hence SH power generated by coupling the fundamental HE_{11} mode into the μ^{th} SH guided mode is given by

$$P_\mu^{(\omega)}(L) = P|a_\mu|^2 = \frac{\omega^2 \varepsilon_o^2 d_{im}^2}{16P^3} P^{(\omega/2)^2} I_g^2 L^2 \left[\frac{\mathrm{Sin}(\Delta\beta L/2)}{\Delta\beta L/2}\right]^2 \qquad (3.2.38)$$

where, P in the denominator of L.H.S. is a normalization factor and has no significance in the calculation of SH power. It cancels out

with that in the field distribution expressions after substitution of the expression for field overlap integral.

Similarly, the square of the amplitude of SH radiated mode is given by

$$|a_\rho{}^{(\omega)}(L)|^2 = \frac{\omega^2\varepsilon_o{}^2 d_{im}^2}{16P^4}\, P^{(\omega/2)^2}\, I_r{}^2 L^2 \left[\frac{\mathrm{Sin}(\Delta\beta L/2)}{\Delta\beta L/2}\right]^2 \qquad (3.2.39)$$

The SH power generated by coupling to radiation field is better expressed in terms of the attenuation coefficient of the fundamental guided mode. In this case high attenuation indicates good conversion efficiency. The radiation field power is given by

$$\Delta P = P\sum \int_0^{n_2 k} |a_\rho|^2 d\rho$$

$$= \frac{\omega^2\varepsilon_o{}^2 d_{im}^2}{16P^3}\, P^{(\omega/2)^2} \int_{-n_2 k}^{n_2 k} L^2 \left[\frac{\mathrm{Sin}(\Delta\beta L/2)}{\Delta\beta L/2}\right]^2 I_r{}^2 \frac{|\beta|}{\rho}\, d\beta \qquad (3.2.40)$$

If 'L' is large (c.f.wavelength), the function $\left[\frac{\mathrm{Sin}(\Delta\beta L/2)}{\Delta\beta L/2}\right]$ is very sharply peaked near $\Delta\beta=0$ (phase-match case), ie

$$\lim_{L\to\infty} \frac{\mathrm{Sin}Lx}{x} = \pi\delta(x) \qquad (3.2.41)$$

Hence, other terms in the integral in equation (3.2.40) can be regarded as constant and can be taken out of the integral sign i.e.

$$\Delta P = \frac{\omega^2\varepsilon_o{}^2 d_{im}^2}{4P^3}\, P^{(\omega/2)^2}\, I_r{}^2 \frac{|\beta|}{\rho} \int_{-n_2 k}^{n_2 k} \left[\frac{\mathrm{Sin}(\Delta\beta L/2)}{\Delta\beta}\right]^2 d\beta \qquad (3.2.42)$$

The integral in equation (3.2.42) can be approximated by

$$\int_{-n_2 k}^{n_2 k} \left[\frac{\mathrm{Sin}(\Delta\beta L/2)}{\Delta\beta}\right]^2 d\beta \approx \int_{-\infty}^{\infty} \left[\frac{\mathrm{Sin}^2 \Delta\beta L/2}{(\Delta\beta)^2}\right] d(\Delta\beta) = \pi\, L/2 \qquad (3.2.43)$$

The change in integration limits has negligable effect, since the integrand contributes to the integral in the immidiate vicinity of $\Delta\beta = 0$.

Hence, equation (3.2.42) can be written as

$$\Delta P = \frac{\omega^2 \varepsilon_o^2 d_{im}^2}{8P^3} \; P^{(\omega/2)^2} \; I_r^2 \; \frac{|\beta|}{\rho} \pi L \qquad (3.2.44)$$

The attenuation coefficient can be defined as

$$\alpha = \frac{\Delta P}{P^{(\omega/2)}_L} \doteq \frac{\omega^2 \pi \varepsilon_o^2 \; d_{im}^2}{8P^3} \; P^{(\omega/2)} \; I_r^2 \; \frac{|\beta|}{\rho} \qquad (3.2.45)$$

where $P^{(\omega/2)}$ is the power in the fundamental mode at z=0 and $\Delta P/L$ is the Sh power radiated power per unit length.

The major difference in the expression for SH power generated by coupling to guided SH mode and to that for SH radiation field is that in the former case SH varies as square of interaction length instead of varying linearly as in the latter case.

The expression for SH power generated by coupling to radiation field was derived by assuming coupling to be weak. However, the above theory can be extended to long interaction lengths as the power coupled into SH radiation is lost into the cladding. The fibre can be considered to be composed of 'n' sections of lengths 'l_c' where, $\alpha l_c << 1$. In this manner the above analysis can be used for calculating SH power generated by each section of length 'l_c' but by using different value of the fundamental power incident on each section. The fundamental power at the n^{th} subsection will be equal to the fundamental power at $(n-1)^{th}$ subsection less power lost due to coupling to SH radiation. The incremental power loss at each section is same and equal to $-\alpha l_c$. Hence, the SH power radiated over the length L of the fibre can be obtained by using following equation.

$$P^{(\omega)}(L) = P(o)^{(\omega/2)} \left[1 - e^{-\alpha L}\right] \qquad (3.2.46)$$

where, $L = nl_c$

Discussion:

The above analysis can be used to make a comparision of SHG efficiencies for SHG by coupling the SH into the radiation field and to a guided mode, and to consider the effects of cladding dispersion on phase matching. Here it is assumed that the phase matching condition is satisfied and the fibre is monomode at the fundamental frequency ie $\nu = 0$. Also, as the field overlap integral is maximum for modes having similar mode field configurations it is assumed that $\mu = \nu$. The expressions for SHG efficiency per unit length for coupling to SH radiation field and SH guided mode can then shown to be given by

For SH in the radiation field

$$\alpha = \frac{8(\omega\varepsilon_o d_{im})^2 (\mu_o/\varepsilon_o)^{3/2} W^4 P(\omega) \int_o^a J_o^2 (U\frac{r}{a}) J_o(\sigma r) r dr}{n(\omega)^2 n(2\omega) \pi^2 a^4 V^4 |J_1(U)|^4 |\rho a J_o(\sigma a) H_1^{(1)}(\rho a) - \sigma a J_1(\sigma a) H_o^{(1)}(\rho a)|^2}$$

note: In this section ω - the fundamental frequency
2ω - the SH frequency (3.2.47)

For SH as a guided mode

$$\frac{P^{2\omega}}{P^{\omega}_L} = \frac{2(\omega\varepsilon_o d_{im})^2 (\mu_o/\varepsilon_o)^{3/2} W^4 W^{1^2} P(\omega)_L \int_o^a J_o^2 (U\frac{r}{a}) J_o(U^1\frac{r}{a}) r dr}{n(\omega)^2 n(2\omega) \pi a^6 V^4 V^{1^2} |J_1(U)|^4 |J_1(U^1)|^2} \quad (3.2.48)$$

In the above expressions the mode field distributions used are of weakly guiding isotropic cored fibres. These expressions can however also be used to determine efficiency per unit length, to an order of magnitude, in weakly guiding uniaxial crystal cored fibres with crystal c-axis along the fibre axis as the effect of difference in the longitudnal index on transverse fields is negligable for birefringence of upto few percent(chapter 2, section 2.3). Consider a monomode benzil crystal cored fibre with following parameters

$n_1^{\omega} = 1.6313$; $n_2^{\omega} = 1.625$; $n_z^{\omega} = 1.66$

$n_1^{2\omega} = 1.6691$; $n_2^{2\omega} = 1.6424$; $n_z^{2\omega} = 1.687$

$a = 2.72\mu m$; $d_{im} = 3.7 \times 10^{-12}$ m/V

The fibre V-value at the fundamental wavelength of 1.064μm is then 2.3. The normalized propagation constant for the fundamental HE_{11} mode at 1.064μm wavelength was computed(Appendix 1) to be 1.627862. This data can then be used to determine SHG efficiencies per unit length for the above two cases.

1. SHG by coupling the fundamental HE_{11} mode into the SH radiation field:

The value for α in this case is 2.6×10^{-3} with 1W of fundamental power. Consequently, SHG efficiency for 10mm of fibre will be 2.6×10^{-3} % . These figures do not include propagation losses of the fundamental and the SH signals. This form of phase matching is rather easy to satisfy by suitably selecting the cladding glass. In figure 3.3 variation of the normalized SHG efficiency per unit length, α_n, in benzil crystal cored fibre as a function of cladding dispersion is given. Also, indicated on the plot is the dispersion of SKN18 glass used as the cladding for benzil crystal cored fibres. α_n is zero for dispersion of upto $n^{2\omega} - n^{\omega}$ as the SH generated cannot couple into radiation field for $\beta^{2\omega} \leq n^{2\omega}$. For greater values of dispersion as $\beta^{2\omega} > n^{2\omega}$ it increases to a maximum value for the optimum dispersion. The value of the optimum dispersion is determined by the overlap integral. The effect of variation of the core radius and/or core refractive index is to change the the fibre V-value and hence the propagation constant at the fundamental wavelength. This will then result in different value for the optimum dispersion. However the variation in the α will not be great for small changes in the fibre V-value in the single mode or in the region just above the cut-off.

2. SHG by coupling the fundamental HE_{11} mode to a SH HE_{1n} modes:

In this case it is rather more difficult to achieve phase matching between the fundamental and SH HE_{11} modes and in practice phase

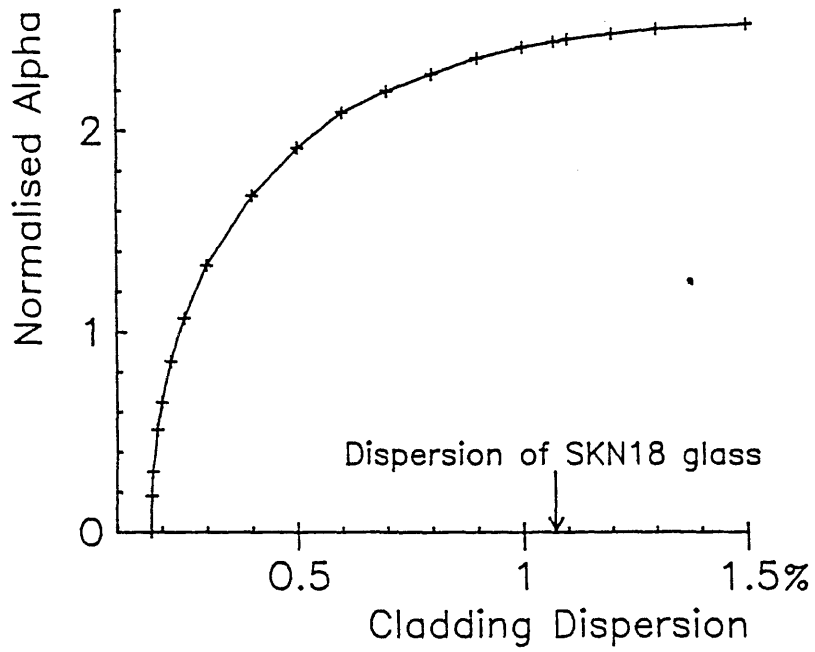

Figure 3.3: SHG efficiency per unit length, α, for benzil crystal cored fibre as a function of the cladding dispersion.

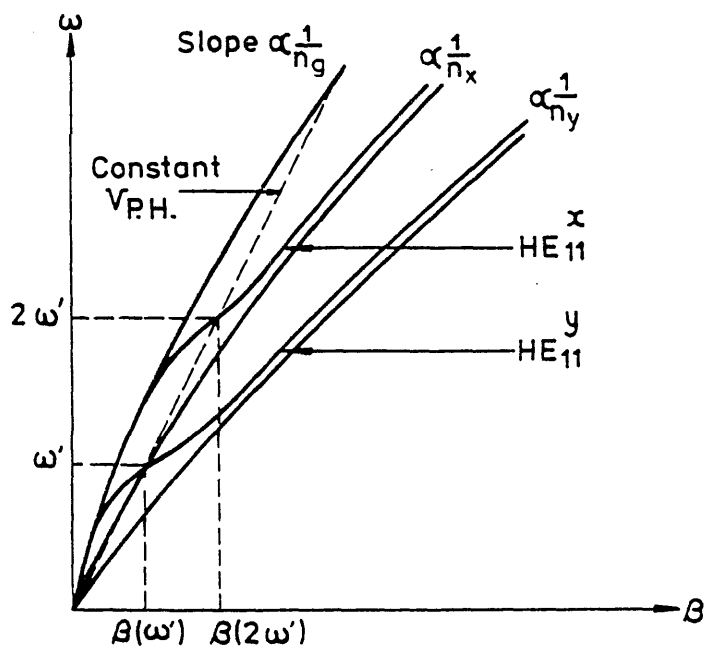

Figure 3.4: ω-β diagram showing phase-matching scheme for guided wave SHG in a biaxial crystal cored fibre with both the fundamental and the SH as HE_{11} modes.

matching is generally satisfied for SH as a higher order mode. This, as discussed earlier, results in lower conversion efficiency due to small value of field the overlap integral. The SHG efficiency for coupling the SH into HE_{12} mode was computed to be 12.4% for a fundamental power of 1W and a 10mm long fibre. This represents an increase of about 4800 as compared with the generation of SH by coupling to the radiation field. This clearly demonstrates advantages in optimisation of the waveguide dispersion for phase-matching.

For a practical device, guided wave SHG is also preferable because of the ease of use. It is possible to maximise the overlap integral by phase matching the fundamental and the SH HE_{11} modes by either using a biaxial crystal material or growing the crystal material in glass capillaries having elliptical bore. In the case of a biaxial core it may be possible to arrange that with the fundamental wave launched in the fibre as HE_{y11} mode, the phase matching condition is satisfied for coupling to the SH HE_{x11} mode. This form of phase matching is shown in figure 3.4. In a similar manner it may be possible to exploit shape dependent birefringence of an elliptical cored fibre by having the fundamental and the SH modes as HE_{o11} and HE_{e11} respectively.

CHAPTER 4

Materials For Growth In Glass Capillaries

4.0 Introduction:

In this chapter criteria used for selection of crystal materials for growth in glass capillaries for non-linear interactions and in particular SHG, are discussed. The two materials selected for growth, after an extensive literature survey, for SHG were acetamide and benzil. Their properties, especially those of benzil, are discussed. Also, in this chapter growth of bulk benzil single crystals is described.

4.1 Selection Criteria Used For Growth Of Crystals In Glass Capillaries For SHG :

There exist a number of non-linear materials which can be used for active device fabrication, however their suitability has to be considered in context of the particular device requirements. Some of the materials possessing large non-linear optical coefficients e.g. $LiNbO_3$, ZnS, KDP, have been used by a number of research workers and their properties are well documented. However, very little data exists for majority of non-centrosymmetric materials regarding their point-group, refractive indices, absorption coefficients etc.. This is because the growth of bulk single crystals and detailed investigation of their physical properties is a time consuming buisness and not always a rewarding exercise. It is possible to make a semi-quantative judgement about the magnitude of non-linear coefficients by comparing the intensity of the SH emitted by their powders with that of some standard eg KDP, quartz. A number of research workers have compiled lists of useful materials for SHG using the above method, principal among them are, Kurtz and Perry (1968), Gott (1971), Davydov (1971), Jerphagnon (1971), and Owen and White (1976). Davydov (1970) and Jerphagnon (1971) have also used a molecular engineering approach to make compounds possessing large non-linear coefficients. This involves replacing some of the

molecules in a compound by those, eg benzene rings, which enhance non-linear effects. However, these materials are not commercially avialable. An extensive literature survey was carried out to find crystals suitable for fabrication of a SH generator in crystal cored fibre form. The method adopted for material selection is illustrated on a flow chart in figure 4.1 and is discussed below.

In weakly guiding fibres the field components in the transverse direction are much greater than those in the longitudnal direction (chapter 2). Hence, for efficient non-linear interactions in crystal cored fibres, the core material non-linear tensor coefficients, which are multiplicative factors with the transverse field components, should have non-zero magnitude. This requirement excludes all the crystal classes with the exception of classes, 1, 2, m, 3, 3m, $\bar{6}$, $\bar{6}$m2, 32.

Of the materials belonging to the above classes , the next consideration is their refractive indices. This is necessary as in order to fabricate a low moded fibre the difference in the core and cladding refractive indices should be in the region of 0.1 . The avialable glasses (Schott) have refractive indices in the range 1.45 to 1.95 (at 0.644μm wavelength). As a result crystals having refractive index greater than 2.0 cannot be used to fabricate crystal cored fibres by their growth in glass capillaries. Because of this consideration some of the very best non-linear materials, e.g. Te, Se, HgS, $LiNbO_3$, $LiTaO_3$, Ag_3AsS_3, $Ca_2Nb_2O_7$, are not useful.

The growth of crystals in glass capillaries is best achieved by crystallization of the melt. As a result materials which decompose on melting were also rejected e.g. hexamine. Also, as the crystal growth is from the melt, the melting point of the material should be less than the glass transformation temperature (temperature at which glass starts to transform from a solid state into a plastic state). This temperature is generally in the range 350°C to 700°C (Schott) depending on the glass type. However, silica capillaries can be used to grow materials possessing high melting points as its softening temperature is 1610°C. In this case the index matching (silica

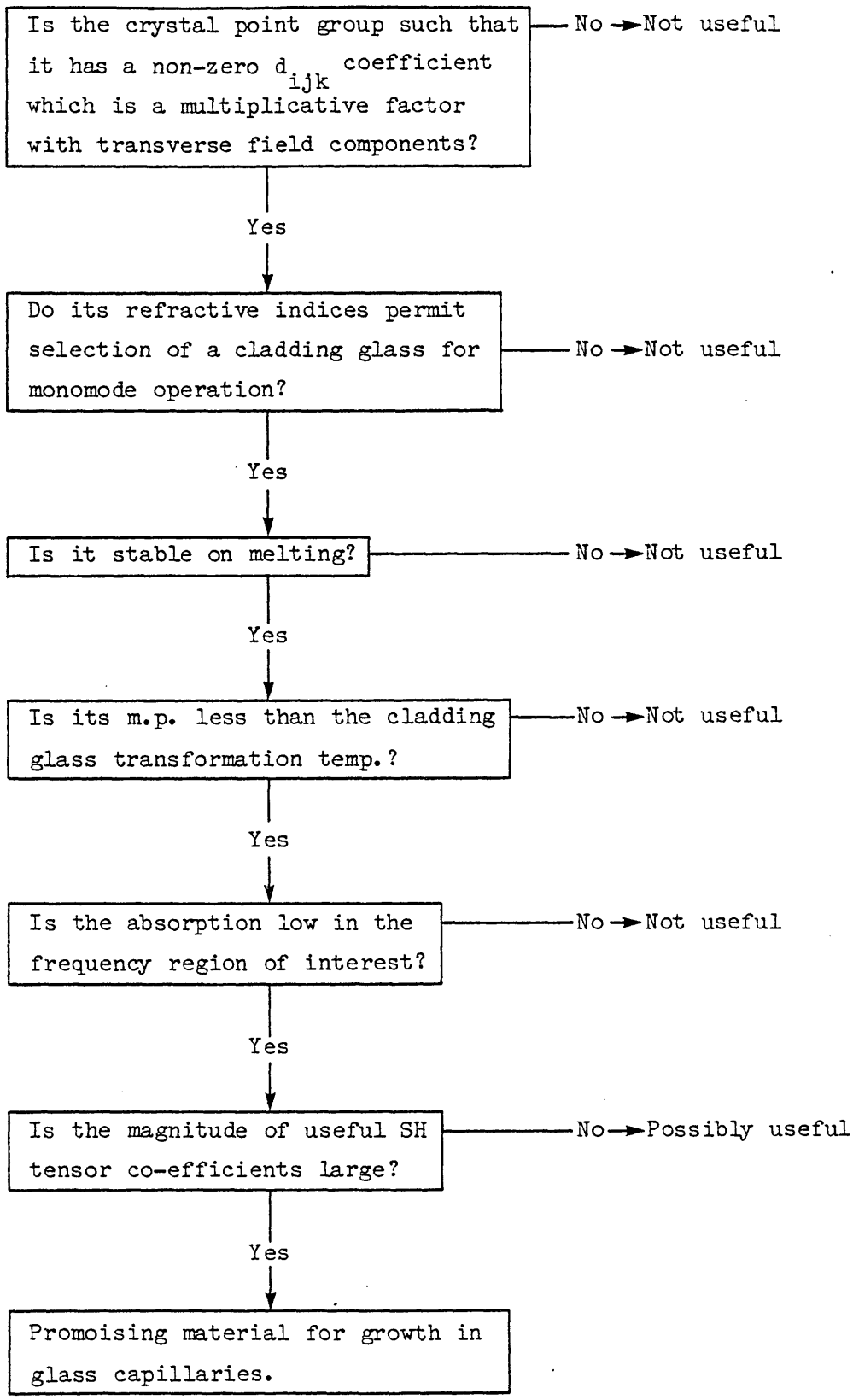

Figure 4.1: Flow chart of the method used in selection of crystals for the fabrication of crystal cored fibres for SHG.

refractive index is 1.455 at 0.633μm) may prevent designing of a useful device.

The other considerations are that the crystal should be transparent in the frequency region of interest and possess large non-linear tensor co-efficients.

The crystal materials for which no data other than SH powder test results was avialable were rejected. The literature survey was carried out to find materials satisfying the above requirements for fabrication of a SH generator. All the materials were found to be unsuitable in at least one aspect. However, two materials, acetamide and benzil, were selected as they appeared to offer a best compromise in material properties.

4.2 Crystal Materials Used For Growth In Glass Capillaries:

Acetamide was the first material selected for growth in glass capillaries. Acetamide is a negative uniaxial crystal belonging to point group 3m. Its properties have been summarised in table 4.1.

The disadvantage of using acetamide is that it is hygroscopic. It was anticipated that it will be possible to prevent water absorption by coating the crystal end faces of the fibre by a thin film of oil or some transparent adhesive. However, the experiments on prevention of water absorption by coating the crystal end face were not successful. The results of these experiments are presented in section 5.1. In view of this growth of acetamide crystals was not carried out in capillaries with bore diameters less than 10μm. Neverthless, the growth of acetamide crystals in large bore capillaries provided useful experience in understanding crystal growth phenomena in glass capillaries.

A search was carried out for an alternative crystal material for growth in capillaries to realise a SH generator. As a result of this exercise benzil was selected. Benzil appeared particularly attractive as it had earlier been successfully grown in capillaries with bore diameters greater than 20μm by Babai (1980). Initially, benzil had

TABLE 4.1

ACETAMIDE

Crystal structure	:	$CH_3.CO.NH_2$
Crystal class	:	trigonal
Point group	:	3m
Melting point	:	82°C
Boiling point	:	222°C at 760mm and 120°C at 20mm
Refractive indices	:	n_o = 1.507; n_e = 1.461(ref.A) at λ = 0.5416μm = 1.54 = 1.46(ref.B)
Other	:	hygroscopic; soluble in alchol, ether, choloroform, glycerol and water.

A: Int. critical tables, vol.1, pp18, McGraw Hill, 1926.
B: Willard M.L. and C. Maresh,'Optical constants of benzamide, its homologs and some aliphatic amides', J. Am. Chem. Soc., 62, 1253(1940).

TABLE 4.2

BENZIL

Crystal Structure	:	$C_6H_5.CO.CO.C_6H_5$
Crystal class	:	trigonal
Point group	:	32
Melting point	:	95°C
Boiling point	:	346°- 348°C at 760mm and 188°C at 12mm
Refractive indices	:	n_o = 1.667; n_e = 1.684 at λ = 0.5461μm
Other	:	yellow in colour; soluble in alchol, acetone, benzene and ether; insoluble in water.

been rejected as it is yellow in colour indicating unsuitability for generation of harmonics with fundamental wavelengths less than 0.84μm and due to small non-linear coefficients. The properties of benzil have been summarised in table 4.2. and some of these are further discussed in section 4.6.

4.3 Purification Of Commercially Avialable Materials:

The commercially avialable materials in general have a high impurity content and as such cannot be used as a starting material for growth of high purity crystals. Infact the crystals grown from material having impurities show a marked concentration gradient of impurities, usually the purest material will be in the bottom section of the boule while the top section has the largest impurity content. This mechanism of purification of crystal material occurs whenever crystal growth is carried out and is exploited in 'zone refining'. This can be illustrated on a phase diagram, figure 4.2, where it has been assumed that the impurities have a lower melting point then the crystal. If the impurity content in the starting material is C_1 then as the melt cools down it stays in liquidus state till it reaches temperature T_1. At this temperature the solid of composition C_2 will crystallize and will co-exist with liquid of composition C_1 in equilibrium. Hence, purer material becomes lost to rest of the material on solidification. The remainder has high impurity concentration, say C_3. When the temperature reaches T_3 further crystallization occurs and material of impurity concentration C_4 comes out . This process goes on and will yield pure crystal material at the bottom with impurities at the top of the crystal.

The other method commonly used for purification of crystal materials is 'fractional crystallization'. In this method crystal material is dissolved in a solvent and then crystallization is allowed to take place either by cooling or partial evaporation of the solvent. By repeated dissolution and crystallization a good seperation of impurities can be achieved.

4.3.1 Purification Of Benzil:

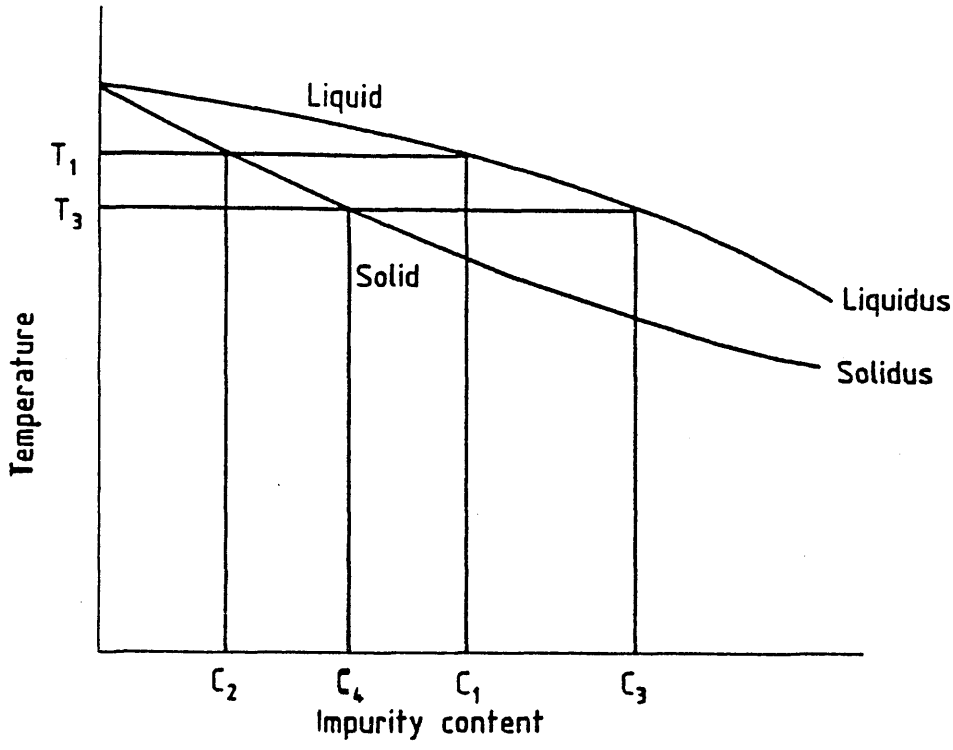

Figure 4.2: Phase-diagram of a crystalline material.

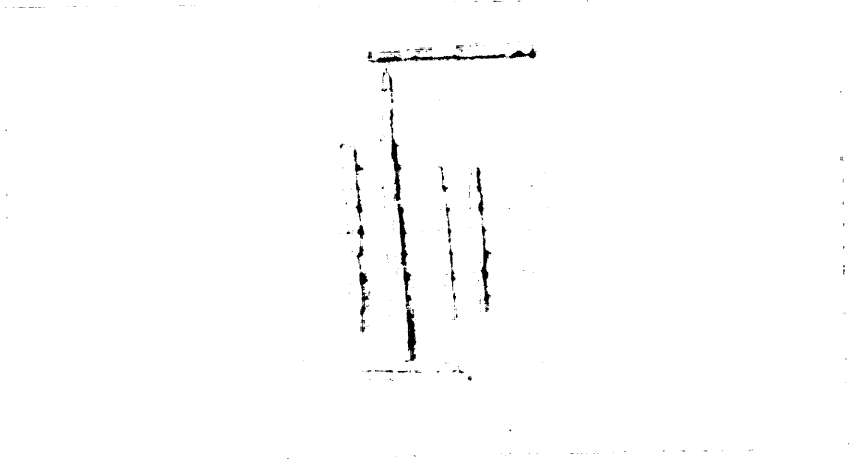

Figure 4.3: A photograph of benzil crystals obtained by evaporation of the super saturated benzil solution in ethyl alchol.

The commercially avialable benzil powder (suppliers: British Drug House) was dissolved in ethyl alcohol, while being heated so as to increase its solubility. The hot benzil solution was filtered twice to remove impurities insoluble in ethyl alchol. The hot benzil solution was then slowly allowed to cool in order to intiate crystallization. Benzil crystals were then seprated from the solution and washed in alchol. This process was repeated. The benzil crystals obtained in this manner were needle shaped having lengths upto 15mm., figure 4.3. The purity of these crystals was assessed by measuring their melting point. The pure materials exhibit a sharp melting point, as can be seen from the phase diagram given in figure 4.2. The melting point of the commercially avialable benzil was measured to be 95.5±0.1°C, while after purification it was measured to be 95.0±0.1°C. The latter value agrees with that quoted in the literature.

4.4 Growth Of Bulk Benzil Single Crystals:

The bulk benzil crystal growth was carried out in order to plot the transmission spectrum in the wavelength range 0.4μm to 2.0μm. Also, bulk benzil crystals could be used as a starting material for growth in glass capillaries as they will have a low impurity content. The growth was carried out using vertical Bridgeman technique. In this technique crystal melt is progressively crystallized as it moves through a temperature gradient.

The furnace used for this purpose was similar to that used McArdle and Sherwood (1974) for growth of phenanthrene. In this furnace two zones which provide the temperature gradient are maintained at constant temperature by the vapour from two boilers. For benzil growth, steam was used for the hot zone while benzene vapour was used for the cool zone (b.p. = 80.1°C). The temperature profile of the furnace is given in figure 4.4. The purified benzil was placed in a thin walled pyrex glass crucible. The tip of the crucible was tapered so that intially only a small volume of melt is supercooled and hence only one nuclei will be formed. If, however, several crystallites are formed then there is a high probability that as the growth interface moves through the taper only one will dominate giving rise to single

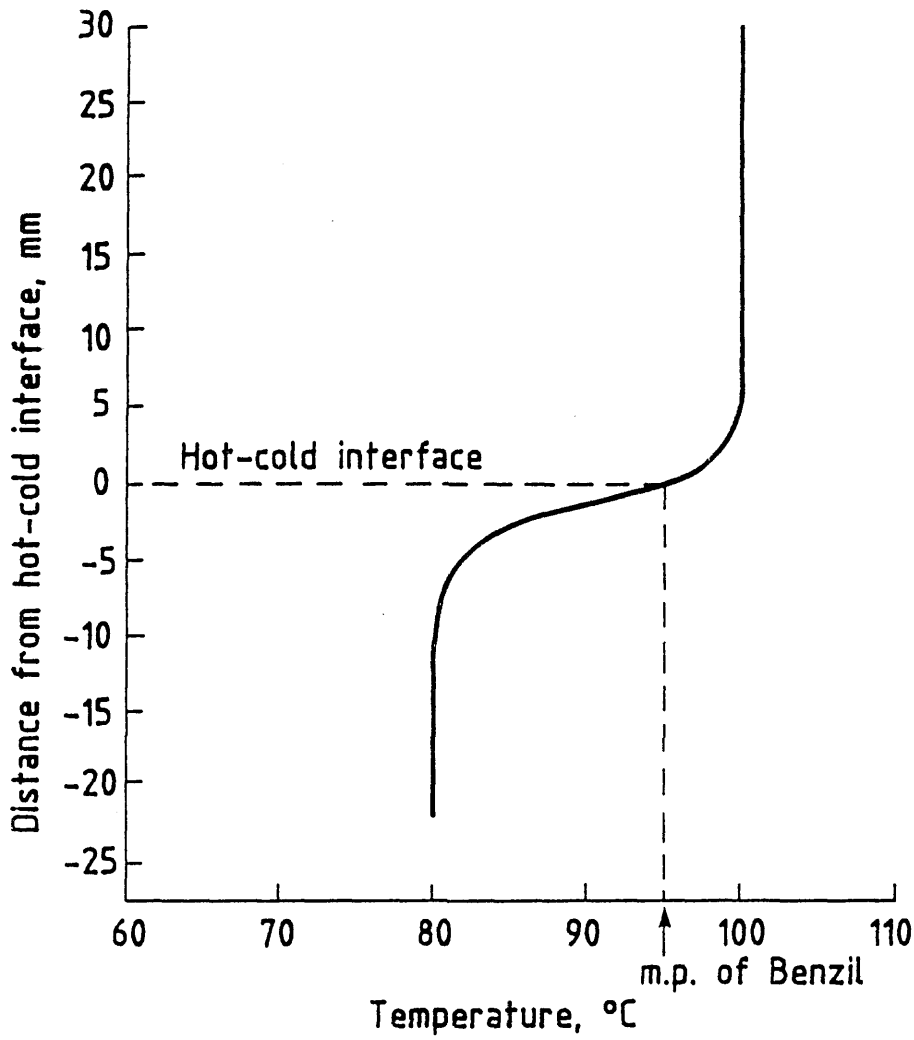

Figure 4.4: Temperature profile of the furnace used for bulk benzil growth from melt.

crystal growth.

The glass crucible was lowered through the zones at the rate of 1mm/hr. Single crystals of lengths upto 40mm and 10mm in diameter were obtained. The crucible was carefully cut at the both ends and the crystal was gently pulled out.

4.5 Assessment And Discussion Of Properties Of Benzil:

In this section properties necessary to design a SH generator and to estimate SHG efficiency are discussed. This requires a knowledge of the following:

1. Refractive indices in the wavelength region of interest.
2. Non-linear SH tensor coefficients.
3. Transmission spectrum.

4.5.1 Benzil's Dispersion:

The refractive indices of benzil are required to be known for both the fundamental and SH wavelengths. The ordinary and extraordinary indices of benzil have been measured by Bryant (1943) in the 0.421μm to 0.656μm wavelength range and Chandrashekar (1954) has derived Sellmeir-Drude formulae to fit refractive index dispersion in this range. These expressions are,

$$n_o^2 = 2.08 + \frac{0.535\lambda^2}{\lambda^2 - (0.24)^2} + \frac{0.015\lambda^2}{\lambda^2 - (0.398)^2} \qquad (4.5.1)$$

$$n_e^2 = 2.35 + \frac{0.37\lambda^2}{\lambda^2 - (0.24)^2} + \frac{0.0138\lambda^2}{\lambda^2 - (0.395)^2} \qquad (4.5.2)$$

where, λ is in micrometers.

Measurements made by Jerphagnon (1971) on SH coherence length in bulk benzil crystals at 1.06μm show that the above formulae could be used to evaluate its refractive index upto 1.06μm without any significant error. A plot of benzil's dispersion as computed from the above

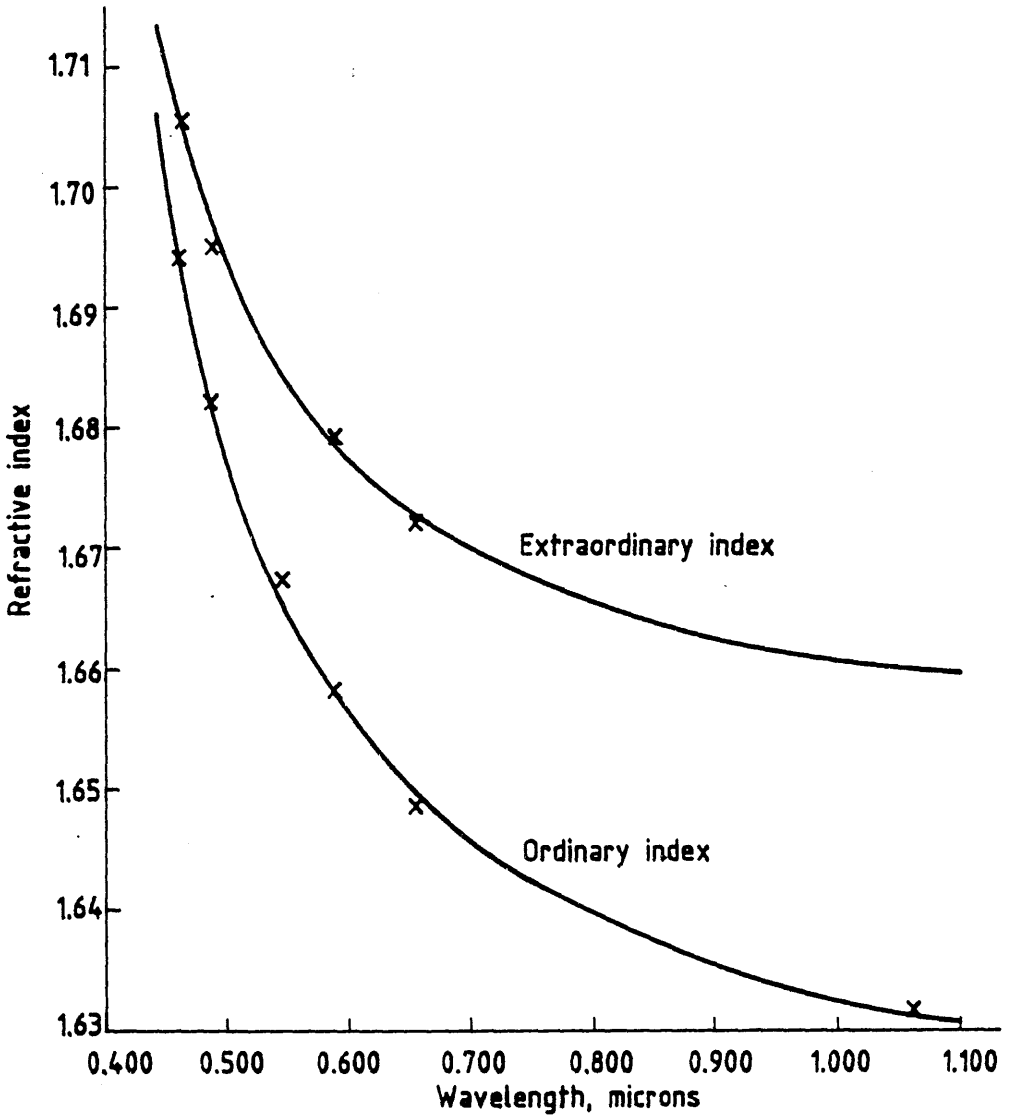

Figure 4.5: Plot of benzil's refractive indices computed from Sellmeir-Drude formulae as a function of wavelength. Also marked are the experimentally measured values.

equations is given in figure 4.5. Also, indicated are reported experimental values of the refractive indices.

4.5.2 Benzil's Non-linear Tensor Coefficients:

Benzil is a trigonal crystal and belongs to point group 32. The SH tensor coefficient for this crystal point group is given by,

$$\begin{vmatrix} d_{11} & -d_{11} & 0 & d_{14} & 0 & 0 \\ 0 & 0 & 0 & 0 & -d_{14} & -d_{11} \\ 0 & 0 & 0 & 0 & 0 & 0 \end{vmatrix} \qquad (4.6.3)$$

Point group 32 crystals generally possess only one independent SH tensor coefficient namely, d_{11}. This is because most of the crystals satisfy the 'Permutation' and 'Klienman's' symmetry for all the tensor elements. However, benzil (Gott (1971)) because of large dispersion does not satisfy these symmetry relations for all the tensor elements. In this case $d_{14} = d_{25} \neq 0$, while $d_{36} = 0$.

Gott (1971) has measured the numerical values for d_{11} and d_{14} as 2xα-quartz and 0.5xα-quartz respectively with 0.694μm as fundamental wavelength. Jerphagnon (1971) has measured d_{11} and the coherence length for a bulk Benzil specimen using Marker fringe technique at 1.06μm to be $(11.5\pm1.5)xd_{11}$ of quartz and 7.10±0.7μm respectively. Gott's values are in error as he did not take into account benzil's strong absorption at 0.347μm (SH wavelength in his case), and he also reports the possibility of errors upto 30% due to various measurement problems present in his technique. In view of this values reported by Jerphagnon are considered to be more accurate and have been used in the analysis.

4.5.3 Transmission Spectrum Of Benzil:

It is necessary to know the signal attenuation due to the crystal in the frequency region of interest. In order to measure the transmission spectrum of benzil, the bulk benzil crystal was cut along its cleavage plane, which in this case is perpendicular to the crystal c-axis. The crystal end faces were then polished using

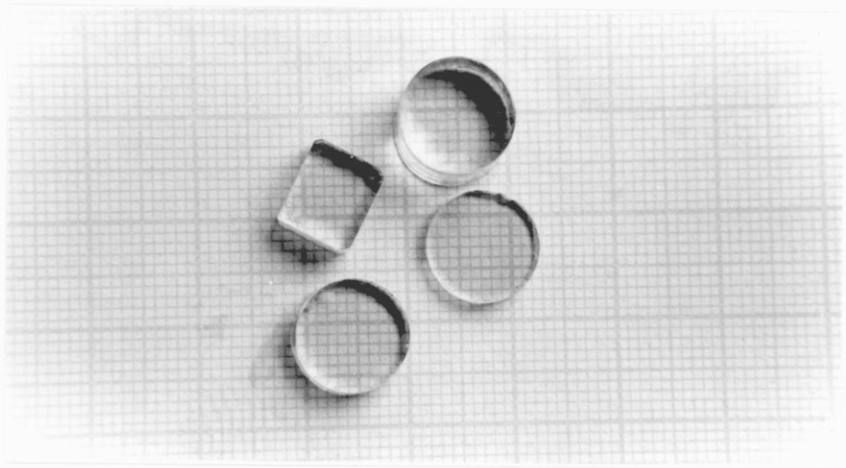

Figure 4.6: A photograph of polished bulk benzil crystals.

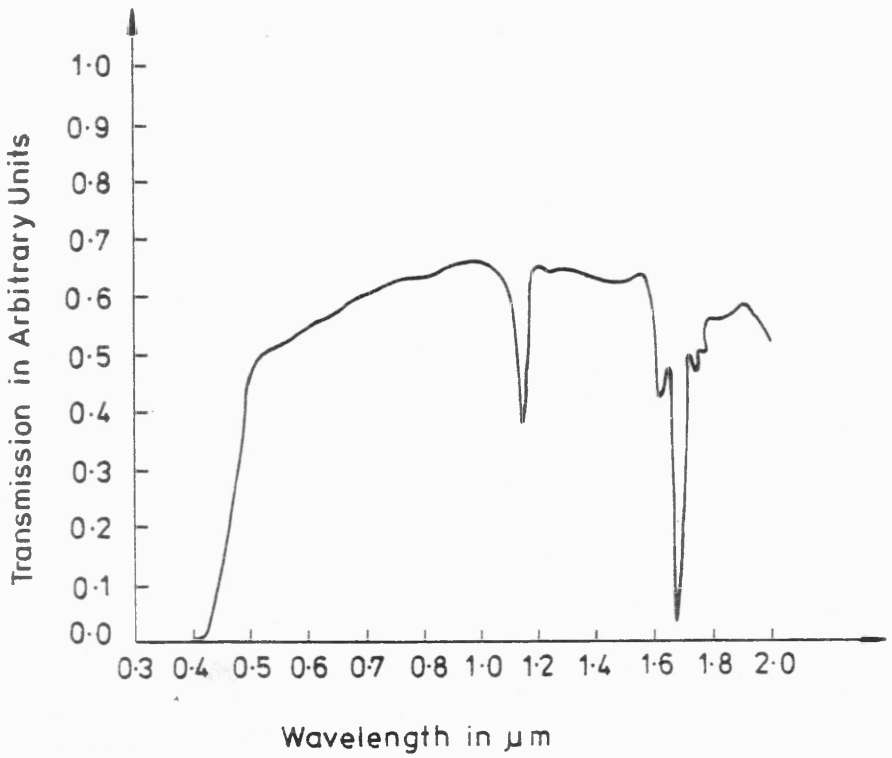

Figure 4.7: Benzil's transmission spectrum.

diamond pastes of varying grades on a cloth lap. A photograph of some of the polished benzil crystals is given in figure 4.6. The transmission spectrum for a 5.49mm long crystal was plotted using a Perkin-Elmer spectrophotometer, figure 4.7. It was not possible to plot it below 0.44μm due to high signal attenuation. In order to investigate transmission in the range 0.2μm to 0.44μm as well, the transmission spectrum of benzil solution in ethanol was plotted. It was found that there exist a major absorption peak at 0.257μm and a relatively weak one at 0.38μm. The absorption peak at 0.38μm is responsible for the charcteristic yellow colour of benzil. The signal attenuation in benzil at 0.633μm wavelength was measured for samples of varying thickness and was found to be -0.9dB/cm. The above measurement of attenuation of benzil in conjunction with its transmission spectra can be used to make an estimate of bulk benzil attenuation at 0.45μm and 0.9μm wavelengths. This gives attenuation of -8.4dB/cm and -0.26dB/cm at 0.45μm and 0.9μm respectively. Rather high attenuation at o.45μm implies that benzil is not a good crystal for SHG with the fundamental wavelength of 0.9μm.

CHAPTER 5

Growth Of Crystal Cored Optical Fibres

5.0 Introduction:

The growth of single crystals in glass capillaries with internal diameters upto 50μm has been reported by Stevenson (1974) and Babai (1977). Stevenson has grown metea-nitroaniline (mNA), while Babai has also grown meta-dinitrobenzene (mDNB), 2-bromo-4-nitroaniline (BNA), formyl-nitrophenylhydrazine (FNPH), and benzil. Babai (1980) has also studied void formation in crystals grown in glass capillaries. This work was directed towards the assessment of the crystal growth mechanism of crystalline materials which are difficult to grow by conventional methods. They have also indicated that the crystal cored fibres could be used as an alternative to 'integrated optic' devices but did not make efforts in that direction. The materials grown by them, with the exception of benzil, are not suitable for SHG device fabrication as they belong to wrong point groups i.e. SH tensor elements multiplying the transverse field components are zero. Also, in order to have single mode or low moded devices the core diameter should be less than 10μm which presents crystal growth problems.

In this chapter first the work on growth of acetamide crystals in glass capillaries having bore diameters upto 10μm is described. This work is used as a basis for discussion of crystal growth mechanism and void formation in glass capillaries. The experiments on prevention of water absorption by coating the end faces of acetamide crystals in glass capillaries are briefly discussed. The selection of glass material for growth of benzil crystals and subsequent capillary drawing from bulk glass is also discussed. Finally, the growth of benzil single crystals in glass capillaries having bore diameters less than 10μm is described.

5.1 Growth Of Acetamide Single Crystals In Glass Capillaries:

Stevenson (1974), (1977), and Babai (1977), (1980), used vertical

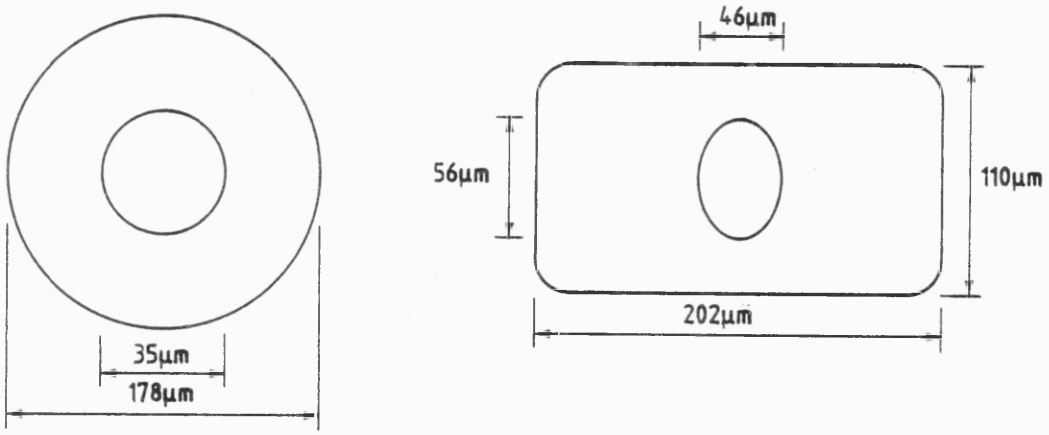

Figure 5.1: Cross-section of pyrex and SF10 glass capillaries used for growth of acetamide crystals.

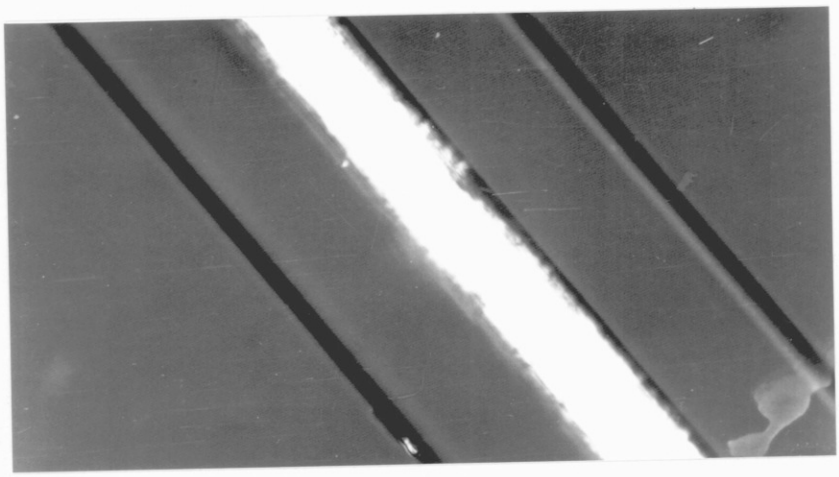

Figure 5.2: A photograph of polycrystalline cored fibre.

Bridgeman method for growth of crystals in glass capillaries. This method was also adopted for our work. In this method the crystal melt is progressively crystallized as it moves through a temperature gradient.

The growth of acetamide was carried out in pyrex (refractive index = 1.475) and Schott SF10 (refractive index = 1.723) glass capillaries. The pyrex capillaries had bore diameters in the range 10μm to 100μm, while SF10 capillaries had bore diameters in the range 20μm to 55μm. The cross-section of these capillaries is shown in figure 5.1.

In our laboratory zone refined acetamide was avialable and this was used as a starting material for the crystal growth. A number of samples of glass capillaries of lengths upto 80mm and varying bore diameters were used for crystal growth. These glass capillaries were filled with the acetamide crystal melt using capillary action in a resistance wire furnace. The furnace was kept at a temperature of about 10°C higher than the acetamide's melting point so as to ensure complete filling of the capillaries. After about 15 minutes the capillaries were withdrawn from the furnace and the melt in them crystallized randomly, figure 5.2. This polycrystalline nature of the core occurs as the melt crystallizes rapidly when the capillaries are brought from a high temperature to room temperature in relatively short time (few seconds).

In order to obtain uniform single crystals it is necessary to allow the crystal melt to traverse steadily a sharp temperature gradient region of the type shown in figure 5.3. It is necessary to have such a sharp temperature gradient as otherwise melt can supercool before the nucleation can take place. As a result when nucleation does take place the crystal growth through the rest of the material will be very rapid and result in polycrystaliization. The slow rate of the growth is necessary to permit time to allow for the latent heat of crystallization to be conducted away and also to help to maintain a planar melt-crystal interface which is necessary to prevent void or dislocation formation. In growth of crystals in glass capillaries this requirement is even more stringent as it is also necessary to match the reduction in the volume of the material on crystallization

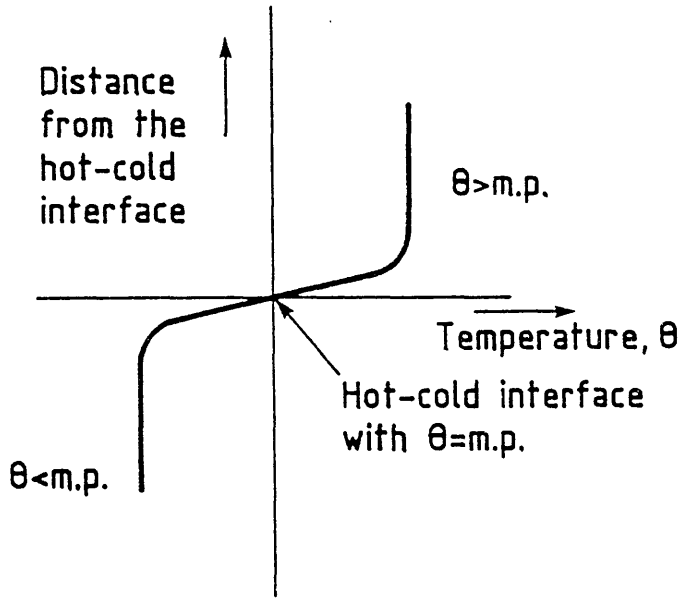

Figure 5.3: Desired temperature profile for single crystal growth.

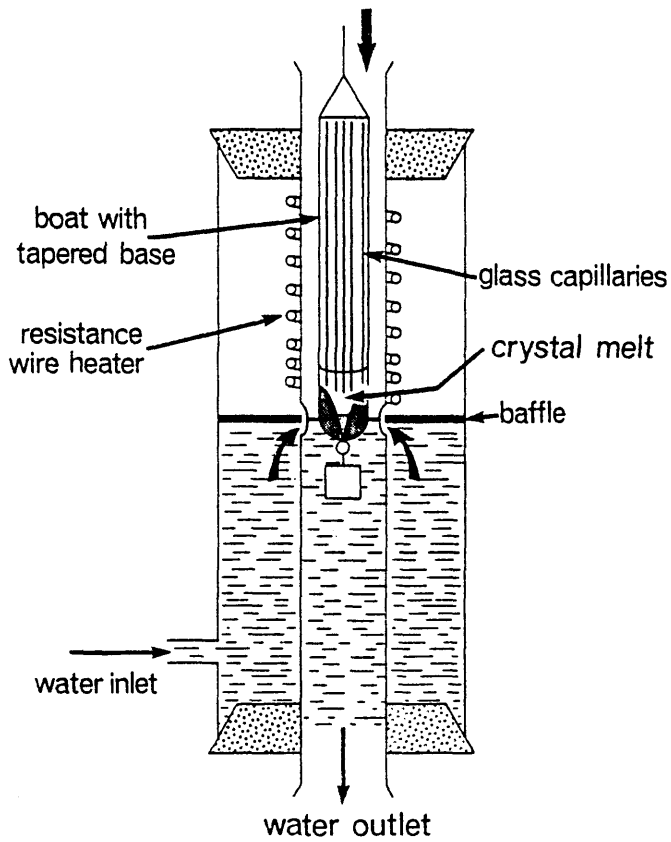

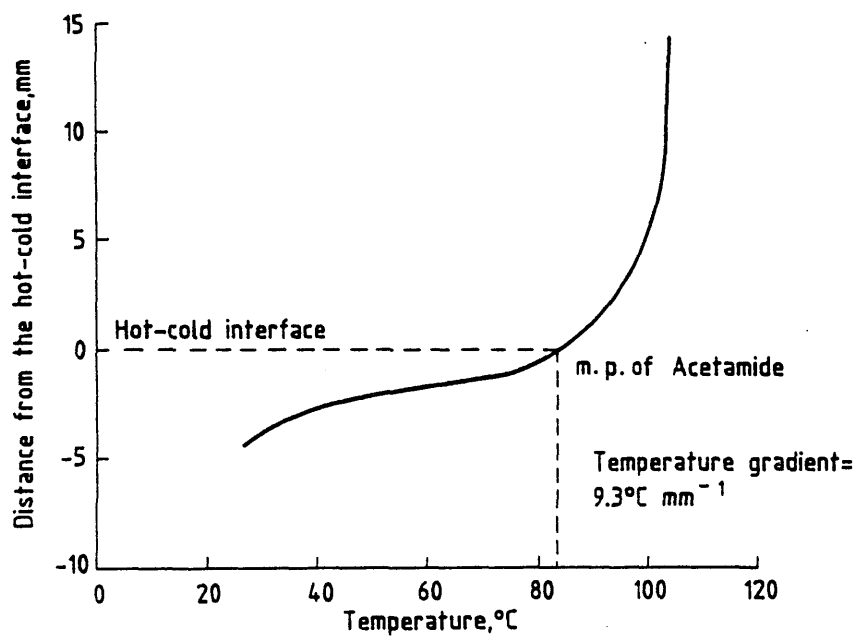

Figure 5.4: Diagram of the furnace along with its temperature profile for growth of single crystals in glass capillaries.

by flow of the crystal melt to the interface.

A furnace having a sharp temperature gradient was built in which controlled recrystallization of the crystal material in the polycrystalline cored fibres could be carried out. This furnace is essentially a resistance furnace but has a water flow arrangement to provide a sharp temperature gradient. The furnace and its temperature profile are shown in figure 5.4. The water suply to the furnace was from a constant water head in order to stabilise the temperature profile and also to keep the hot-cold interface at a fixed position in the furnace. The fibres could be lowered down the furnace with speeds in the 10 to 50 mm/hr range by means of a pulley, having different radii, connected to the shaft of a motor.

As the process of recrystallization of polycrystalline core of the fibres is slow a number of fibres were used in each run. This was done by placing them in a small diameter thin walled pyrex glass container which was then lowered into the furnace using the motor with the pulley arrangement. Before, recrystallization was started it was always ensured that there was a short section (few mms) of polycrystalline cored fibres in the region having temperature below the melting point of the crystal. This was done to prevent the melt from supercooling. The yield of the void free crystals grown in this manner was 1 to 5% in each run. The maximum lengths of single crystal obtained were 4 to 5 mm for capillary bore diameters in the region of 35μm. The fibres were assessed for their core quality using a polarising microscope with magnification upto x500. A number or different types of defects/voids were observed and they can be categorised as follows:

1. Bubbles/Small Voids (maximum size equal to the bore diameters): During melting of the polycrystalline core many microbubbles are released and in some cases they can join together to give rise to bubbles having dimensions of upto bore diameter. On subsequent crystallization of the melt these bubbles are 'frozen' in the core. In figure 5.5 a picture of a typical void of this form is given.

2. General voids and those between the crystal and the walls of the

capillary:
These can occur as on crystallization there is a decrease in the volume of the material and if this volume is not filled by the flow of melt (by gravity in this case) to the crystal face a void will be generated. Pictures of this type of void in the fibre core are given in figure 5.6. However, in a few cases a break in the crystal core was observed and this is shown in figure 5.7. Interesting feature of this defect is that the crystal alignment is preserved through the void. This type of void was found to be more prevalent in growth of crystals in small bore capillaries and possible mechanisms responsible for this are discussed in section 5.5.

3. Non-uniform axis alignment:

In some crystal cored fibres it was observed that the direction of the crystal c-axis varied along the length of the fibre. This can occur if the melt-crystal interface is concave in which case there is a possibility of the growth of spurious nuclei which could maintain growth over short lengths. A photograph of such a fibre between the cross polarisers is given in figure 5.8.

It was considered that type 1 defects, above, could be eliminated by filling of the crystal melt and carrying out the subsequent crystallization in the same furnace. On implementation of the above scheme it was observed that the number of the voids was significantly reduced. The maximum length of single void free crystal obtained in the above manner was 20mm in a capillary of 40μm bore diameter. During the growth at times the melt will supercool and as a result the crystal core will be polycrystalline for a few centimeters after which single crystal growth was observed. The occurence of this was prevented by introducing a crystal seed into the melt container, after it had traversed a few millimeters in the cold region, to initiate the crystal growth. It was also found that it was very important to ensure that the water level in the furnace remained constant during the crystal growth. If it were to suddenly rise, then the melt in the length of capillary now in the region of temperature below crystal's melting point will crystallize randomly. As a result there will be sections of single crystal core seperated by sections

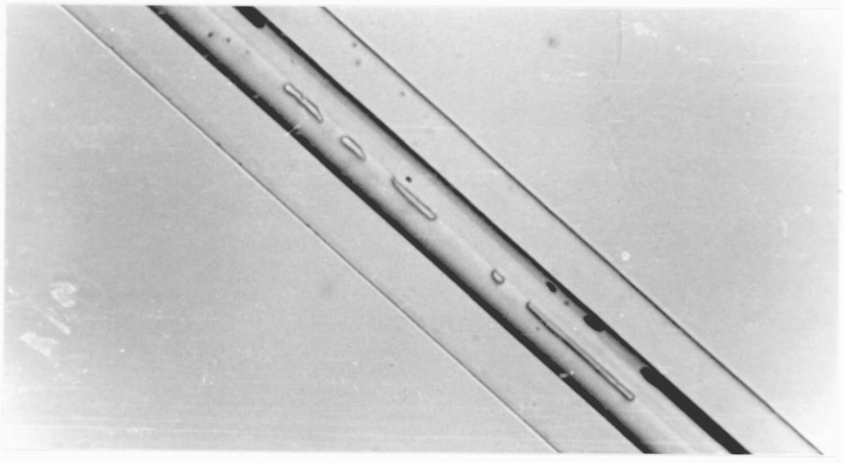

Figure 5.5: A photograph showing voids in a fibre due to presence of bubbles in the melt.

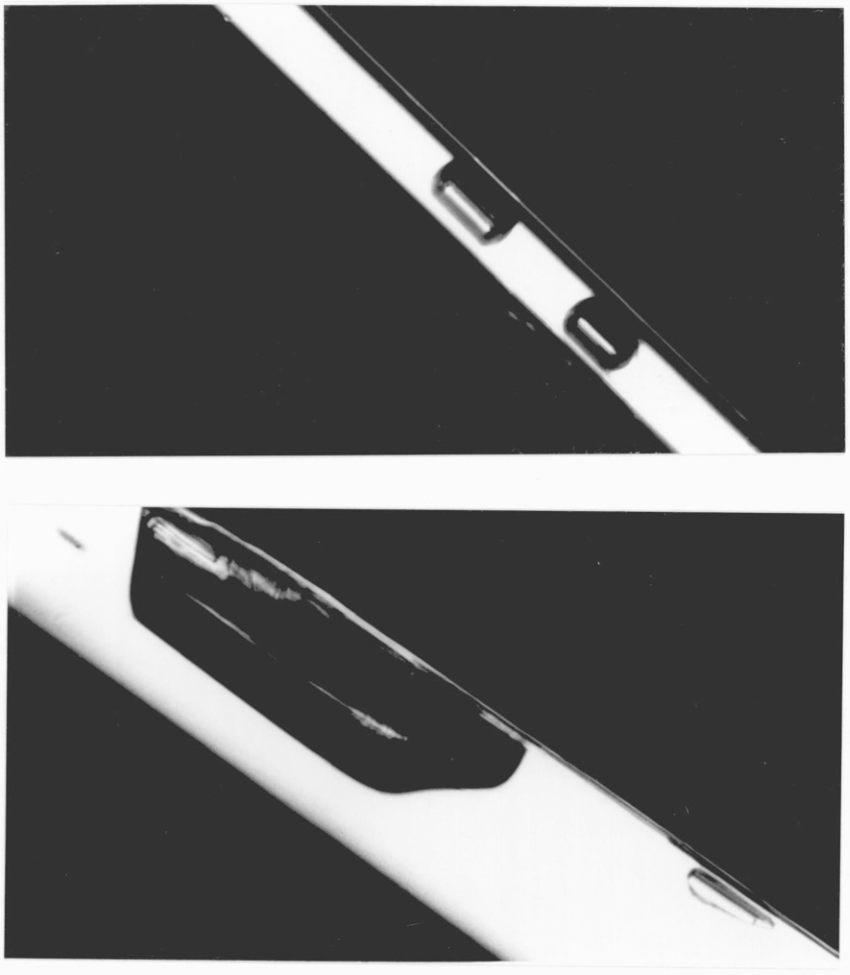

Figure 5.6: Photographs showing fibre voids generated due to the insufficient flow of melt to the crystal face.

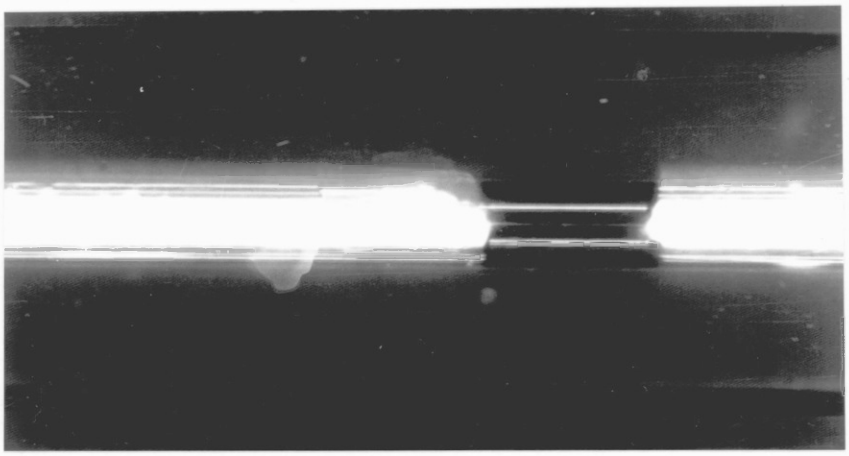

Figure 5.7: A photograph showing break in the crystal core due to a large void.

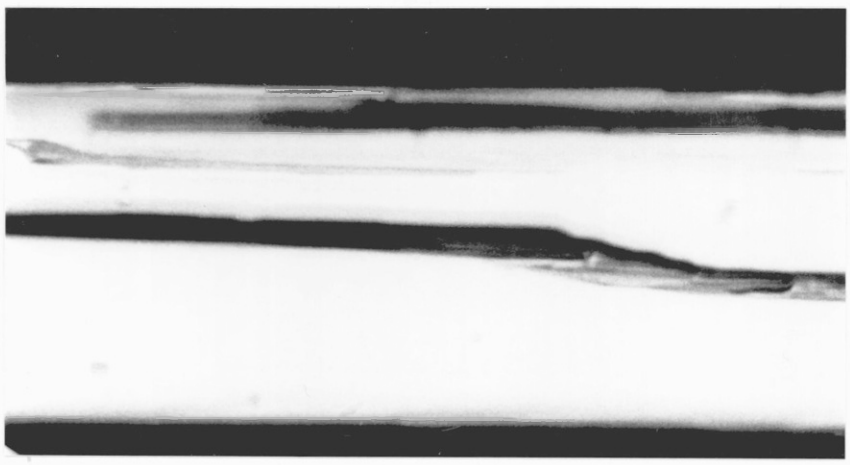

Figure 5.8: A photograph of fibre with variation in the crystal axis along the length.

of polycrystalline core. Also, it is necessary to prevent any thermal or mechanical perturbations during the growth to realise uniform single crystal growth.

To grow crystals in capillaries with pulling speeds of 10mm/hr it takes upto 6hrs for the growth to be completed. In the furnace used control of the water level for upto this period was found to be unsatisfactory. The water flow arrangement was modified and this is shown along with the furnace's temperature profile in figure 5.9. The temperature gradient of this furnace was less than that of the previous one ie 4.75°C/mm instead of 9.30°C/mm. However, decrease in the temperature gradient did not adversely effect the quality of crystals grown. It was possible to obtain single crystals of lengths upto 30mms in capillaries having bore diameters in 30μm to 40μm range. The optimum pulling rate for crystal growth in capillaries with bore diameters <40μms was found to be 18mm/hr.

The quality of crystals grown in capillaries with bore diameter >50μms was poor. The maximum single crystal lengths were only a few millimeters. This is because for large diameter crystal growth the pulling speed has to be very low too allow the melt to reach crystal face and also to permit the latent heat of crystallization to be conducted away through the crystal and capillary walls. Additionally the requirements of stable temperature profile and isolation from mechanical disturbances are more stringent than for growth in small bore capillaries. Hence, a furnace has to be designed taking above considerations into account. As our interest was in growth of crystals in small bore capillaries, ie <40μms, no further improvements were incorporated in the furnace design.

A few single crystals were also grown in capillaries with bore diameters down to 10μm. The quality of the growth was found to be satisfactory and void free single crystals of lengths upto 30mms. were easily obtained.

The crystals were assessed for their quality using a polarising microscope with magnification in the 25 to 500 range. A photograph of a good quality acetamide crystal cored fibre taken between cross-

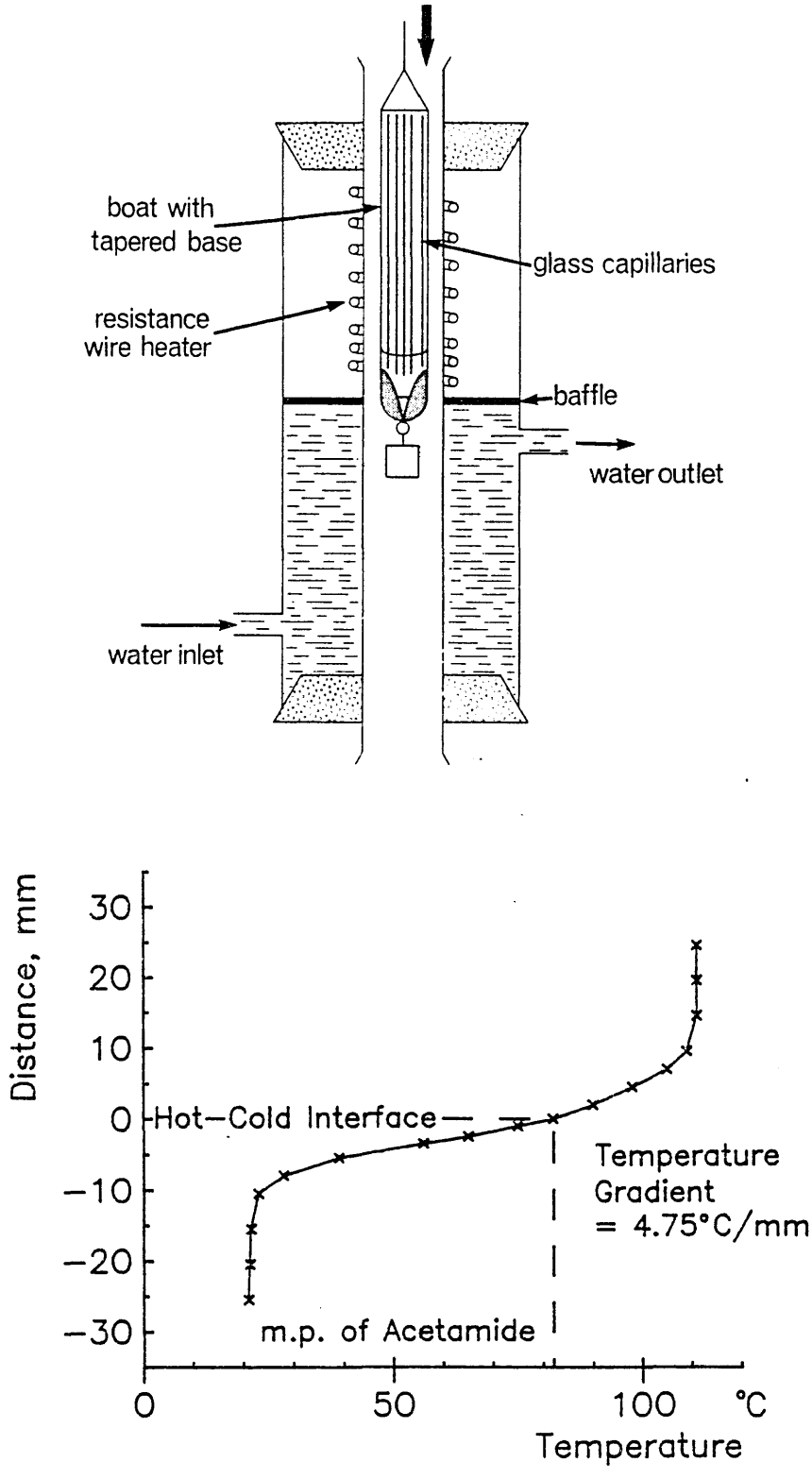

Figure 5.9: Improved furnace along with its temperature profile for growth of void free single crystals in capillaries.

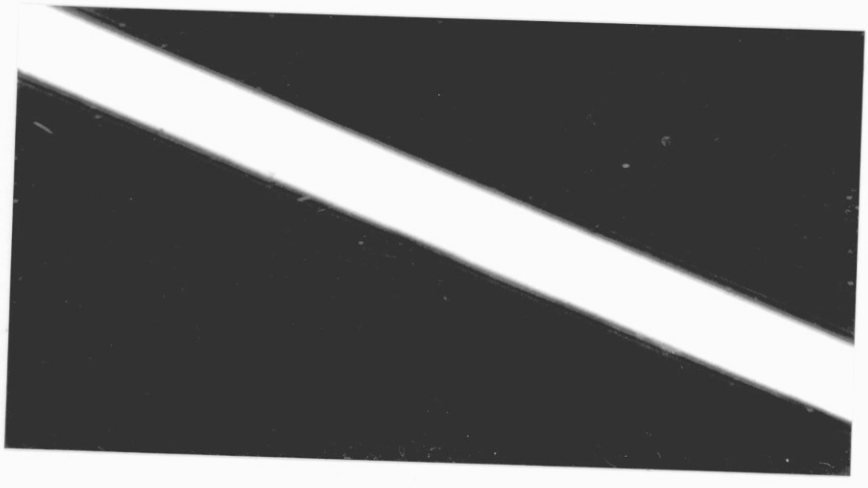

Figure 5.10: A photograph of a void free single acetamide crystal cored fibre.

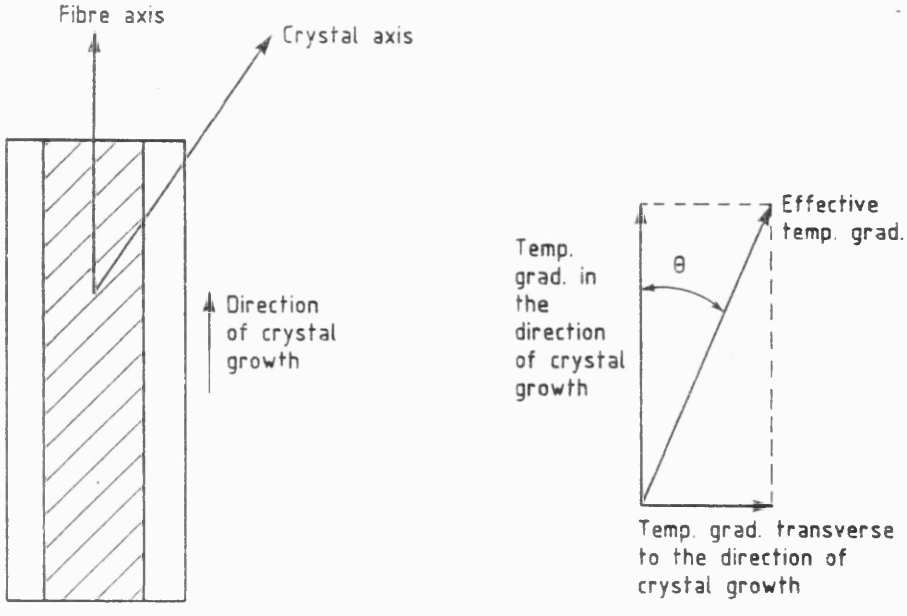

Figure 5.11: Diagram showing the influence of transverse temperature gradients on the direction of crystal growth in capillaries.

polarisers is given in figure 5.10. The deviations of the crystal axis from the fibre axis was also determined. It was found that the crystal axis was not always along the fibre axis and deviations of upto 10° were measured. However, in majority of the samples deviation of the crystal axis from the fibre axis was less than 2°. The crystal axis alignment in the fibre will be along the direction which is favoured by the temperature gradient, which in this case is along the fibre axis, in absence of any mechanical or thermal perturbations during the growth. The crystal axis deviations could also have been caused by the presence of small transverse temperature gradient, see figure 5.11. However, for growth in capillaries having small diameters this effect should not be significant. The major cause of the deviations thus seems to be that the crystal alignment in the fibre is determined by the direction of intial nucleation. This effect could then be eliminated by pulling at faster rates. In this case if the intial nucleation direction is not along the fibre axis, the crystal growth along this direction will not be able to match the pulling rate thereby leading to supercooling of the melt and subsequent nucleation of crystallite having crystal axis along the fibre axis. It was decided to verify the above hypothesis by increasing the pulling speed. The fibres pulled in this manner had crystal axis along the fibre axis but the void content was found to be unacceptably high. This was so as melt did not have sufficient time to reach the crystal face to occupy the space generated by reduction in volume on crystallization. As a result of this it was decided to select fibres with crystal axis along the fibre axis for SHG experimentation rather than to further improve the furnace design. The birefringence fringes obtained using sodium light with acetamide cored fibre, indicating good optical quality of the crystal core, are given in figure 5.12. Their symmetrical behaviour indicates that the crystal axis is along the fibre axis.

The growth of acetemide crystals in capillaries having bore diameters <10μms was not carried out as experiments to prevent water absorption by the crystal end faces by coating them with a thin protective layer were unsuccessful. The coating of the crystal faces was attempted by using fine layer of quick setting adhesives e.g. cyanoacrylate, bostick, Lacquer adhesives etc. All the adhesives used reacted with

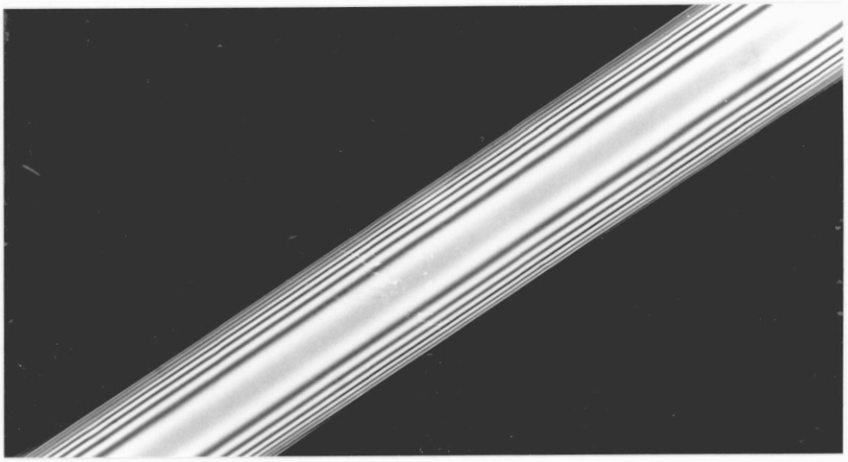

Figure 5.12: A photograph of birefringence fringes obtained using a void free single acetamide crystal cored fibre.

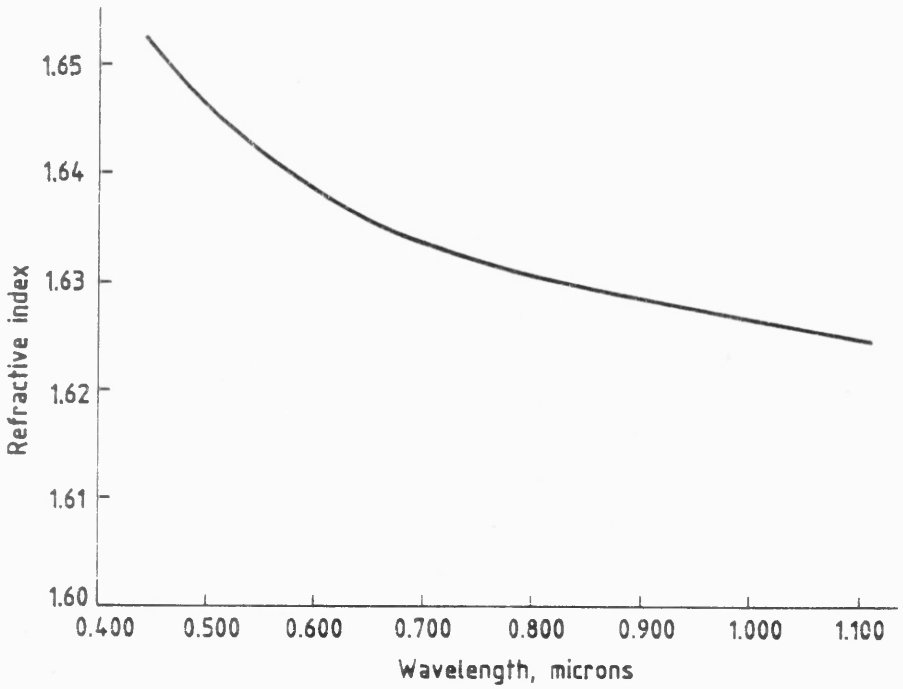

Figure 5.13: Plot of SKN18 glass's dispersion.

the lengths of upto 100μm of acetamide crystal from the end face. The other disadvantage was that they left a non-uniform film of adhesive at the fibre end and this would have significantly reduced the efficiency of launching light into the fibre. The other possibility tried was application of water blocking barrier e.g. cedarwood oil, vaseline, grease, and parafin oil to the crystal face. All these materials also reacted with the crystal face with rates varying from 1.5μm/min to 11μm/min. Failure to find any suitable material to prevent water absorption by acetamide led to reassessment of its suitability for SHG experimentation. Also, as there was not sufficient data avialable on acetamides refractive indices in the near infra-red, it was decided to find an alternative crystal material for SHG. Benzil was then selected and its growth in capillaries with bore diameters less than 10μms is discussed in section 5.5.

5.2 Selection Of Capillary Glass For The Fabrication Of Benzil Crystal Cored Fibres:

In order to make an optical waveguide it is necessary that the cladding refractive index be less than that of the core. For single mode operation in a uniaxial crystal cored fibre, with crystal axis along the fibre axis, cladding index is given by (equation 2.3.9),

$$n_2 \leqslant \left[n_1^2 - \left[\frac{2.405(n_1/n_z)}{k_o a} \right]^2 \right]^{\frac{1}{2}} \qquad (5.2.1)$$

It is generally preferable to have a large core diameter and to make the core-cladding index difference small so that the light can easily be launched into the fibre. For non-linear interactions to occur it is necessary to have high field strengths in the fibre core. In which case small core size can be used to exploit non-linear effects with low powers. In order to optimise between the two it was decided to select a glass which will give single mode operation with core diameters less than 10μm. The Schott glass SKN18 was found to be best for fabrication of single mode benzil crystal cored fibres. Its dispersion has been plotted in figure 5.13. Hence for single mode operation at the wavelength of 0.9μm , the core diameter should be 4.45μm.

The refractive index of the SKN18 glass supplied by the manufacturer was measured at 0.633μm wavelength using an Abbe refractrometer and was found to agree with the manufacturer's quoted value.

5.3 Prepration Of Glass Capillaries:

The glass supplied by the manufacturer was in the form of a large rectangular block. A glass sliver was melted and large bore capillary formed by blowing an air bubble through it. The typical dimensions of these preforms were,
outer diameter = 6mm
Inner diameter = 0.8mm
Length = 34mm
These capillaries were then roughly annealed over a period of 12 hours as otherwise they tended to crack upon heating them upto their glass transformation temperature. These preforms were then used by a glass blower to draw capillaries, having small bore diameters, by hand. The capillaries obtained in this manner had bore diameters down to 20μm and bore was uniform to upto 10mm in length. The attempted pulling of smaller bore diameter capillaries generally resulted in bore collapse.

In order to pull capillaries with bores <20μm, a hypodermic tube furnace was used. A brass hypodermic tube of 75mm length and approximately 300μm bore diameter was connected to mains via a current transformer and a Variac. The glass capillaries drawn by the glass blower having diameters in the range

$25\ \mu m \leq i.d. \leq 75\ \mu m$

$90\ \mu m \leq o.d. \leq 175\ \mu m$

were used as preforms for drawing small bore capillaries. The preform was threaded through the furnace with one end fixed while a weight (3 to 5 gms) was attached to the other end. On increasing the Variac voltage the preform started pulling. By trial and error pulled down ratios of 1:10 could be obtained. The fibres pulled down using this furnace had uniform bores over lengths upto 20 to 30 mm.

During, the course of above work a resistance furnace developed by

Handerek(1982) to pull glass capillaries for fabrication of single mode liquid filled guides became avialable. This furnace had a short hot zone allowing pull down ratios of 1:20 to be obtained. The furnace was approximately 2 metres above the floor level, as a result it was possible to draw uniform bore capillaries. The pulling of large bore diameter preform (i.d. = 0.8mm) was done in two stages. This gave pulled down ratio of 1:400 and single mode size capillaries having uniform bore over lengths of upto 40mms were easily obtained. A picture of the cross-section of one of the capillaries pulled was taken using an electron microscope, figure 5.14. As the bore in the starting preform was not always circular, the final pulled down bore in some cases had an elliptical cross-section.

5.4 Change In Glass Refractive Index On Capillary Drawing:

Glass manufacturer's do not specify the change in glass refractive index that occurs on heating it to temperatures above glass transformation temperature as this change is not a well defined function. In prepration of glass capillaries for crystal growth the glass was heated a number of times to temperatures above the transformation temperature. Hence, it is necessary to determine the refractive index of the pulled down glass capillaries in order to estimate the core diameter with which single mode operation at a given wavelength is possible.

The refractive index of glass capillaries was measured using 'immersion method'. In this method liquids of known refractive indices are used as immersion media. The sample is placed in the successive immersions till the sample is indistinguishable in an immersion. This will occur when the sample index equals that of the immersion. While viewing the sample in an immersion using a microscope, on lowering the stage a bright line is seen to move into the region out of the two having higher refractive index. This line is referred to as 'Becke´ line' and can be used in conjunction with the 'immersion method' to determine the refractive index of the pulled down glass capillaries. In order to measure the refractive index SKN18 capillaries, mixtures of 1-bromonapthalene and iodobenzene, were used as immersion media to give refractive indices

in the range 1.612 to 1.651. The refractive index of the mixtures was determined using the Abbé refractometer. The glass capillary was placed in successive mixtures having increasing refractive index and with the aid of Becke line it was found that the glass index, n_g, was such that

$$1.6237 < n_g < 1.6245$$

It was not found possible to mix the liquids in right proportions to give an index within the above range. Hence, the refractive index of SKN18 capillary was assumed to be given by the mean of the above interval i.e. 1.6241. However, as only an estimate of the typical change in the refractive index was required (as no two capillary drawing runs are identical) no attempt was made to improve on the above accuracy. This value indicates reduction in the SKN18 refractive index by 0.78% on drawing it into capillaries by the method discussed in the previous section.This change in the refractive index is very large in comparison with the core-cladding index difference which was used in selection of SKN18 glass to give single mode operation. In view of this, for single mode operation at 0.9μm wavelength the core diameter needs to be 2.67μm.

The glass refractive index changes whenever it is heated to its transformation temperature and subsequently cooled to ambient temperature. This change occurs as a result of residual stresses which occur on cooling and can vary depending upon the thermal history of the glass during the cooling process from the transformation temperature to the ambient temperature. It is however possible by fine annealing to prevent change in refractive index and glass manufacturers have developed annealing schedules to permit processing of glasses without introducing stress birefringence. The change in refractive index on annealing for borosilicate glasses has been shown by Lillie(1954) to be given by

$$n' = n - K.\ln(R'/R) \qquad (5.4.1)$$

where, n and n' are the refractive indices of glass annealed at rates R and R' respectively and K is a constant for a given glass

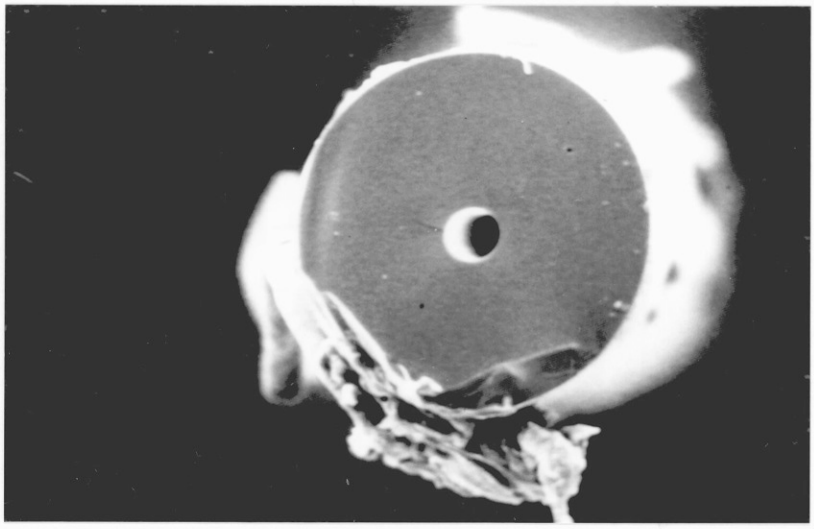

Figure 5.14: A photograph of SKN18 capillary taken using scanning electron microscope.

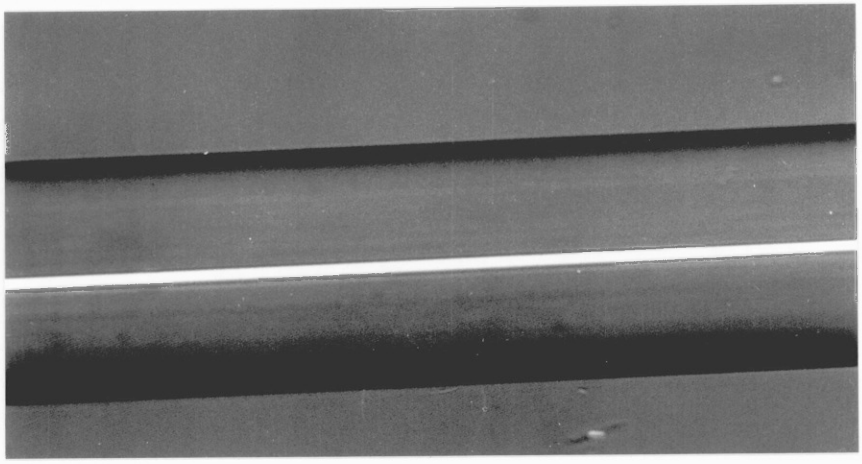

Figure 5.15: A photograph of void free benzil single crystal monomode fibre.

type.

This problem of change in glass refractive index was encountered in the latter part of the research program. It was decided not to develop a fine annealing routine as this in itself would have been a detailed study and especially as SKN18 glass capillaries could be used despite of change in their refractive index for fabrication of monomode benzil crystal cored fibres.

5.5 Growth Of Benzil Crystals In Small Bore Capillaries:

The growth of benzil crystals in small bore capillaries was attempted using the furnace given in figure 5.9. The capillaries had bore diameter <10μm and were about 55mm in length. In some of the intial growth attempts it was observed that at times nucleation did not take place even though the melt had moved into the cold zone of the furnace. The supercooling of the benzil in this case could be attributed to the high purity of the melt. In order to initiate nucleation, a taper was incorporated in the boat, figure 5.9. A pulling speed of 18mm/hr and a temperature gradient of 5°C/mm were found to give optimum conditions for void free single crystal growth. Void free monomode benzil crystal cored fibres of lengths upto 50mm were obtained. The crystal length was limited by the furnace design and, in principle, it should be possible to obtain longer lengths of void free fibre. A photograph of a void-free monomode benzil crystal cored fibre between the cross polarisers is given in figure 5.15. The direction of benzil crystal axis in glass capillaries was determined using a polarising microscope and was found to be along the fibre axis. At times deviations of upto 5° were observed and these were, as discussed in section 5.1, due to the presence of transverse temperature gradients in the furnace.

The defects observed in the growth of benzil crystals in small bore capillaries were of similar type as those observed in the case of large bore acetamide cored fibres. In figure 5.16 photographs of typical voids observed are given. However, in this case break in the crystal core was found to occur more often than for crystals grown in large bore capillaries. The seperation between single crystal

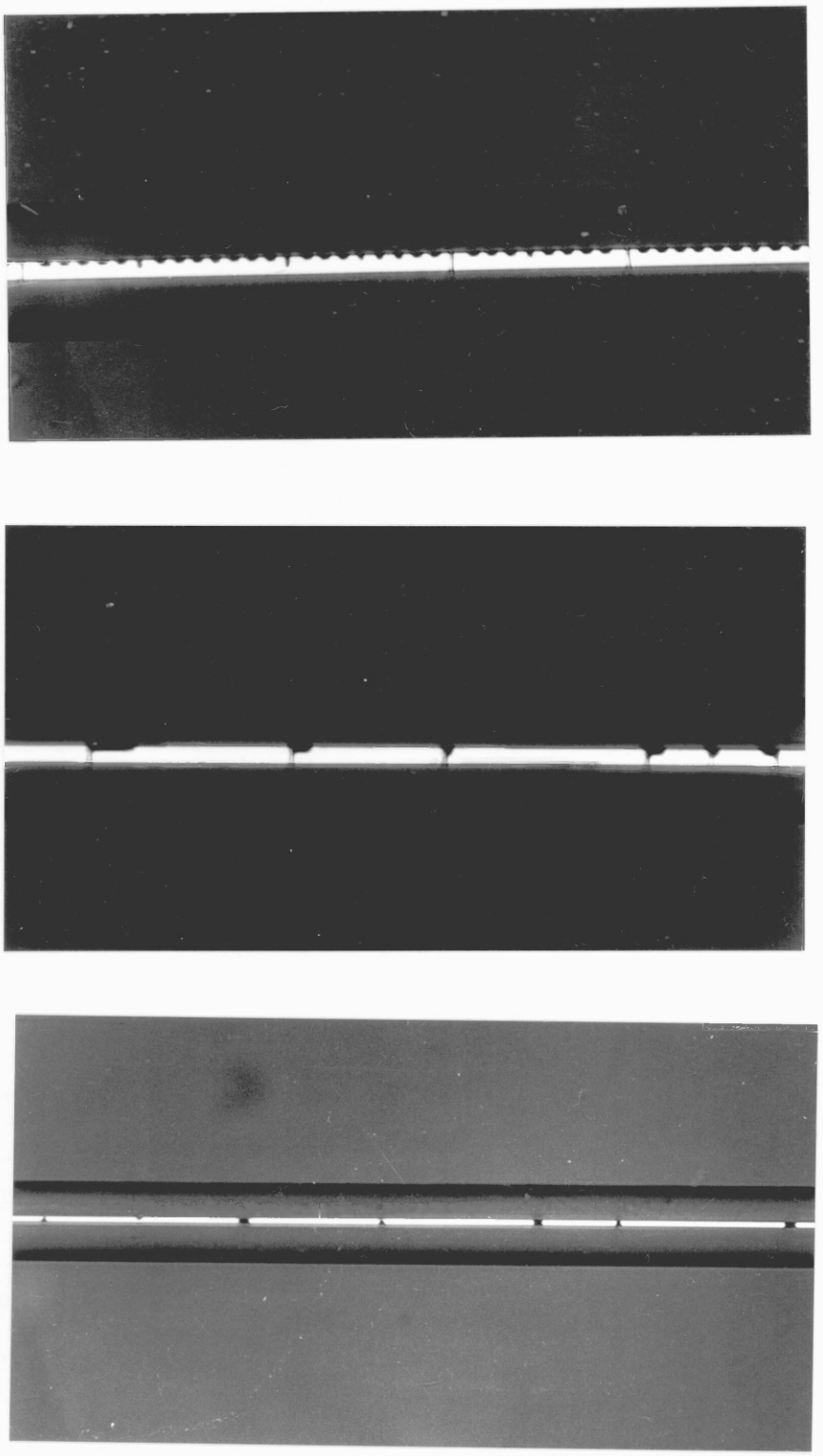

Figure 5.16: Photographs showing typical voids in benzil crystal cored fibres.

sections varied from few microns to upto five times the bore diameter. The intresting nature of this defect is that the crystal alignment is preserved through the void. The explanation for this behaviour is that the small bore size of the capillary initiates nucleation along the direction determined by the temperature gradients in the furnace and as these are constant for a given crystal growth run, the direction of crystal nucleation is same along the length of the fibre. The greater incidence of this type of defect in small bore capillaries cf large bore capillaries, is because of the reduced volume of melt there is a need of greater degree of optimisation between the temperature gradient and the pulling speed. No further work was carried out on crystal growth as with the growth conditions discussed above it was easily possible to obtain void free fibres for SHG experiments.

CHAPTER 6

Optical SHG Experiments Using Benzil Crystal Cored Fibres

6.0 Introduction:

In this chapter results of optical SHG experiments using benzil crystal cored fibres are presented. The benzil crystal cored fibres were fabricated to demonstrate optical SHG by coupling SH to the radiation field. Intially, experiments were conducted to demonstrate SHG using a GaAs laser, operating at 0.9μm wavelength, as the fundamental source. These experiments did not lead to observation of SHG primarily because of insufficient optical intensities at the fundamental wavelength, due to poor fibre end quality, and high attenuation of the SH wavelength in benzil. The experiments were then conducted using a high power Nd:YAG laser operating at 1.06μm wavelength. In this case SHG was demonstrated by coupling the SH to the radiation field.

6.1 SHG Experiments Using GaAs Laser:

The GaAs laser was selected as the fundamental source, to demonstrate SHG in benzil crystal cored fibres, as it can be made to emit high peak powers in the pulsed mode and is an inexpensive laser source. The lasing wavelength for GaAs lasers is generally between 0.8 to 0.9μm and as a result SH will be in the blue region of the spectrum. A demonstration of efficient SHG, in this case, could be of use for printing applications where there is a requirement for a cheap, miniature and high intensity source in the blue and near ultra-voilet region.

For this work a RCA high power GaAs laser, type SG2012, rated to deliver pulses of 20W peak power, for 36A threshold current, with maximum pulse width of 0.2μs and duty factor of 0.1% was chosen. To drive this laser a circuit capable of supplying low duty cycle high current pulses was designed. This essentially comprised of a co-axial line in series with a spark gap and the laser diode, figure

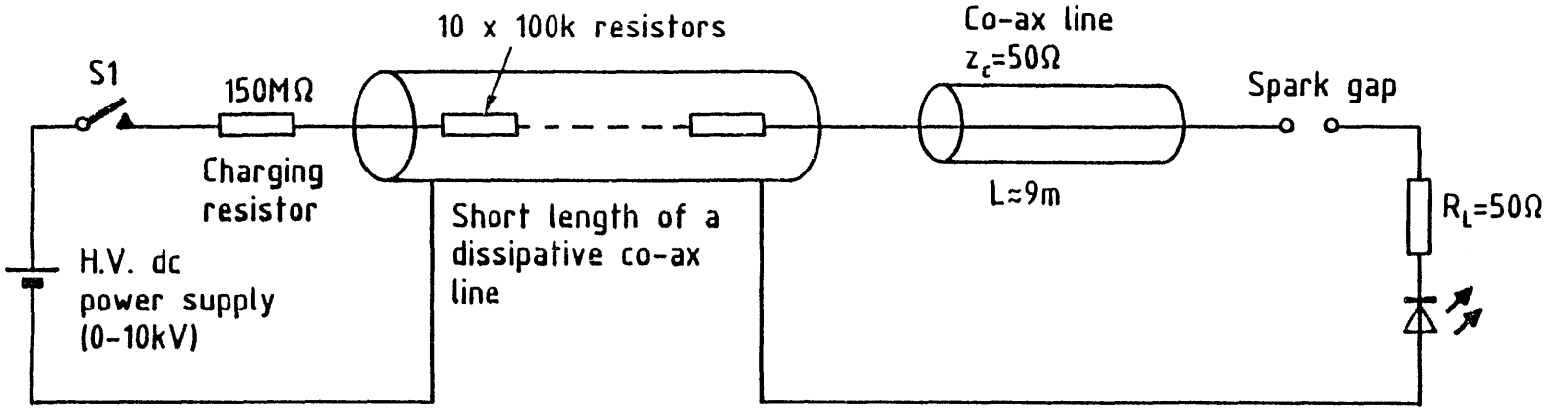

Figure 6.1: Diagram of the laser drive circuit.

6.1. On application of the switch S1, the transmission line starts charging until a breakdown voltage, V, develops across the spark gap. At the onset of breakdown in the spark gap, a current pulse, I, is injected into the laser diode and its magnitude is given by

$$I = V/(2Z_o)$$

where, Z_o is the load impedance and for maximum power transfer it was made equal to the line characteristic impedeance.

The magnitude of the current pulse is dependent on the spark gap breakdown voltage and can therefore be set to give any desired value by adjusting the spark gap. The current pulse duration, δt, is dependent upon the transmission line length and can be shown using transmission line theory to be given by

$$\delta t = 2l\epsilon^{1/2}/c$$

where,

l is the length of the transmission line.

c is the velocity of light in vacuum.

ϵ is the relative permittivity of the dielectric material in the co-axial line and for PTFE its value is 2.25.

The pulse repetation rate is determined by the charging time of the line and is given by

$$T = CR = \delta tR/(2Z_o)$$

where, C and R are the line capacitance and the charging resistance respectively.

A co-axial line of 50ohm characteristic impedance and 9m length was used with a line charging resistance of 150Mohm to give laser drive current pulses of 90ns width at a reptetion rate of 22Hz.

The spark gap was generally arranged to give peak laser output power in 30 to 45W range. It was attempted to obtain higher peak powers with increased injection current but this resulted in laser facet damage after few hours of operation. The laser pulse width was measured at FWHM points to correspond to 80ns and the repetition rate was measured to be 23Hz.

The laser radiation was collimated using a x10 microscope objective

and then launched into a single mode benzil crystal cored fibre using a x45 microscope objective. The peak optical power at the focus of x45 objective was arranged, by suitably adjusting the spark gap, to be equal to 40W. This corresponds to optical intensity of about $25MW/cm^2$. The launch efficiency in this case for a monomode fibre with 5μm core diameter was only about 10% as the spot size dimensions at the focus of x45 objective were approximately 2μm x 100μm. This large value of the spot size is as a result of the laser output having assymetrical radiation pattern. The estimation of the launch efficiency is further complicated by the fact that it is dependent on the fibre end quality which for organic crystal cored fibres can be highly variable. It is however possible to estimate the launch efficiency and the fibre attenuation by monitoring the output power. The fibre output power was measured for a number of fibres, having lengths in the 2 to 4cm range, to vary from about 1mW to 1.5W. This measurement of the output power also includes some of the cladding power as it is not possible to completely strip the cladding modes over these small lengths. Also, power can be coupled into the cladding by the voids/defects in the core. This large variation in the measured output power indicates that the fibre ends were of variable quality as care was taken to use void free fibres. The fibre ends were prepared by scribbing the cladding glass using a diamond scriber and followed by gentle pressure to obtain a clean break. This often resulted in benzil crystal broken some distance in the capillary(2 to 25μm). The preferred method of end perpartion would be to polish the fibre ends but this is not feasible because of the large variation in the hardness of organic crystals and glass. Despite of the shortcomings of the method used for making fibre ends it was possible, in many cases, by preparing new ends to obtain peak output powers in the 0.25 to 1.5W range. At these output powers the intensity of the fundamental in the fibre core is not high but should be adequate for SHG measurement using a sensitive detection arrangement.

To detect the SH signal, the fibre output was collimated using a microscope objective and monitored through 0.9μm absorbing filters using a cooled photomultiplier. In this case as the average fundamental power is low the SH would not be visible to the naked eye

and it is necessary to ensure that SH power measurement does not give errorneous results due to the noise associated in detection of weak optical signals. The test for SH observation is that the output power should be proportional to the square of the fundamental power and for coupling of the SH to radiation field be proportional to the interaction length. In this case the former test was adopted as it would not have been possible to obtain reproducibile launch efficiencies on preparation of new fibre ends. Also, as the crystal quality can vary along the fibre length, the variation of the SH power with fibre length is not a reliable test for demonstration of SHG. The SH measurements made did not lead to demonstration of SHG even though this experiment was carried out using over 50 fibre samples. The principal reasons identified for the failure to observe SHG with the GaAs laser are insufficient fundamental intensity in the fibre core due to poor end quality, low value of benzil's SH tensor coefficient and high attenuation of the SH in the fibre. The attenuation of the SH wavelength in the bulk benzil crystals was estimated from its transmission spectra to be approximately -8.4dB/cm. This value is high because of the close proximity of the SH wavelength to the benzil's UV absorption band.

6.2 SHG Experiments Using Nd:YAG Laser

The advantages with the use of Nd:YAG laser, at 1.064μm, for SHG with benzil crystal cored fibres are very high peak and average optical powers are avialable and the SH wavelength will not suffer significant attenuation as it is well away from the benzil's UV absorption edge.

For this work Quantronix Q-switched Nd:YAG laser rated to deliver peak powers of 12kW with pulse duration of 0.1μs and repetition rate of 500Hz was used. The laser output was attenuated using neutral density filters and launched into single mode benzil crystal cored fibres using a x10 microscope objective. The higher magnification objectives were not used so as to prevent optical damage in benzil at very high optical intensities. In a typical experiment, light was launched into a 3cm long fibre having approximately 3.75μm core diameter and 0.2 numerical aperture. The SH so generated was seen to

Figure 6.2: Optical SHG in benzil crystal cored fibre by coupling to the SH radiation field.

be guided in the cladding and could be seen on a screen to correspond to the far field pattern of the cladding, figure 6.2. This observation implies that the optical SHG is as a result of coupling the SH to radiation field. The SH conversion efficiency of 2×10^{-3} % has been estimated with fundamental power of 400W by comparing the intensity of SH output with that of a signal of an equivalent intensity. The value of SHG efficiency obtained is rather low. This is due to the small value of benzil's SH tensor coefficient and since the SH wave is guided in the cladding it may destructively interfere with the SH generated at later instants. This interference process is quite complex as the SH propagates in the cladding as a number of different modes, the cladding being a multimode dielectric waveguiding structure. This problem arises because of the long coherence length of the Nd:YAG laser and will not arise with high power semiconductor lasers.

CONCLUSION

In the thesis results of the study on fabrication of a waveguiding structure using organic non-linear crystal materials for phase matched optical SHG have been presented. There is considerable interest in fabrication of efficient frequency doublers, mixers and parametric amplifiers which also require low input optical powers. The use of organic materials in fabrication of these devices is especially attractive as they have high non-linear susceptibilties, high optical damage thresholds and it is possible to optimise the material properties using molecular engineering.

The form of waveguiding structure used involved growth of a single crystal from melt in glass capillaries. The use of glass cladding is attractive as it overcomes the disadvantages of lack of mechanical strength and tendency of chemical attack in organic materials. The other advantage is that for a given core material it is easy to find a suitable cladding glass as glasses are avialable having wide range of refractive indices. This method of crystal growth was successfully used to grow void free single crystals of acetamide and benzil in glass capillaries having bore diameter in the 10μm to 50μm range. The growth of acetamide which is a hygroscopic material was not pursued after attempts to find a suitable water barrier to coat the fibre ends were unsuccessful. The growth of benzil crystals was successfully extended to capillaries having bore diameter in the 2μm to 10μm range for single mode propagation. The lengths of void free single crystals grown were typically in the 30 to 50mm range. The upper limit was essentially dependent on the furnace design and it is anticipated that growth of single crystals of lengths upto 100mm should not pose significant problems. These lengths of crystal cored fibres can result in very efficient non-linear devices. The major mechanisms for void formation were identified to be presence of bubbles during filling of the capillaries with the melt and on crystallization as a result of insufficient flow of the crystal melt to the crystal face. The former type of voids were eliminated by ensuring that the melt was free of bubbles prior to filling of the capillaries and the latter type of voids were minimized by optimisation of the furnace temperature gradient and the pulling

speed.

The wave propagation in these fibres is very similar to that in silica fibres. The wave propagation in weakly guiding isotropic cored fibres has been discussed and developed to describe propagation in crystal cored waveguides. As the core material is usually anisotropic the effects of anisotropy on mode propagation have also been discussed. A computer program was written to study propagation in uniaxial crystal cored fibres with the crystal axis along the fibre axis. This program was used to show that for core birefringence of upto 10 percent the variation in the normalised propagation constant as a function of the core-cladding refractive index is less than 1.72% . This small variation in propagation constants is due to the fields being very nearly transverse. The wave propagation in biaxial crystal cored fibres and in uniaxial crystal cored fibres with crystal axis not along the fibre axis, is more difficult to describe as analytical solutions do not exist. For these guides a perturbation method has been discussed which could be used to compute the propagation constants. It has been shown that in fibres with highly dispersive cores it is necessary to take material dispersion into account for designing waveguides in which phase matching has to be achieved for non-linear interactions.

The theory of optical SHG in crystal cored fibres has been developed in some detail and it can easily be adapted to other three wave interactions. The two important considerations for efficient guided wave interactions are the phase-matching and the need to maximise the overlap integral. These both are intimately related and the highest efficiencies are only possible when the fundamental and the SH modes are of the same type. This in practice is rather difficult to achieve due to waveguide dispersion. A much simpler form of phase matching is to couple the SH to the radiation field. This form of SHG is not as efficient as the guided wave SHG as the overlap integral is small and the conversion efficiency is guide length dependent rather than the length square as for the guided wave SHG. For benzil crystal cored fibres SHG efficiency by coupling the SH to radiation field was computed for a 10mm long fibre with V-value of 2.3 at the fundamental wavelength of 1.064μm and input power of 1W to be $2.6 \times 10^{-3}\%$ while

that for coupling the SH into the HE_{12} guided mode was 12.4%. High efficiencies obtainable with the guided wave SHG hold the key to the success of this type of device for three wave mixing processes. It should be possible to achieve even higher conversion efficiencies by either using an elliptical cored guide or a biaxial crystal core where depending upon the crystal class it should be possible to achieve phase-matching between the fundamental and SH HE_{11} modes. At present time there are number of research groups trying to develop organic materials with even higher values of second order non-linearity. As an example with the use of 2-methyl-4-nitroaniline(MNA) (Levine et al 1979) the SHG efficiency will increase by a factor of 1890 as compared with that for benzil crystal core due to the MNA's exceptionally large value of the SH tensor co-efficient.

For this study it was decided to demonstrate SHG by coupling the SH to the radiation field. Benzil crystal cored fibres were fabricated by growing single void free crystals in Schott SKN18 glass capillaries. These fibres were designed to be monomode at 0.9μm with bore diameter of about 4.5μm. However, it was found that the glass refractive index changed upto a percent on drawing small bore capillaries due to residual stresses. As a result only the fibres with bore diameter of less than 3μm were monomode at 0.9μm wavelength. In order to obtain an estimate of the lower transmission loss limit in these fibres bulk benzil crystals were grown and their transmission spectra was measured along with attenuation measurements at 0.633μm wavelength. The transmission loss of benzil crystal cored fibres was measured at 0.633μm to be in the range -1.5 to -1.9dB/cm while the bulk attenuation was found to be -0.9dB/cm. The SHG experiments were first conducted using 0.9μm GaAs laser source. These experiments were not successful because of the insufficient fundamental launch powers and high attenuation of the SH signal in benzil. The experiments were then conducted using a high power Nd:YAG laser operating at 1.064μm wavelength. In this case SH generated was observed to couple into the cladding glass. This experiment clearly demonstrates that the phase-matching condition has been satisfied. The SH conversion efficiency was estimated to be 2×10^{-3}% for a 30mm fibre with 400W peak input power. Further investigation of these fibres was not possible due limited access to the Nd:YAG laser. The

phase matched SHG in benzil crystal cored fibres is significant as it demonstrates that materials which cannot be phase-matched in the bulk can be exploited for three wave mixing using guiding structures. Also, this is believed to be the first demonstration of a phase matched three wave mixing process using an organic material in a cylinderical waveguiding stucture.

APPENDIX 1

Description and listing of the computer program used to determine propagation constants of modes in fibres:

The propagation constants of modes in uniaxial crystal cored fibres with the crystal axis along the fibre axis and isotropic cored fibres can be evaluated from their respective transcendental equations given in chapter 2. The transcendental equation for an isotropic cored fibre is a special case of that for the uniaxial guide with $n_z = n_1$.

A computer program, TRANS, was written to solve the transcendental equation for a uniaxial crystal cored fibre with its crystal axis along the fibre axis. To solve the transcendental equation, the program requires an intial guess for the root which is then used to find the exact root using a modified Newton-Raphson method. The intial guess value for the propagation constant is chosen to be slightly greater than the propagation constant in the cladding ie $n_2 k_o$, as otherwise overflow is generated due to very large values of the K-Bessel's functions. The accuracy of the computer program is also evaluated by substituting the root back into the transcendental equation and evaluating its numerical value. To check the accuracy of the computations the results were compared with the values of propagation constants reported in the open literature by other researchers and good agreement was obtained. As an example in table A1 the results obtained using TRANS are compared with that reported by Yeh(1977). No comparision of results for uniaxial crystal cored fibres was made as this is believed to be the first such study.

TABLE A1

Method of computation	$k_0 a$	$\beta_n = \beta/k_0$	Numerical value of the transcendental equation
Subroutine TRANS	5.13593	1.501042	-0.80
	10.19825	1.507002	-0.0018
	26.13023	1.513001	-0.00032
Yeh's results	5.13593	1.501000	33.98
	10.19825	1.507000	0.0073
	26.13023	1.513000	0.0025

```
      SUBROUTINE TRANS(WAVE,RI1,RI2,RIZ,CR,NN,MM,UC,ANS,R,ACC)
      EXTERNAL F
      COMMON V,A,PK1,PK2,PKZ,RZR1,N,M,ID
C
C
C     ..................................................................
C
C     PURPOSE
C        CALCULATION OF U AND BETA FOR MODES OF AN OPTICAL FIBER
C     WITH ISOTROPIC OR UNIAXIAL CORE FROM THE TRANSCEDENTAL EQUATION
C     FOR WAVE PROPAGATION IN AN OPTICAL FIBER.
C     INPUT DATA REQUIRED
C         WAVE- WAVELENGTH OF THE OPTICAL SIGNAL
C         RI1- CORE RI ALONG X- AND Y- AXES
C         RI2- CLADDING RI
C         RIZ- CORE RI ALONG Z-AXES
C         CR- CORE RADIUS
C         NN AND MM SPECIFYING THE MODE NUMBER
C         UC- SET TO 0.0, UNLESS THE ACCURACY OF U CALCULATED BY SOME
C         OTHER ROUTINE AS TO BE TESTED
C         ACC- ACCURACY TO WHICH ROOT REQUIRED -- SET TO 1.0E-04
C
C     OUTPUT
C         R- COMPUTED U- VALUE FOR A PARTICULAR MODE
C         ANS- GIVES THE ACCURACY OF THE COMPUTATION BY SUBSTITUTING
C         THE VALUE U OBTAINED INTO THE TRANSCEDENTAL EQUATION
C
C     METHOD
C        FIRST THE VALUES OF J ARE FOUND WHICH LIE ON THE EITHER SIDE
C        OF THE ROOT OF THE TRANSCEDENTAL EQUATION, THEN USING
C        SUBROUTINE C02AAF(A,B,EPS,ETA,F,X,IFAIL) OF N.A.G. LIBRARY
C        THE ROOT(I.E. U), OF THE TRANSCEDENTAL EQUATION IS CALCULATED
C        TO A SPECIFIED ACCURACY.
C
C     ERROR MESSAGE DUE TO C02AAF
C        IFAIL=1 FUNCTION HAS SAME SIGN AT THE INTERVAL LIMITS
C         THE ABOVE ERROR WILL NOT OCCUR IN ROUTINE
C
C     ..................................................................
C
      A=CR
      N=NN
      M=MM
      PI=4.0*ATAN(1.0)
      RZR1=RIZ/RI1
      PK=(2.0*PI)/WAVE
      PK1=PK*RI1
      PK2=PK*RI2
      PKZ=PK*RIZ
      DELTA=((RI1**2)-(RI2**2))**0.5
      V=PK*A*DELTA
      IF(UC.GT.0.0)GOTO154
      IF(N.NE.1.OR.M.NE.1)GOTO87
      IF(V.GT.3.5)GOTO91
      GOTO88
   87 IF(V.GT.4.75)GOTO90
   88 U=V
      ID=1
      GOTO95
   90 U=V-1
   95 DO100I=1,100
      FUN=F(U)
      IF(I.EQ.1)PREVF=FUN
      IF(FUN)13,14,15
   13 P=U
      IF(PREVF.GT.0.0)GOTO17
      GOTO16
   15 Q=U
      IF(PREVF.LT.0.0)GOTO17
   16 IF(N.NE.1.OR.M.NE.1)GOTO98
      IF(V.GT.3.5)GOTO96
      GOTO97
   98 IF(V.GT.4.75)GOTO96
   97 U=V-V*(FLOAT(I)/100.0)
      W=((V**2)-(U**2))**0.5
      PREVF=FUN
      GOTO100
   96 W=V-V*(FLOAT(I)/100.0)
      U=((V**2)-(W**2))**0.5
      PREVF=FUN
  100 CONTINUE
      WRITE(6,155)P,Q
  155 FORMAT(10X,E15.8,10X,E15.8)
   17 EPS=ACC
      ETA=ACC
      IFAIL=0
      CALL C05ACF(P,Q,EPS,ETA,F,R,IFAIL)
      IF(IFAIL.EQ.0)GOTO70
      WRITE(6,153)IFAIL
  153 FORMAT(//,25X,"IFAIL =",I4)
      GOTO70
   14 R=U
      GOTO70
  154 R=UC
   70 ANS=F(R)
      RETURN
      END
```

```
      FUNCTION F(P)
      COMMON V,A,PK1,PK2,PKZ,RZR1,N,I,ID
      U=P
      IF(I.NE.1)GOTO10
      IF(ID.EQ.1)GOTO11
      W=V
      GOTO12
   11 W=0.1
      GOTO12
   10 W=((V**2)-(U**2))**0.5
   12 SQA=A**2

      U2=U**2
      W2=W**2
      UM=RZR1*U
      BETA=((PK1**2)-((U/A)**2))**0.5
      SIDER=FLOAT(N**2)*(BETA**2)*SQA*(((1.0/U2)+(1.0/W2))**2)
      D=1.0E-6
      CALL BESJ(U,N,BJ,D,IER)
      BJNU=BJ
      IF(IER.EQ.0)GOTO170
      WRITE(6,21)IER
   21 FORMAT(//,25X,"IER =",I4)
  170 NS1=N-1
      CALL BESJ(U,NS1,BJ1,D,IE1)
      BJNS1U=BJ1
      IF(IE1.EQ.0)GOTO190
      WRITE(6,22)IE1
   22 FORMAT(//,25X,"IE1 =",I4)
  190 NA1=N+1
      CALL BESJ(U,NA1,BJ2,D,IE2)
      BJNA1U=BJ2
      IF(IE2.EQ.0)GOTO210
      WRITE(6,23)IE2
   23 FORMAT(//,25X,"IE2 =",I4)
  210 CALL BESK(W,N,BK,IE3)
      BKNW=BK
      IF(IE3.EQ.0)GOTO230
      WRITE(6,24)IE3
   24 FORMAT(//,25X,"IE3 =",I4)
  230 CALL BESK(W,NS1,BK1,IE4)
      BKNS1W=BK1
      IF(IE4.EQ.0)GOTO250
      WRITE(6,25)IE4
   25 FORMAT(//,25X,"IE4 =",I4)
  250 CALL BESK(W,NA1,BK2,IE5)
      BKNA1W=BK2
      IF(IE5.EQ.0)GOTO270
      WRITE(6,26)IE5
   26 FORMAT(//,25X,"IE5 =",I4)
  270 CALL BESJ(UM,N,BJ3,D,IE6)
      BJNUM=BJ3
      IF(IE6.EQ.0)GOTO280
      WRITE(6,27)IE6
   27 FORMAT(//,25X,"IE6= ",I4)
  280 CALL BESJ(UM,NS1,BJ4,D,IE7)
      BJNS1UM=BJ4
      IF(IE7.EQ.0)GOTO290
      WRITE(6,28)IE7
   28 FORMAT(//,25X,"IE7= ",I4)
  290 CALL BESJ(UM,NA1,BJ5,D,IE8)
      BJNA1UM=BJ5
      IF(IE8.EQ.0)GOTO300
      WRITE(6,29)IE8
   29 FORMAT(//,25X,"IE8= ",I4)
  300 R1=((BJNS1U/BJNU)-(BJNA1U/BJNU))*(0.5/U)
      R2=((BKNA1W/BKNW)+(BKNS1W/BKNW))*(0.5/W)
      R3=((BJNS1UM/BJNUM)-(BJNA1UM/BJNUM))*(0.5/U)
      SLB1=R1-R2
      SLB2=(PK1*PKZ*(A**2))*R3-((PK2*A)**2)*R2
      SIDEL=SLB1*SLB2
      F=SIDEL-SIDER
      RETURN
      END
```

```
      SUBROUTINE BESJ(X,N,BJ,D,IER)
C
C
C     .................................................................
C     PURPOSE
C        COMPUTE THE J BESSEL FUNCTION FOR A GIVEN ARGUMENT AND ORDER
C
C     USAGE
C        CALL BESJ(X,N,BJ,D,IER)
C
C     DESCRIPTION OF PARAMETERS
C        X -THE ARGUMENT OF THE J BESSEL FUNCTION
C        N -THE ORDER OF THE J BESSEL FUNCTION
C        BJ -THE RESULTANT J BESSEL FUNCTION
C        D -REQUIRED ACCURACY
C        IER -RESULTANT ERROR CODE
C             IER=0 NO ERROR
C             IER=1 N IS NEGATIVE
C             IER=2 X IS ZERO OR NEGATIVE
C             IER=3 REQUIRED ACCURACY NOT OBTAINED
C             IER=4 RANGE OF N COMPARED TO X NOT CORRECT (SEE REMARKS)
C     REMARKS
C        N MUST BE GREATER THAN OR EQUAL TO ZERO. BUT IT MUST BE
C        LESS THAN
C        2.+1.*X-X**2/3       FOR X LESS THAN OR EQUAL TO 15
C        90.+X/2              FOR X GREATER THAN 15
C
C     METHOD
C        RECURRENCE RELATION TECHNIQUE
C
C     .................................................................
C
      BJ=0.0
      IF(N)10,20,20
   10 IER=1
      RETURN
   20 IF(X)30,33,31
   30 IER=2
      RETURN
   33 BJ=1.0
      RETURN
   31 IF(X-15.0)32,32,34
   32 NTEST=IFIX(2.0+1.0*X-(X**2)/3.0)
      GOTO36
   34 NTEST=IFIX(90.0+X/2.0)
   35 IF(N-NTEST)40,38,38
   38 IER=4
      RETURN
   40 IER=0
      BPREV=0.0
C
C     COMPUTE STARTING VALUE OF M
C
      IF(X-5.0)50,60,60
   50 MA=IFIX(X+6.0)
      GOTO70
   60 MA=IFIX(1.4*X+60.0/X)
   70 MB=N+IFIX(X)/4+2
      MZERO=MAX0(MA,MB)
C
C     SET UPPER LIMIT OF M
C
      MMAX=NTEST
      DO190M=MZERO,MMAX,3
C
C     SET F(M),F(M-1)
C
      FM1=1.0E-28
      FM=0.0
      ALPHA=0.0
      IF(M-(M/2)*2)120,110,120
  110 JT=-1
      GOTO130
  120 JT=1
  130 M2=M-2
      DO160K=1,M2
      MK=M-K
      BMK=2.0*FLOAT(MK)*FM1/X-FM
      FM=FM1
      FM1=BMK
      IF(MK-N-1)150,140,150
  140 BJ=BMK
  150 JT=-JT
      S=1+JT
  160 ALPHA=ALPHA+BMK*S
      BMK=2.0*FM1/X-FM
      IF(N)180,170,180
C
  170 BJ=BMK
  180 ALPHA=ALPHA+BMK
      BJ=BJ/ALPHA
      IF(ABS(BJ-BPREV)-ABS(D*BJ))200,200,190
  190 BPREV=BJ
      IER=3
  200 RETURN
      END
```

```
      SUBROUTINE BESK(X,N,BK,IER)
      DIMENSION T(12)
C
C     ..................................................................
C
C     SUBROUTINE BESK
C
C     PURPOSE
C        COMPUTE THE K BESSEL FUNCTION FOR A GIVEN ARGUMENT
C
C     USAGE
C        CALL BESK(X,N,BK,IER)
C
C     DESCRIPTION OF PARAMETERS
C        X -THE ARGUMENT OF THE K BESSEL FUNCTION
C        N -THE ORDER OF THE K BESSEL FUNCTION
C        BK -THE RESULTANT K BESSEL FUNCTION
C        IER -RESULTANT ERROR CODE
C             IER=0 NO ERROR
C             IER=1 N IS NEGATIVE
C             IER=2 X IS ZERO OR NEGATIVE
C             IER=3 X.GT.170, MACHINE RANGE EXCEEDED
C             IER=4 BK.GT.1.0**70
C
C     REMARKS
C        N MUST BE GREATER THAN OR EQUAL TO ZERO
C
C     METHOD
C        COMPUTES ZERO ORDER AND FIRST ORDER BESSEL FUNCTIONS USING
C        SERIES APPROXIMATIONS AND THEN COMPUTES N TH ORDER FUNCTION
C        USING RECURRENCE RELATION.
C
C     ..................................................................
C
      BK=0.0
      IF(N)10,11,11
   10 IER=1
      RETURN
   11 IF(X)12,12,20
   12 IER=2
      RETURN
   20 IF(X-170.0)22,22,21
   21 IER=3
      RETURN
   22 IER=0
      IF(X-1.0)36,36,25
   25 A=EXP(-X)
      B=1.0/X
      C=SQRT(B)
      T(1)=B
      DO26L=2,12
   26 T(L)=T(L-1)*B
      IF(N-1)27,29,27
C
C     COMPUTE K0 USING POLYNOMIAL APPROXIMATION
C
   27 C0=A*(1.2533141-0.1566642*T(1)+0.0881128*T(2)-0.0191395*T(3)
     E+0.1344596*T(4)-0.2299850*T(5)+0.3792410*T(6)-0.5247277*T(7)
     E+0.5575368*T(8)-0.4262633*T(9)+0.2184518*T(10)-0.0668097*T(11)
     E+0.0189383*T(12))*C
      IF(N)20,28,29
   28 BK=C0
C
      RETURN
C
C     COMPUTE K1 USING POLYNOMIAL APPROXIMATION
C
   29 C1=A*(1.2533141+0.4699927*T(1)-0.1468583*T(2)+0.1280427*T(3)
     E-0.1736432*T(4)+0.2847618*T(5)-0.4599434*T(6)+0.6283381*T(7)
     E-0.6632295*T(8)+0.5050239*T(9)-0.2581304*T(10)+0.0788001*T(11)
     E-0.0164282*T(12))*C
      IF(N-1)20,30,31
   30 BK=C1
      RETURN
C
C     FROM K0,K1 COMPUTE KN USING RECURRENCE RELATION
C
   31 DO35J=2,N
      CJ=2.0*(FLOAT(J)-1.0)*(C1/X)+C0
      IF(CJ-1.0E70)33,33,32
   32 IER=4
      GOTO34
   33 C0=C1
   35 C1=CJ
   34 BK=CJ
      RETURN
   36 B=X/2.0
      A=0.5772156649+ALOG(B)
      C=B*B
      IF(N-1)37,43,37
C
C     COMPUTE K0 USING SERIES EXPANSION
C
   37 C0=-A
      X2J=1.0
      FACT=1.0
      BJ=0.0
      DO40J=1,6
      RJ=1.0/FLOAT(J)
      X2J=X2J*C
      FACT=FACT*RJ*RJ
      BJ=BJ+RJ
   40 C0=C0+X2J*FACT*(BJ-A)
      IF(N)43,42,43
   42 BK=C0
      RETURN
C
C     COMPUTE K1 USING SERIES EXPANSION
C
   43 X2J=B
      FACT=1.0
      BJ=1.0
      C1=(1.0/X)+X2J*(0.5+A-BJ)
      DO50J=2,8
      X2J=X2J*C
      RJ=1.0/FLOAT(J)
      FACT=FACT*RJ*RJ
      BJ=BJ+RJ
   50 C1=C1+X2J*FACT*(0.5+(A-BJ)*FLOAT(J))
      IF(N-1)31,52,31
   52 BK=C1
      RETURN
      END
```

APPENDIX 2

Evaluation of the field overlap integral for SHG in crystal cored fibres:

The field overlap integral determines the modes among which coupling can take place and it also determines the strength of coupling. It was shown in chapter 2 to be given by

$$I = \int_{-\infty}^{\infty}\int_{-\infty}^{\infty} \underline{\mathcal{E}}_{\nu t}^{(\omega/2)^2} \cdot \underline{\mathcal{E}}^{*(\omega)}_{(\mu,\rho)t} \, dxdy \qquad (A2.1)$$

where, it has been assumed that the fundamental ν^{th} mode couples into μ^{th} SH guided mode or SH radiation field.

In cylinderical co-ordinate system it can be re-rewritten as

$$I = \int_{0}^{a}\int_{0}^{2\pi} \underline{\mathcal{E}}_{\nu t}^{(\omega/2)^2} \cdot \underline{\mathcal{E}}^{*(\omega)}_{(\mu,\rho)t} \, rdrd\phi \qquad (A2.2)$$

In the case of coupling to the μ^{th} SH guided mode the overlap integral, I_g, can be rewritten using the field expressions, given in chapter 2, for these modes, as

$$I_g = A_\nu^2 A_\mu \int_0^a \int_0^{2\pi} J_\nu^2 (U^{(\omega/2)}\tfrac{r}{a}) J_\mu (U^{(\omega)}\tfrac{r}{a}) \begin{Bmatrix}\cos^2 \nu\phi \\ \sin^2 \nu\phi\end{Bmatrix} \begin{Bmatrix}\cos \mu\phi \\ \sin \mu\phi\end{Bmatrix} rdrd\phi \qquad (A2.3)$$

where, A_ν and A_μ are the mode field amplitudes and are given by equation (2.2.9).

This integral can be re-written in a simplified notation as

$$I_g = A_\nu^2 A_\mu I_\phi I_d \qquad (A2.4)$$

where,

$$I_d = \int_0^a J_\nu^2 (U^{(\omega/2)}\tfrac{r}{a}) J_\mu (U^{(\omega)}\tfrac{r}{a}) \, rdr \qquad (A2.5)$$

and it gives the magnitude of the coupling strength for coupling the

fundamental ν^{th} mode into various μ^{th} modes. For $\nu = \mu$ ie similar mode field configurations, the coupling strength is maximum.
and

$$I_\phi = \int_0^{2\pi} \begin{Bmatrix} \cos^2 \nu\phi \\ \sin^2 \nu\phi \end{Bmatrix} \begin{Bmatrix} \cos \mu\phi \\ \sin \mu\phi \end{Bmatrix} d\phi \qquad (A2.6)$$

and it gives the radial symmetry of the modes among which coupling can take place and only for modes which have $I_\phi = 0$ can the coupling take place.

Similarly, for coupling to the SH radiation field the expression for the overlap integral is obtained by using the appropriate field expressions, from chapter 2, for the SH radiation field ie

$$I_r = A^2_\nu A^1 \int_0^a \int_0^{2\pi} J_\nu^2 (U^{(\omega/2)}\frac{r}{a}) J_\mu (\sigma r) \begin{Bmatrix} \cos^2 \nu\phi \\ \sin^2 \nu\phi \end{Bmatrix} \begin{Bmatrix} \cos \mu\phi \\ \sin \mu\phi \end{Bmatrix} r dr d\phi \qquad (A2.7)$$

where, A' is the field amplitude of the SH radiation mode and is given by equation (2.2.21).

The field overlap integrals for coupling to SH guided modes and SH radiation field cannot be solved analytically and consequently have to be numerically evaluated using a computer.

REFERENCES:

Anderson D.B. and J.T. Boyd, Appl. Phys. Letts., 19, 266(1971).

Armstrong J.A., N. Bloembergen, J. Ducuing and P.S. Pershan, Phys. Rev., 127, 1918(1962).

Babai F.H., E.A.D. White and R.B. Dyott, J. Mats. Sci., 12, 869(1977).

Babai F.H. and E.A.D. White, J. Cryst. Growth, 49, 245(1980).

Ballentyne D.W.G. and S.M. Al-Shukri, J. Cryst. Growth, 48, 491(1980).

Bloembergen N.,'Non-linear Optics', W.A. Benjiman Inc., 1965.

Bloembergen N. and Sievers A.J., Appl. Phys. Letts., 17, 483(1970).

Boyd G.D. and Patel C.K.N., Appl. Phys. Letts., 8, 313(1966).

Bryant W.M.D., J. Amer. Chem. Soc., 65, 96(1943).

Burns W.K and A.B. Lee, Appl. Phys. Letts., 24, 222(1974).

Chandrasekhar S., Indian Academy of Science Proceedings- section A, 39, 243(1954).

Chen B.U., C.L. Tang and J.M. Telle, Appl. Phys. Letts., 25, 495(1974).

Chen B.U., C.C. Ghizoni and C.L. Tang, Appl. Phys. Letts., 28, 651(1976).

Cozens J.R., Electronics Letts., 12, 413(1976).

Dewey C.F. and Hocker L.O., Appl. Phys. Letts., 26, 442(1975).

Davydov B.L., L.D. Derkacheva, V.V. Dunina, M.E. Zhabotinshii, V.F. Zolin, L.G. Koreneva and M.A. Samokhina, Sov. Phys. J.E.T.P. Letts., 12, 16(1970).

Davydov B.L., V.V. Dunina, V.F. Zolin and L.G. Koreneva, Sov. Phys. J.E.T.P. Letts., 118(1971).

Franken P.A., A.E. Hill, C.W. Peters and G. Wienreich, Phys. Rev. Letts., 7, 118(1961).

Franken P.A. and J.F. Ward, Rev. Modern Phys., 35, 23(1963).

Garrett C.G.B. and F.N.H. Robinson, IEEE J. Quantum Electron., 2, 328(1966).

Garrett C.G.B., IEEE J. Quantum Electron., 4, 70(1968).

Giordmaine J.A. Phys. Rev. Letts., 18, 19(1962).

Gloge D., Applied Optics, 10, 2252(1971).

Gott J.R., J. Phys.- B: Atom. Molec. Phys., 4, 116(1971).

Handerek V.A., 'Polarised light in circular and elliptical optical fibres', Ph.D. Thesis, London University, 1982.

Hopkins M.M. and A. Miller, Appl. Phys. Letts., 25, 47(1974).

Ito H., N. Uesugi and H. Inaba, Appl. Phys. Letts., 25, 385(1974).

Ito H. and H. Inaba, Optics Letts., 2, 6(1978).

Jerphagnon J. IEEE J. Quantum Electron., 7, 42(1971).

Kaminow I.P., ' An Introduction to Electro-optic Devices', Academic Press, 1974.

Kao K.C. and Hockham G.A., Proc. IEE, 113,1151(1966).

Kapany N.S., 'Fiber Optics', Academic Press, 1967.

Kapany N.S. and J.J. Burke, 'Optical Waveguides', Academic Press, 1972.

Klienman D.A., Phys. Rev., 126, 1977(1962).

Kurtz S.K. and T.T.Perry, J. Appl. Phys., 39, 3798(1968).

Kutz S.K. and F.N.H. Robinson, Appl. Phys. Letts., 10, 62(1967).

Lax B., J.G. Mavroides and D.F. Edwards, Phys. Rev. Letts., 8, 166(1962).

Levine B.F., C.G. Betha and R.A. Logan, Appl. Phys. Letts., 26, 375(1975).

Levine B.F., C.G. Betha, C.D. Thurmond, R.T. Lynch and J.L. Berstein, J. Appl. Phys., 50, 2523(1979).

Lillie H.R. and H.N. Ritland, J. Am. Ceram. Soc., 37, 466(1954).

Longaker P.R. and C.S. Roberts, IEEE Microwave Theory and Techniques, 11, 543(1963).

Maker P.D., R.W. Terhune, M. Nisenoff and C.M. Savage, Phys. Rev. Letts., 18, 21(1962).

Marcuse D., 'Light Transmission Optics', Van Nostrand Reinheld, 1972.

Marcuse D., ' Theory of Dielectric Optical Waveguides', Academic Press, 1974.

McArdle B.J. and J.N. Sherwood, J Crystal Growth, 22, 193(1974).

Midwinter J.E.,'Optical Fibres for Transmission', John Wiley, 1979.

Miller R.C., Appl. Phys. Letts., 5, 17(1964a).

Miller R.C., Phys. Rev., 134, A1313(1964b).

Miller R.C., G.D. Boyd and A. Savage, Appl. Phys. Letts., 6, 77(1965).

Owen J.R. and E.A.D. White, J. Mats. Sci., 11, 2165(1976).

Robinson F.N.H., Bell Sys. Tech. Journal, 913(1967).

Rosenbaum F.J., IEEE J. Quantum Electron., 1, 367(1965).

Rosenbaum F.J. and L. Kraus, Applied Optics, 16, 2204(1977).

Schott, 'Catalogue of optical glasses', Jenaer Glaswerk Schott and Gen., Mainz (West Germany).

Singh S., 'Non-linear optical materials', pp489-507, Handbook of Lasers, The Chemical Rubber Company, 1971.

Snyder W.A., IEEE Microwave Theory and Tech., 17, 1130(1969).

Somekh S. and A. Yariv, Optics Commn., 6, 301(1972a).

Somekh S. and A. Yariv, Appl. Phys. Letts., 21, 140(1972b).

Stevenson J.L. and R.B. Dyott, Electron. Letts., 10, 449(1974).

Stevenson J.L., J. Crystal Growth, 37, 116(1977).

Stolen R.H., J.F. Bjorkholm and A. Ashkin, Appl. Phys. Letts., 24, (1974).

Suematsu Y., Y. Sasaki and K. Shibata, Appl. Phys. Letts., 23, 137(1973).

Szilagyi A., A. Hordvik and H. Schlossberg, J. Appl. Phys., 47, 2025(1976).

Tang C.L. and P.P. Bey, IEEE J. Quantum Electron., 9, 9(1973).

Thompson D.E., J.D. McMullen and D.B. Anderson, Appl.Phys. Letts., 29, 113(1976).

Tien P.K., R. Ulrich and R.J. Martin, Appl. Phys. Letts., 17, 447(1970).

Uesugi N. and T. Kimura, Appl. Phys. Letts., 29, 572(1976).

Uesugi N., K. Daikoku and K. Kubota, Appl. Phys. Letts., 34, 60(1979).

Van der Ziel J.P., R.C. Miller, R.A. Logan, W.A. Norland jr. and R.M. Mikulyak, Appl. Phys. Letts., 25, 238(1974).

Van der Ziel J.P. and M. Llegems, Appl. Phys. Letts., 28, 437(1976a).

Van der Ziel J.P., M. Llegems, P.W. Fay and R.M. Mikulyak, Appl. Phys. Letts., 29, 775(1976b).

Winchell A.N., 'The optical properties of organic compounds', Academic Press, 1954.

Yacoby Y., R.L. Aggarwal and B. Lax, J. Appl. Phys., 44, 3180(1973).

Yariv A., 'Quantum Electronics', John Wiley, 1975.

Yeh C. and G. Lindgren, Applied Optics, 16, 483(1977).

Zemon S., R.R. Alfano, S.L. Shaprio and E. Conwell, Appl. Phys. Letts., 21, 327(1972).

Zernike F. and J.E. Midwinter, 'Applied Non-linear Optics', John Wiley, 1973.

Publications:

Nayar, B. K., 'Optical second harmonic generation in crystal cored optical waveguides', Technical Digest, Sixth topical meeting on integrated and guided wave optics, Pacific Grove, USA, Jan. 1982.

In Print:

Nayar, B.K., 'Nonlinear optical interactions in organic crystal cored fibres', Non-linear Optical Properties of Organic and Polymeric Materials, Ed: D.J. Williams, ACS Symposium Series, No.233, American Chemical Society, USA.

ThA2-1

OPTICAL SECOND HARMONIC GENERATION IN CRYSTAL CORED FIBERS

B K NAYAR

British Telecom Research Laboratories

Martlesham Heath

Ipswich, Suffolk IP5 7RE

UK

Optical Second Harmonic Generation (SHG) has been reported in planar waveguides, using waveguide dispersion to phase match the fundamental and Second Harmonic (SH) modes[1-6]. The optimum waveguide dispersion is generally achieved by the correct choice of waveguide dimensions. In practice however the inability to maintain uniform guide dimensions has limited the useful interaction length for SHG to less than 2 cms.

Whilst a number of authors[7-8] have reported the fabrication of cylindrical crystalline cored optical fibers, SHG in these structures has not been previously demonstrated. The use of such a fiber for SHG should be more efficient than the conventional planar waveguide since longer lengths of this type of structure can readily be produced with uniform guide dimensions. In addition since this structure has cylindrical geometry, coupling to other optical components will be simpler.

For SHG in these fibers the core material should be a chemically stable, non-centrosymmetric crystal having a large transverse non-linear optical coefficient. In addition the crystal should have a low refractive index and low melting point to facilitate the use of a suitable cladding glass. The majority of inorganic materials having large non-linear optical coefficients eg $LiNbO_3$, ADP etc, do not satisfy all the above criteria. For the purpose of this work therefore the organic material Benzil ($C_6H_5.CO.CO.C_6H_5$) was selected for the core material.

Crystal cored optical fibers were fabricated by growing single crystals in glass capillaries using a modified vertical Bridgeman technique. The glass capillaries were initially filled with the crystal melt by capillary action in the 'hot' zone of the furnace. The melt in the capillary was then progressively crystallized by slowly moving the fiber through a sharp temperature gradient. In this manner void free single Benzil crystal cored fibers with lengths up to 5 cm have been grown in glass capillaries with diameter in the range 5-10 μm. However, longer lengths of crystal cored fiber may be fabricated since it is possible to produce capillaries with uniform bores using established fiber pulling techniques. In figure 1, a photograph of a void free Benzil single crystal cored fiber viewed between crossed polarisers is shown.

Optical SHG in a cylindrical single mode crystal cored fiber can take place either by coupling the fundamental wave in the HE_{11} mode into a SH guided mode or into SH radiation field. In practice it is more difficult to achieve phase matched interaction for the former case since precise control of the waveguide dispersion is required. The latter method is simpler to implement and was adopted for this initial study. The cladding glass was so selected that the SH propagation constant, $\beta^{(2\omega)}$, lay in the continuum of the radiation field ie $\beta^{(2\omega)} < k_0 n_2^{(2\omega)}$, where k_0 is the free space propagation constant and $n_2^{(2\omega)}$ is the cladding refractive index at the SH frequency. This form of phase matching is shown in the ω-β diagram, figure 2. The SH radiation will exit from the fiber core at an angle α given by

$$\text{Cos}\alpha = \beta^{(2\omega)} / k_0 n_2^{(2\omega)}$$

where, $\beta^{(2\omega)} = 2\beta^{(\omega)}$, and $\beta^{(\omega)}$ is the propagation constant of the fundamental HE_{11} mode. It can be shown from a theoretical analysis that the angle α in practice is very small and consequently the generated SH wave will be guided in the cladding.

A Nd:YAG laser operating at 1.06 μm was used to demonstrate optical SHG in the Benzil crystal cored fiber by coupling the SH to the radiation field. The visible SH so generated was guided in the cladding and was observed on a screen as a ring corresponding to the far-field pattern, figure 3. A discussion of these theoretical and experimental results will be presented at the meeting.

In conclusion void free Benzil crystal cored monomode optical fibers have been fabricated and phase matched SHG in these structures demonstrated. The use of such a structure could also find application for other non-linear processes such as optical mixing and parametric amplification.

ACKNOWLEDGEMENTS

The autnor is grateful to J R Cozens of Imperial College, London and R B Dyott of Andrew Corporation, Illinois, for many useful discussions during the course of this work and to the Director of British Telecom Research Laboratories for permission to publish this paper.

REFERENCES

1 P.K. Tien, R. Ulrich and R.J. Martin, Appl. Phys. Letts., 17, 447 (1970).

2 D.B. Anderson and J.T. Boyd, Appl. Phys. Letts., 19, 266 (1971).

3 Y. Suematsu, Y. Sasaki and K. Shibata, Appl. Phys. Letts., 23, 137 (1973).

4 W.K. Burns and A.B. Lee, Appl. Phys. Letts., 24, 222 (1974).

5 N. Uesugi, K. Daikoku and K. Kubota, Appl. Phys. Letts., 34, 60 (1979).

6 H. Ito and H. Inaba, Optics Letts., 2, 139 (1978).

7 J.L. Stevenson and R.B. Dyott, Electronics Letts, 10, 449 (1974).

8 F.H. Babai, R.B. Dyott and E.A.D. White, J. of Mats. Sci., 12, 869 (1977).

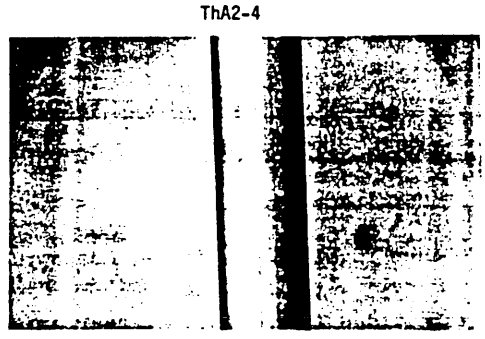

FIGURE 1. Monomode Benzil Crystal cored fiber viewed between crossed polarisers

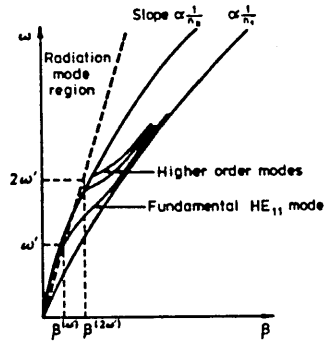

FIGURE 2. ω-β diagram showing the phase matching scheme employed

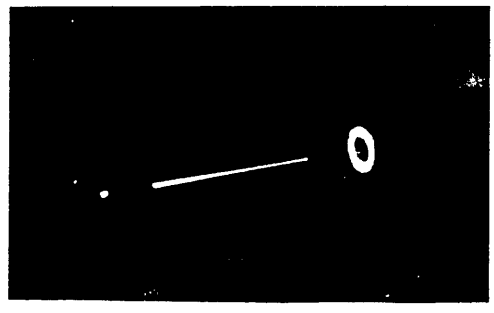

FIGURE 3. Far-field ring pattern corresponding to the visible SH in the cladding